Synthesis and characterization of a chromophore -functionalized novel non-symmetrical ditopic ligand with *N,N*-functions and it's zinc complexes

Ansa Mushtaq

MASTER'S THESIS

Inorganic Chemistry

International Master's Program for Research Chemists

656/2020

Synthesis and characterization of a chromophore-functionalized novel non-symmetrical ditopic ligand with *N,N*-functions and it's zinc complexes

Ansa Mushtaq, 300291
University of Eastern Finland, Department of Chemistry
Supervisor: Professor Igor Koshevoy
Joensuu 19.05.2020

Abstract

The development of versatile coordination supramolecular structures is imperative for several technical and industrial fields due to their fascinating structures, enthralling properties and potential applications, i.e., optoelectronic devices, drug delivery, gas preservation, sensing, segregation purposes, solar cells, rectifiers, molecular flasks, bio-imaging, and catalysis. Metallo-supramolecular chemistry field is devoted to rational design of polymeric aggregates, metal–organic polyhedral, heterometallic macrocycles and cages by using different combinations of metal ions and organic ligands thus paving way to design new molecules with different chemical and photophysical properties. Nitrogen containing heterocyclic is a class of ligands found ubiquitous in the organometallic and supramolecular chemistry with potential multi-binding capacities to metal ions. Amongst nitrogen containing compounds, ditopic ligands with *N,N*-functions and their zinc complexes have extraordinary stability, enthralling structure, riveting characteristics and appealing photophysical features. Thus, they have attained ever-increasing attention in academic and industrial researchers.

The effort of this project discovers the new synthetic attempts to design a chromophore-functionalized novel non-symmetrical ditopic ligand with *N,N*-functions (**LF**) by incorporating secondary chromophore based on phenyl-bipyrdine motif to the phenanthrol-imidazole-pyridine based primary chromophore with less electronic communication between constituting moieties. The ditopic ligand is capable to coordinate with different metal ions through bipyridine and pyridyl-imidazole moieties to form organo-metallic complexes. Th zinc complexes, **LF-(Zn (OAc)$_2$)$_2$** and **LF-Zn (OAc)$_2$**, were synthesized and characterized by XRD crystallography, NMR spectroscopy, elemental and photophysical analysis. Crystallographic XRD data revealed that ligand and complexes have ability to self-assembled to construct supramolecular structures due to intermolecular interactions from acetylene to pyridine and phenyl fragments, hydrogen bonding (N···H, O···H) and π···π stacking. Moreover, photophysical measurement demonstrates two absorption bands due to phenanthrene-localized $\pi \rightarrow \pi^*_{phen}$ transitions (LC) and phenanthrene → pyridyl intra-ligand charge transition (ILCT) with maximum absorption intensity (λ_{ab}) at 262 and 325 nm due to presence of electron deficient moiety (bpy) that increases energy gap between HOMO LUMO orbitals resulting decrease in absorption wavelength. The outcomes of this work would contribute in comprehensive support to expand novel molecular structures with improved chromophore functionality.

Contents

Abbreviations

HOMO	-Highest occupied molecular orbital
LUMO	-Lowest unoccupied molecular orbital
ES/GS/TS	-Excited states/ground states/triplet state
ECF	-Electrostatic crystal field
CT/ET	-Charge transfer/energy transfer
MMCT	-Metal-metal charge transfer
LMCT	-Ligand-metal charge transfer
MLCT	-Metal-ligand charge transfer
1D/2D/3D	-One/two/three-dimensional
SmS	-Supramolecular structures
MSm	-Metallo-supramolecular
OL/AL	-Organic ligand/auxiliary ligand
MOPs	-Metal–organic polyhedra
MOFs	-Metal–organic frameworks
SBUs	-Secondary building units
DL/DimL	-Ditopic ligand/Diimine ligands
NH	-Nitrogen heterocycles
NDDO	-Neglect of diatomic differential overlap
PL-QY	-Photoluminescence quantum yield
UV/WL/IR)	-Ultraviolet/white light/infrared
MRI	-Magnetic-resonance imaging
LPL	-Long persistent luminescence

1. Introduction

1.1. Ligands and their types

In coordination chemistry, a coordination complex is made up of core metallic atom or ion and bounded with several molecules or ions named as ligands. A ligand is a functional specie that can coordinate with core metal atom by contributing variable electron pairs. The ligand to metal bond has covalent to ionic nature and usually ligands act as Lewis bases but rarely can behave like Lewis acids. Metal ion binds with ligand to generate sets of highest occupied molecular orbital (HOMO) and lowest unoccupied molecular orbital (LUMO) orbitals. These molecular orbitals characterize reactivity and properties of the metal complex. As a result, five degenerate d-orbitals of metal ion splits up in two sets of doubly degenerate (eg): d_z^2 and $d_{x^2-y^2}$ (excited states (ES)) and triply degenerate orbitals (t_2g): d_{xy}, d_{xz} and d_{yz} (ground states (GS)) in octahedral electrostatic crystal field (ECF). While doubly degenerate (eg): d_z^2 and $d_{x^2-y^2}$ orbitals are GSs and triply degenerate orbitals (t_2g): d_{xy}, d_{xz} and d_{yz} are ESs in tetrahedral ECF.[1] The energy difference between doubly and triply degenerate orbitals are represented by Δ_o and Δ_t for octahedral and tetrahedral complexes depending upon strong or weak field ligands (**Figure 1**).[2]

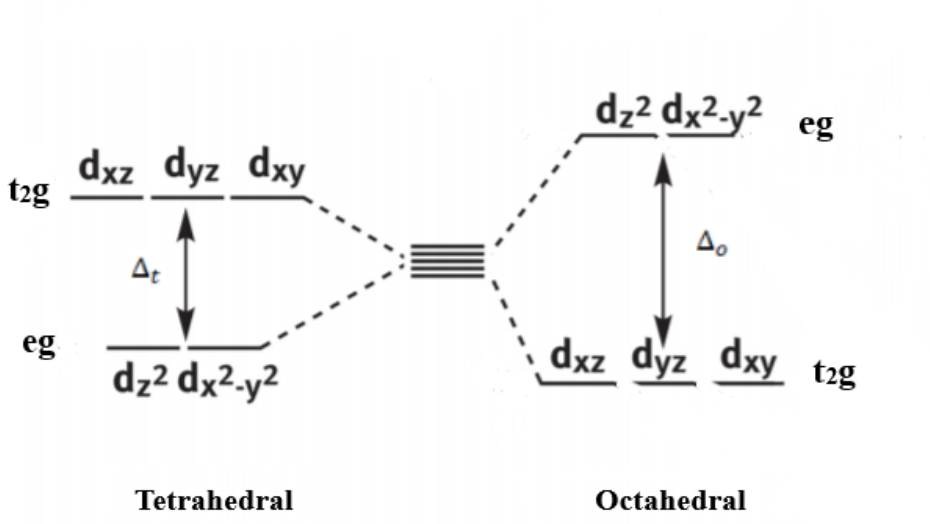

Figure 1: Energy level diagram illustrating influence of octahedral and tetrahedral ECFs on d-orbitals.[2]

Ligands are categorized in different manners depending upon charge, size, the number of contributing electrons in coordination (denticity or hapticity) and types of coordinating atoms. Ligands have ability to bind with metal ions by multiple sites because of the presence of lone pairs on more than one atom. There are two possibilities either ligand can bind to a single metal ion widely known as chelating ligand or can bind with two or more metal ions known as bridging ligand. Depending upon the binding ability, the ligands are classified as monodentate, bidentate, tridentate and polydentate (one, two, three and poly binding sites respectively) (**Figure 2**)[3]. There is another category of ligand depending upon their function, which may include trans-spanning ligands, ambidentate

ligand, bridging ligand, bi-nucleating ligand, spectator ligand and bulky ligands (chiral and hemilabile ligands).[3] The types of coordinating atoms and their examples is as follows, oxygen donor ligand (e.g., carbonyl and ethers), nitrogen donor ligand (e.g., amine and imine), multi-bond donor ligand (e.g., alkenyl and phenyl) and other donor ligands such as sulphur, halogen, phosphorus etc.[4] Ligands can be classified into another three classes: σ-donor (alkyl/aryl group (R), water, ammonia), the second one σ -donor, π-acceptor or π-acids (nitrogen monoxide, carbon monoxide, cyanide), and third one, σ -donor, π-donor or π-donors (bromide, fluoride, chloride, iodide, oxide, sulphide, nitride, η^3 -C_3H_5).

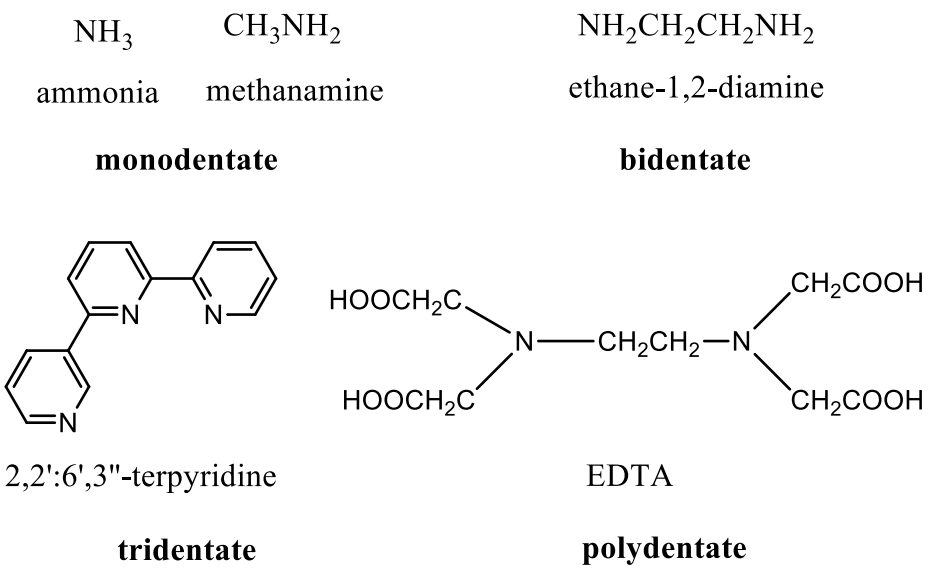

Figure 2: Classification of ligands depending upon binding sites.[3]

1.1.1. Charge transfer (CT) mechanism and properties

Charge transfer (CT) transitions occurs, when the electron migrates between molecular orbitals of metal and ligand. The CT transitions can be classified as metal to metal (MMCT) or ligand to metal (LMCT) or metal to ligand (MLCT). LMCT occurs when metal ion contains low-lying vacant orbitals (in high oxidation state) and ligand has high energy lone pairs (non-bonding electrons) and these bands can be seen in the visible region with intense colour. MLCT occurs, when metal ion in low oxidation state (it's d-orbitals comparatively close in energy to vacant ligand orbitals) and ligand has low-lying empty (π*/acceptor) orbitals particularly aromatic ligands and these bands can be seen in the visible region at low energy. MLCT mostly observed for diimine ligands that contain two N donor atoms, e.g., 2,2′-bipyridine (bpy), 1,10-phenanthroline (phen) (**Figure 3**)[5]. A complex, tris (bpy) ruthenium (II) shows orange colour, it's excited states (due to CT) have the lifetime of microseconds and these transitions were studied by Resonance Raman spectroscopy.[6] In octahedral coordination compounds, LMCT occurs in d^6-complexes and MLCT in d^5-complexes depending upon ligand shows following transitions patterns (**Figure 4, 5**).[1]

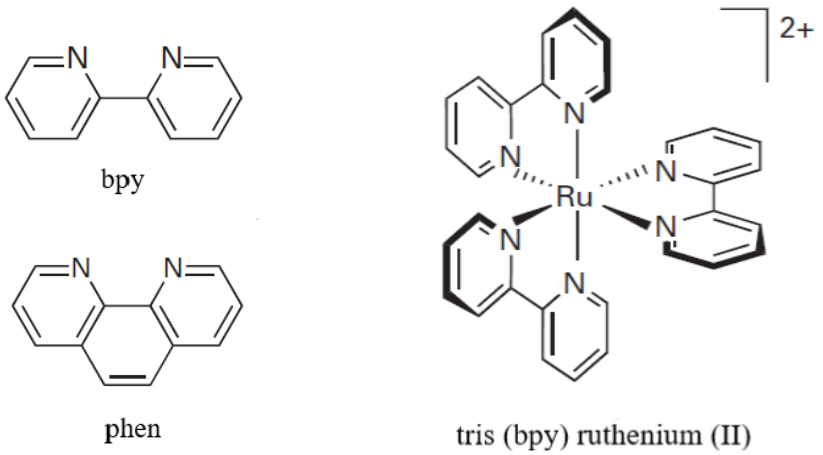

Figure 3: Structure of bpy, phen and Ru complex.[5]

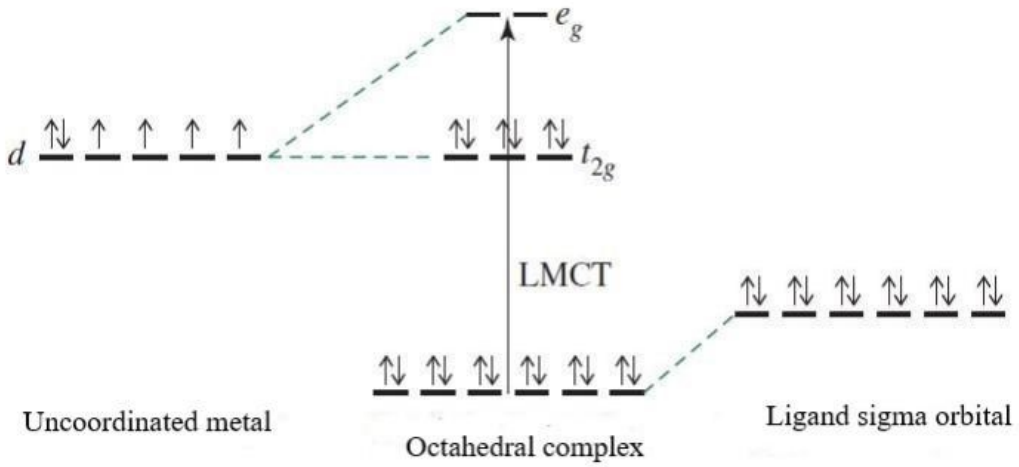

Figure 4: LMCT in octahedral d^6-complex.[1]

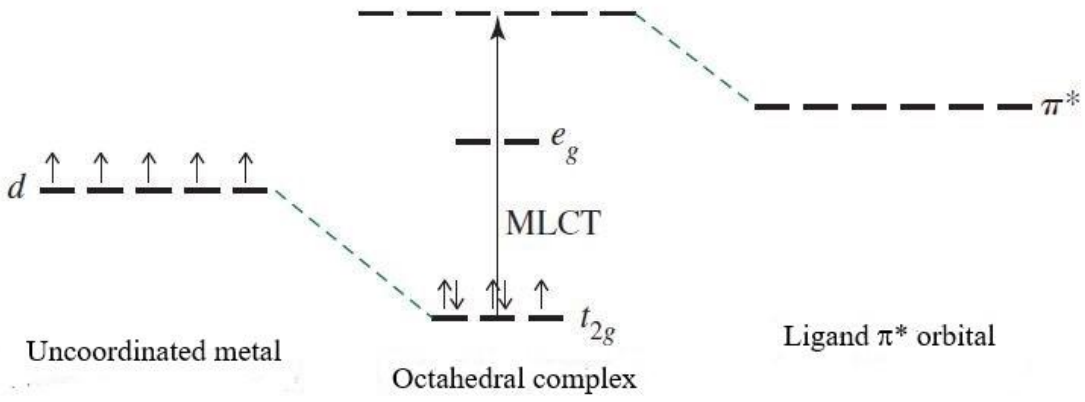

Figure 5: MLCT in octahedral d^5-complex.[1]

In octahedral complexes LMCT occurs showing four type of transitions (**Figure 6**).[7] ν_1 transition has lowest energy with the narrow band due to the involvement of nonbonding π and π^* orbitals and whenever $\pi^*(t_2g)$ orbital is filled (d^6 complexes) this band is missing. ν_2 is broad band having lowest energy in t_2g d^6-complexes due to transition from nonbonding to antibonding orbitals, while ν_3, ν_4 bands are weak and beyond the observed region.[3]

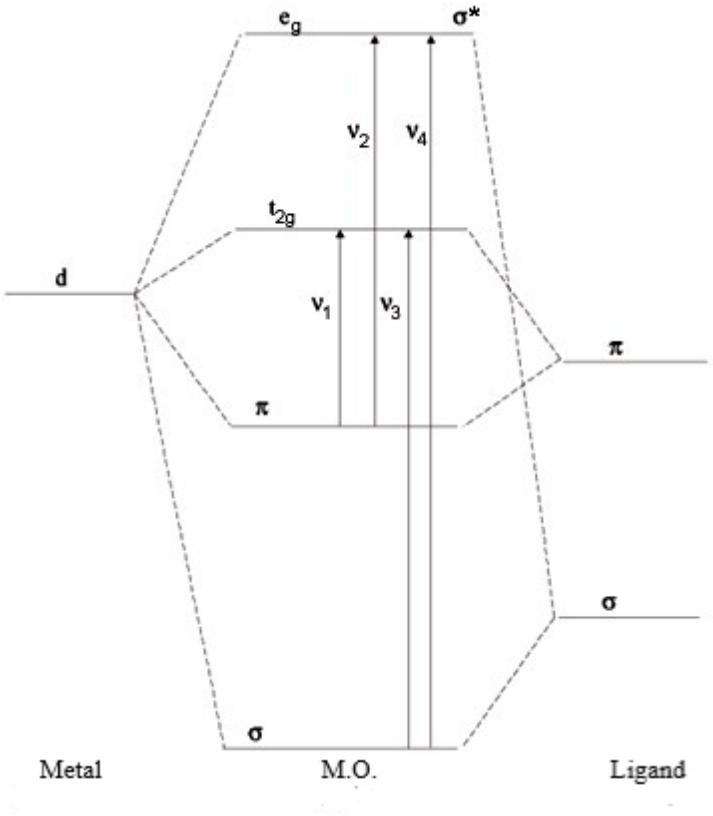

Figure 6: LMCT transitions in octahedral complexes.[7]

MLCT occurs from metal (bonding) to ligand (antibonding) orbitals, resulting π-bonding interactions. Three types of bands from medium to strong strength appear in this type of transition in octahedral complexes.[3] The absorption energy or wavelengths of CT band specifically depend on nature of donor and acceptor molecules. The electron donating ability is defined by ionization potential (E_I, energy needed to remove electrons from HUMO), while electron accepting ability is measured by electron affinity (E_A, energy released to add electrons to LUMO). The overall energy ΔE is determined by the difference between acceptor's E_A and donor's E_I, adjusted by electrostatic attraction (J). CT absorptions bands are intense and can be seen in the ultraviolet or visible region of a spectrum. The colour of complexes can be seen due to the transfer of charge from donor to acceptor molecule and in solution form, the electron density changes resulting variations in colour due to the solvent permittivity.[8]

1.2. Occurrence and chemistry of nitrogenous compound

The neutral nitrogen atom comprises two outer valence orbitals with five electrons $2s^2\ 2p^3$. It has ability to share three electrons with another nitrogen or other atom to complete the octet of valence electrons. The nitrogenous compounds exist in different forms such as ammonia (NH_3), hydrazine (N_2H_4), azides, amines, nitrogen oxides, nitro alkanes and nitro arenes, nitroso compounds, amides (Primary, secondary, tertiary amides and quaternary ammonium Ion ($R\text{-}NH_2$, $R_2\text{-}NH$, $R_3\text{-}N$, $R_4\text{-}N^+$ respectively) and used in drug, medicines, industry, explosives and propellants.[9]

Nitrogen is found in all living organisms in the form of amino acids, peptides, proteins, glycoproteins, enzymes, vitamins (vitamin B_6), antibiotics (penicillins and cephalosporin C), purines, pyrimidines, nucleosides, nucleic acids (DNA and RNA), neurotransmitters, alkaloids, secondary metabolites, Porphyrins, Chlorins and Cobalamins (macrocyclic ligands, haem for oxygen transport, coenzyme B_{12} for liver functions and chlorophyll).[9] Nitrogen containing ligands are of various kinds, such as heterocycles (pyrazoles, pyridine, indazole, phenanthroline, triazole etc.), saturated macrocycles (tetraazacycloalkanes, oxaor thia-azamacrocycles), unsaturated networks (porphyrins, salophens, BODIPYs etc.), 3D architectures, cryptands, supramolecular aggregates and nanoparticles.

1.3. Importance of ligands in supramolecular chemistry

From the past few decades, a significant attention has been dedicated to the coordination supramolecules due to their fascinating structures, enthralling properties and potential applications, i.e., to recognize molecules, for gas preservation and segregation purposes, drug delivery and catalysis.[10] To successfully accomplish this goal, the sensible choice of metal ions and organic ligands (OL) are vital. It plays important role in revealing the desired organometallic supramolecular structures (SmS) and structure-dependent properties, flexible backbone, conformation and symmetry of OL. To attain this aim, OL are changed to modify properties of coordination supramolecules, that gives motivation for further research in coordination supramolecular architectures, i.e., spheres, polyhedra, cages, wires, rings, wheels and grids.[11] In this perspective, Lehn[12], Stang[13], Fujita[14], Raymond[15], Newkome[16], Nitschke[17] and many other[18,19,20] groups are founder of various approaches to build up several metallo-supramolecular (MSm) designs.

MSm chemistry engages in practise of specific combinations of OL and metal ions to create discrete, polymeric aggregates, metal–organic polyhedra (MOPs), heterometallic macrocycles and cages. For this reason, it needs to be paid special attention in the incorporation of heterocyclic rings and arene cores in special ligand design. Nitrogen containing heterocyclic structures broadly operates for instance of bridging ligands in organometallic coordination and MSm chemistry.[21] Pyrazine is the simplest ligand which is used in the construction of binuclear complexes (Creutz-Taube ion) and for the building up larger aggregates i.e. discrete (molecular squares) or extended (coordination polymers)

(**Figure 7**).[21] Ligand designs is important for regulating distance between metals and aggregate's dimensions. As an example, pyrazine is a linear bridge ligand that create a distance of ca. 7 Å between two metal centres, similarly, 4,4-bipyridine ligand creates metal separations of ca. 11Å.[22] The well organized and well-regulated assemblies of discrete organometallic supramolecular architectures generally depend upon the combinations and arrangement of linear or angular constituents' elements. These components reasonably join and assemble to form expected structures by using directional information e.g., 2-dimensional (2D) polygons (double squares and hexagons) and 3D polyhedral (cubes and dodecahedra)[13] (**Figures 8**[23]**, 9**[24]). Usually, self-assembly controlled procedure attained through means of rigid structures of ligands, but this methodology is restricted to few highly symmetrical molecular structural designs.[13]

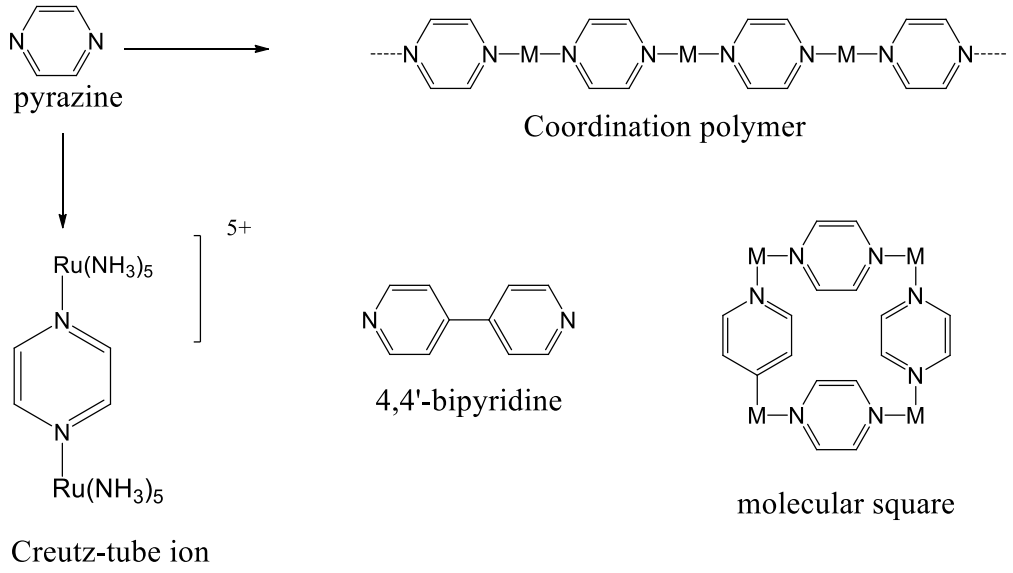

Figure 7: Pyrazine containing complexes.[21]

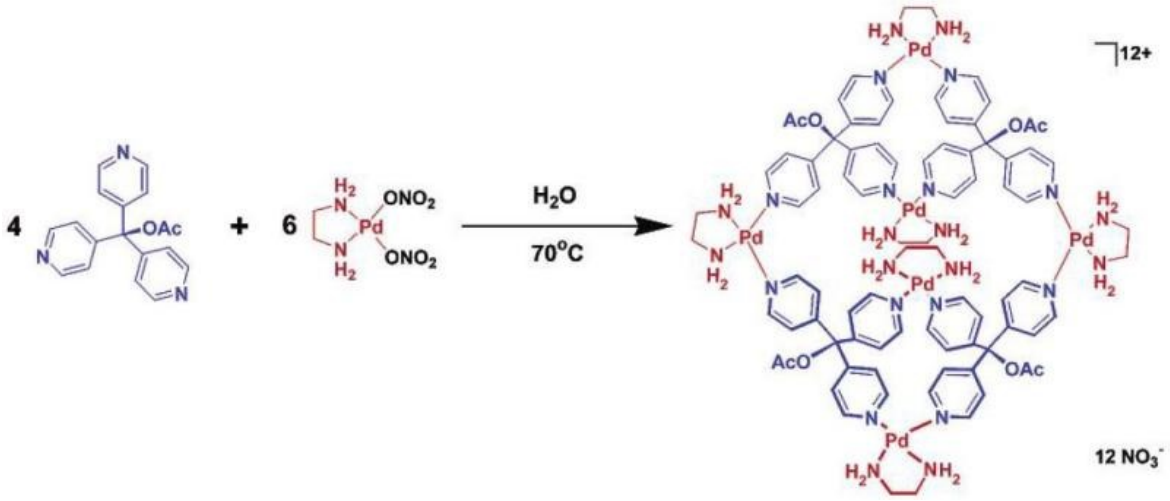

Figure 8: Self assemble two-dimensional polygons e.g. double squares.[23]

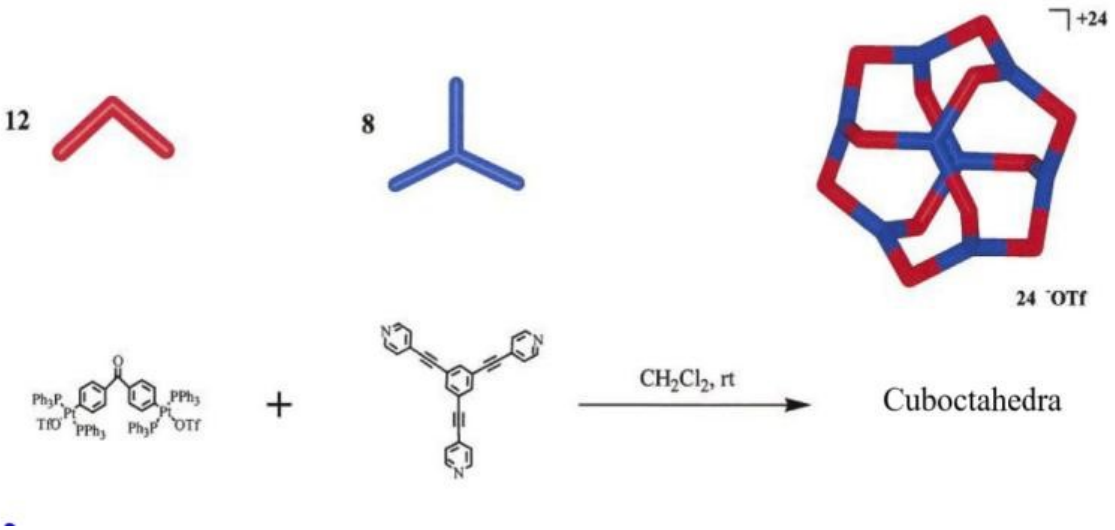

Figure 9: Self assemble three-dimensional polyhedral e.g. cuboctahedra. [24]

Recently, other approaches are being used by incorporating flexibility in the conformation of ligand (alkyl chains).[25] Thus, chemists concerned with manufacturing innovative heterocyclic ligands aimed at organometallic, coordination and MSm of chemistry. From past few years, NH ligands was synthesized for construction of complexes, e.g., simple binuclear complex, discrete and polymeric multinuclear aggregates.[21] Such compounds as pyrazine, pyrazoles, quinoline, imidazoles and 1,2,5-triazole were integrated into chelating or bridging ligands to get heterocycles.[26] Physicochemical properties of metal complexes depend on the design, structure, geometry and symmetry of heterocyclic ligand e.g., pyridine are σ-deficient, hence good σ-acceptors while five-membered pyrazole are σ-excessive and so σ-donors. Similarly, there are a lot of factors (presence of different of substituent groups, steric hindrances, chirality, etc.) of heterocyclic ring systems that can significantly change the properties of metal complexes.[26]

Complexes can fabricate into assemblies owed by non-covalent interactions that includes metal coordination, electrostatic forces, hydrogen bonding, weak Van der Waals forces and hydrophobic forces according to dynamic study of supramolecules.[27] Metal–organic polyhedral (MOPs) constructions considered to be 3D, organic polymers (1D) and organometallic polygons (2D include squares, triangles, rhomboids and rectangles etc.) architectures.[28] Wu et. al.[28] put a lot of struggles for the geometrical study of MOPs and successfully find out the following, tetrahedrons, octahedrons, rhombic dodecahedrons, cuboctahedrons, cubes, prisms and large spherical structures. Metal–organic frameworks (MOFs) have the larger surface area and used in adsorption and separation of gases.[29] A principal synthetic approach for the creation of MOPs and MOFs is the joining of secondary building units (SBUs) with linkers (**Figure 10**[30]**, 11**[31]). MOPs are nano-sized and have specific outer and inner surface areas, thus can be used in catalysis, photoreactions, molecule sensing, gas sequestration, drug delivery and stabilization of reactive species. Raymond[32] and Nitschke[33] paid special attention on synthesis and applications of MOPs, tetrahedra with the minimum edges, vertices and faces, that has great symmetry and chirality from chiral ligands. The advantages of this methodology are

extraordinary improvement for complexity in only one step, tetrahedral assembly can be modified to obtained desired properties and conversion into new structural forms by imine exchange.[33]

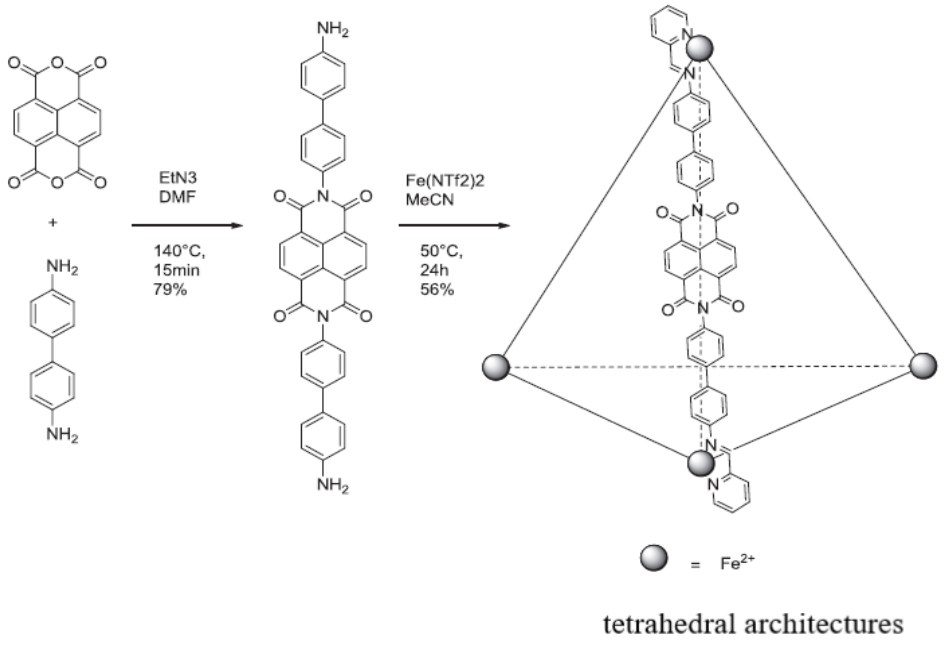

Figure 10: Formation of MOPs, a self-assembled tetrahedral architecture by using SBUs and longer linkers.[30]

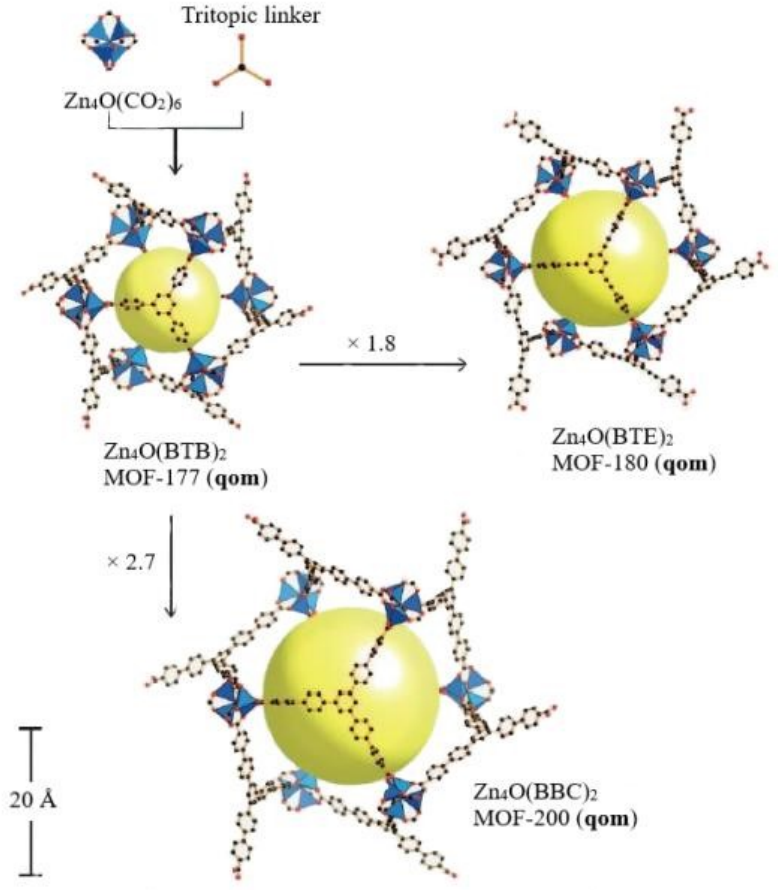

Figure 11: MOFs structure, a combination of inorganic SBUs with tritopic organic linkers.[31]

Self-assembly of polyhedral cage complexes in which bis-bidentate ligand comprising of pyrazolyl-pyridine units associated with central aromatic spacer and a transition metal (CN=6). Complex cation $[Co_8(L^{1,5\text{-naph}})_{12}]$ $[BF_4]_{16}$ having 4 ligands (tetrafluoroborateanions) are situated in the central space of six faces of the cube (**Figure 12**).[34] The cages exhibit fascinating properties such as host–guest chemistry due to the central cavity, aromatic stacking containing fluorophores (naphthyl and anthracenyl groups) enhance stability and improved fluorescence properties.[35]

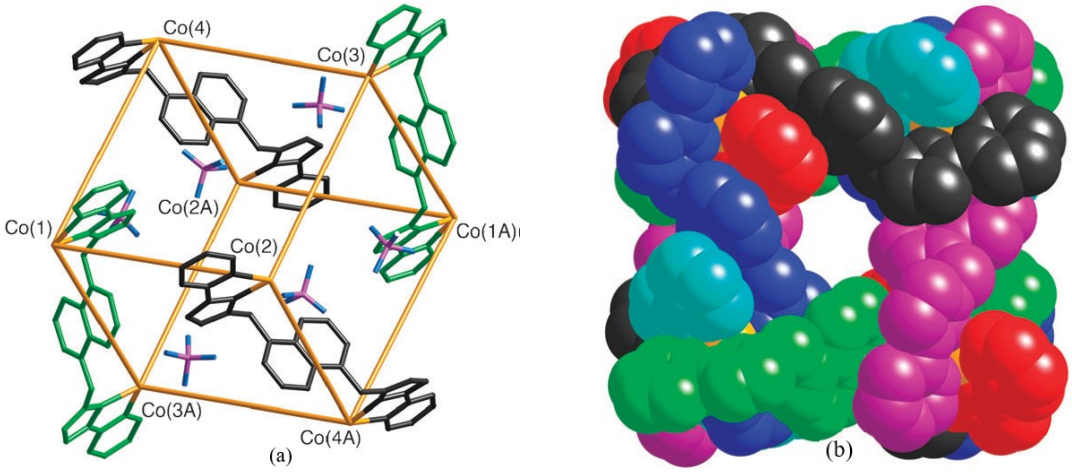

Figure 12: (a) Structure of complex cation $[Co_8(L^{1,5\text{-naph}})_{12}]$ $[BF_4]_{16}$ and (b) space-filling view of the cage.[34]

In supramolecular chemistry wide variety of structures can be formed by noncovalent intermolecular interactions which may include biological enzyme, sensors, molecular devices, liquid crystals, wires, rectifiers and molecular flasks.[36]

1.4. Ditopic ligands (DL)

A ditopic ligand (DL) has two binding sites to coordinate with metal ion by dative covalent bond. The organic DL used in coordination chemistry primarily are derivatives of N-, O-, S-, and P- comprising ligands, N-containing ligands (terpyridine (tpy), bipyridine (bipy) and azoles, etc.), O-comprising (Schiff-base, β-diketonates, 8-hydroxyquinolates, carboxylates, etc.), DL containing P and S (disulfide, thiophene, phosphine, phosphole, etc.), combination of N, O-, N, S-, and N, P- DL and organometallic complexes were studying from few past decads.[37] Coordination complexes with tpy moiety having N-donor, N, O-donor and N, S-donor ligands have been studies from several years due to the outstanding behaviour of tpy ligand, that exhibit 4-substitution with variable coordination and retains its symmetry. A rigid DL, N, S-comprising on tpy and thiophene but shows binding guest through nitrogen atom (**Figure 13**).[38]

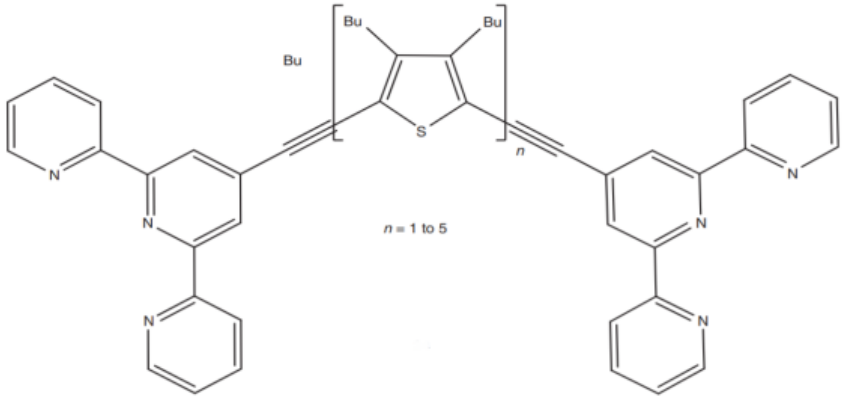

Figure 13: N, S-comprising DL grounded upon tpy and thiophene with nitrogen coordinating sites.[38]

Metallodendrimers consists of one centred and 6 outlying $[Re_6(\mu\text{-}Se)_8]^{2+}$ groups associated with pyridyl bridge have been described.[39] Ligands containing fluorene or carbazole bipy undergo cross-coupling reactions with Re $(CO)_5X$ (X = Cl, Br) in the presence of Pd to produce ring closure product that aid in manufacturing of self-assemblies of SmS (**Figure 14**).[40] DL containing fluorene and carbazole accelerate the creation of trimetallic triangles and cyclic dimers respectively.[40]

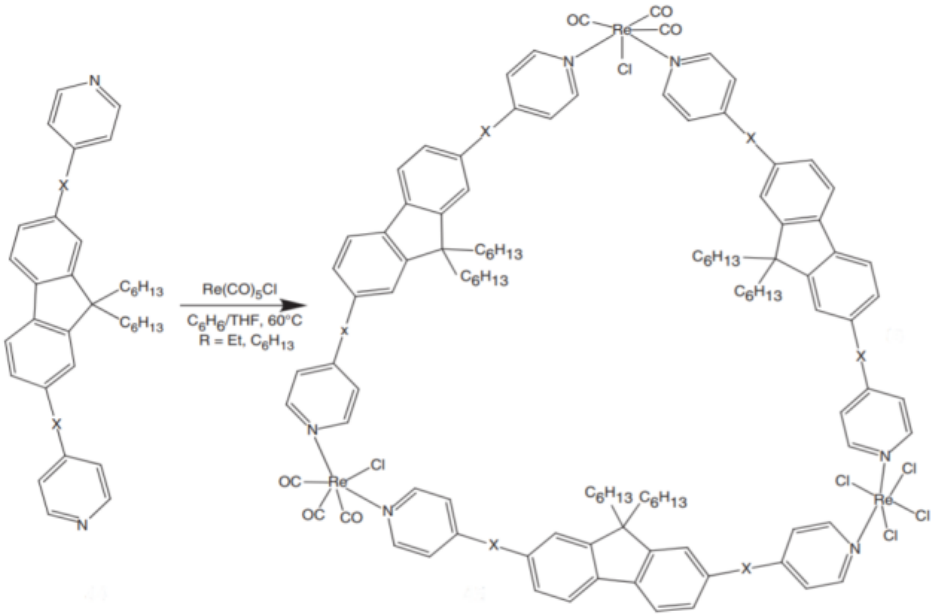

Figure 14: DL containing fluorene bipy synthesized supramolecular trimetallic triangle.[40]

2,5-pyrazinedicarboxaldehyde reacts with acyl-/aryl-hydrazine to yield a DL 2,5-Pyrazinedicarboxaldehyde-acyl-/aryl-hydrazine (**Figure 15**).[41] This ligand reacts with $[Cu_2L(tpy)_2]$ $(OTf)_4$ to synthesize dinuclear Cu complex and its magnetic studies disclosed the existence of antiferromagnetic intramolecular interactions in this complex.[41]

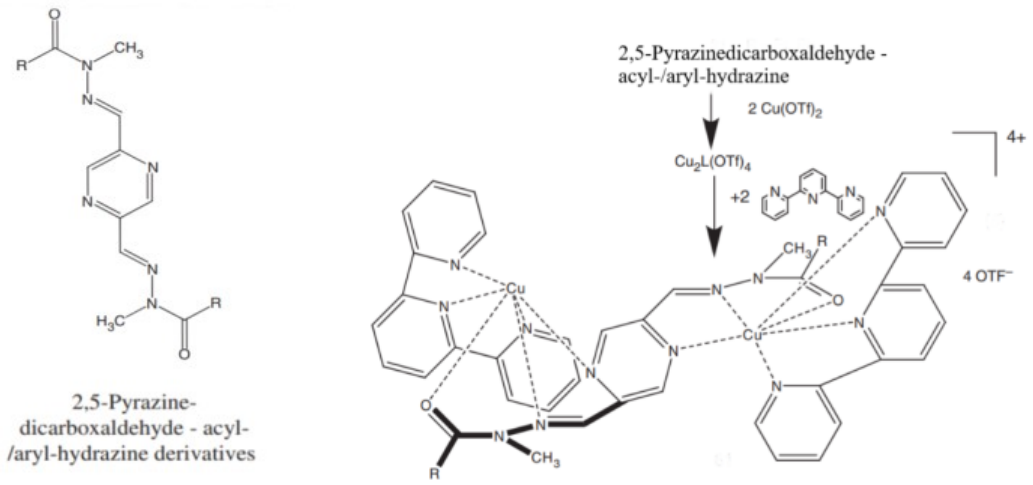

Figure 15: Structure of 2,5-Pyrazinedicarboxaldehyde-acyl-/aryl-hydrazine forms rack-like Cu complex showing intermolecular interactions.[41]

Ditopic ligands exhibiting luminescent properties due to specific coordination ability of a ligand design to form multinucleated complex have been studied from past few decades. Recently, transition-metal luminophores have been used in the form of mixed d−f complexes because of the energy donating ability of various d-block luminophores due to the prolonged triplet ES, which is variable by using different types of ligand and substituents. Hybrids d−f complexes of Ir(III)/Ln and cyclometalated phenyl-pyridine are dynamic energy donors for creating luminescent properties from ln, such as Tb(III), Eu(III), Yb(III) and Nd(III) have significant application in bioimaging.[42,43,44] In addition, transition-metal complexes with triplet-based phosphorescence effectively quenched by molecular oxygen, this approach can be used for oxygen screening (vivo/vitro) for diagnostics and treatment purposes because O_2 has vital importance in numerous physiological processes (e.g., ATP generation).[45] Photosensitive oxygens screening and imaging are procedures that give quantitative, non-invasive method for screening the concentration of intercellular oxygen.[46] Luminescent d-block complexes of Pt(II), Pd(II), Ru(II) and Ir(III) were reported aimed at oxygen detection, for example, complex of Ir·Eu and Ir·Gd have the luminescent group $[Ir(F_2ppy)_2(phen)]^+$ associated with ln (III) polyamino-carboxylatechelate (L1) exhibits specific features (**Figure 16 a, b**).[45]

Specific features founded on design, effective ET occurs by Ir(III) → Eu(III) owed by the conjugation between two metal centers, ET needs electronic coupling which follows single or two-photon excitation of Ir to generate combination of green and red coloured emission. In addition, MLCT transitions involve two-photon absorption due to the extended conjugation to help in imaging and rigidity of complex increase relaxitivity for Gd (III) used for dual-mode luminescence and magnetic-resonance imaging (MRI).[45]

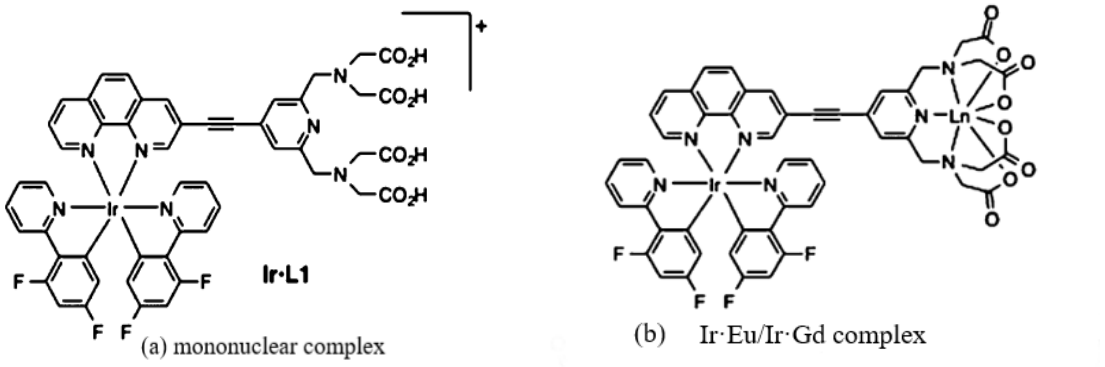

Figure 16: (a) Mononuclear complex (b) (Ir·Eu/Ir·Gd) binuclear complex.[45]

Long persistent luminescence (LPL) is an optical phenomenon to stock energy of electromagnetic radiation for succeeding emission after eliminating the excitation source. LPL substances were figured and manufactured from few past decades owed by extensive usages including, LEDs, sensors, military night-visions, anticounterfeiting barcodes, bio-imaging labels etc. Most common LPL materials are inorganic doping with noble transition metals, e.g., Zn^{2+}, Cr^{3+}. However, organic LPL substances were manufactured by using numerous approaches, e.g., host-guest co-crystals, organometallic hybrids and frameworks. LPL material can be excited by the absorption of one photon of UV or visible white light (WL) while excitation through near- IR radiations shows blank that is valuable fact for biological imaging.[47] Instead of that, fluorescence occurs due to the excitations by two photon absorptions of visible/NIR that generate higher energy emission. A LPL material, D-π-A type OL, originated from tpy, shows one/two photon absorptions, form complex with Cd (II) to manufacture M_2L_2 rectangular box. This supramolecular structure has heavy atom effect of central metal, π-stacking, inter/intramolecular packing and J aggregation states to accelerate extraordinary excitations of UV, WL and NIR through one/two photon absorption mechanisms (**Figure 17**).[48]

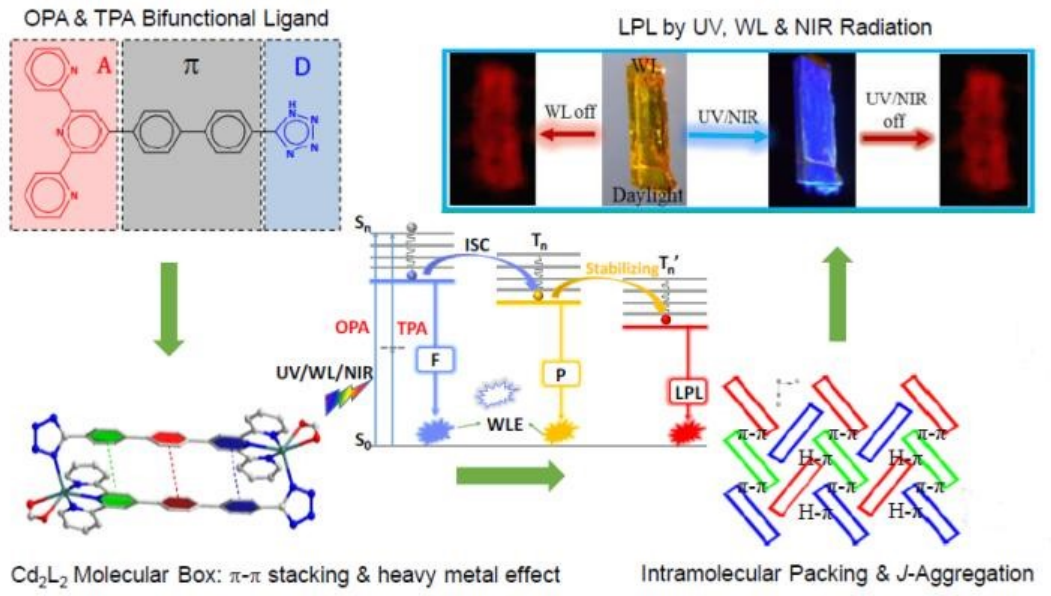

Figure 17: M_2L_2 supramolecular assembly containing D-π-A type ligand, heavy metal, π-stacking and J aggregation states.[48]

1.5. Diimine ligands (DimL) with *N-N* functions

An organic compound that has two imine (RCH=NR') groups are known as diimine. The most common derivatives of diimines are 1,2-diimine, 1,3-diimine, and they are used as ligands and precursors of heterocycles in coordination chemistry (**Figure 18**).[49]

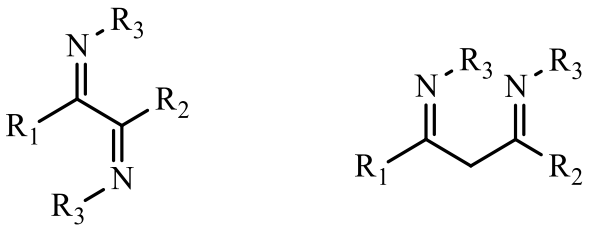

Figure 18: DimL, 1,2-diimine and1,3-diimine.[49]

Diimine ligands and their complexes have been gained special interest in organometallic chemistry from past few decades due to their interesting structure, luminescence properties, fascinating characteristics and potential applications in different fields of chemistry. The synthesis, characterization and photophysical studies of a DimL based on toluene-bipyridines (tolbpy) and its zinc complex have been reported. XRD studies was also carried out on complex [$Zn(tolbpy)Cl_2$] crystals in acetonitrile (MeCN) solvent, the molecular structure of complex is illustrated (**Figure 19 a**).[50] The selected bond distances

(Å) were observed for Zn(1)–N(1), Zn(1)–N(2), Zn(1)–Cl(1), Zn(1)–Cl(2) as 2.093, 2.078, 2.243 and 2.232 respectively. The bpy moiety has planar configuration with torsion angle of 5.26, bpy and toluene substituents has torsion angle of 10.43 between them and zinc ion gained tetrahedral geometry in complex. The photophysical studies of ligand and complex was carried out in MeCN solvent that revealed, ligand shows maximum absorption intensity (λ_{ab}) at 302 nm and maxima emission intensity (λ_{em}) at 360 with fluorescence quantum yields (Φ_F=0.17). Zinc complex shows λ_{ab} at 326 nm, λ_{em} at 403, 423sh and emission wavelength is red shifted as compared to absorption wavelength. Moreover, DFT studies on ligand demonstrated HOMO and LUMO orbitals with π character (π and π∗) delocalized throughout the conjugated aromatic rings (**Figure 19 b**).[50] It seems that, lone pairs of N-atoms donated to HOMO-1 (n-orbital) and n–π∗ and π–π∗ ES exist. But upon Coordination with zinc metal, N-atoms of bpy contributes its lone pair resulting fluorescence due to π–π∗ transition.[50]

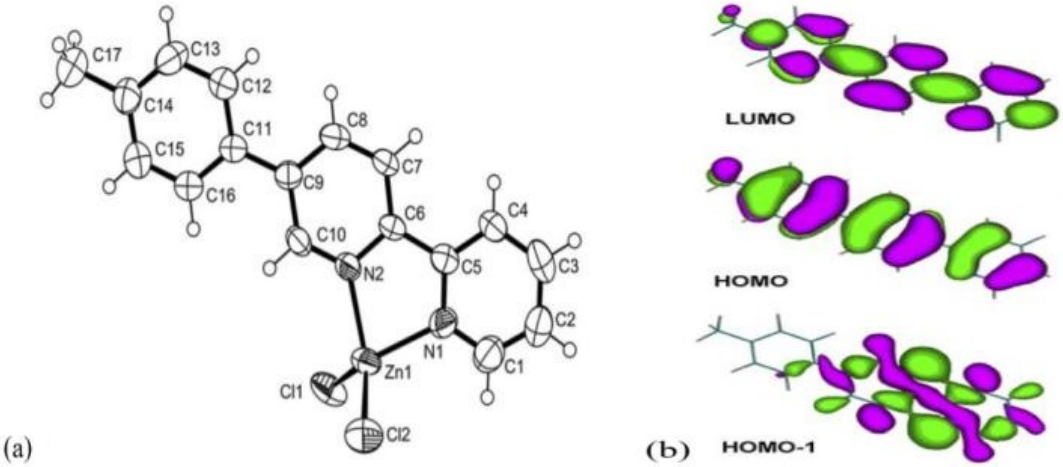

Figure 19: (a) Molecular structure of [Zn(tbpy)Cl_2] and (b) Pictorial arrangement of HOMO and LUMO of tolbpy ligand.[50]

The synthesis of DimL containing pyridyl-imidazole moiety and ten zinc complexes have been reported and one of them complex 5 is discussed here. The crystal structure of five-coordinated complex is square pyramid in which two ligands chelated to zinc ion (**Figure 20 a**).[51] The bond distance between zinc and N-atom of imidazole and pyridine was found to be 1.993 A˚ and 2.242 A˚ respectively. Normally, Zn–N bond distance with pyridine fragment ranging from 2.1 to 2.2 A˚.[52] Photophysical measurements was carried out for ligand and complex 5, and excitation and emission spectra for ten complexes is illustrated (**Figure 20 b**).[51] The complex 5 shows blue emission in solid and solution form because of luminescence due to π∗–π transition in ligand structure. The luminescence of complex is strong as compared to free ligand in visible region and bathochromic shift was observed in maxima emission intensity of complex as compared to ligand emission wavelength λ_{em} of 369 nm. Complex also has water molecule that's why it shows three times more luminescence as compared to complexes without water.[51]

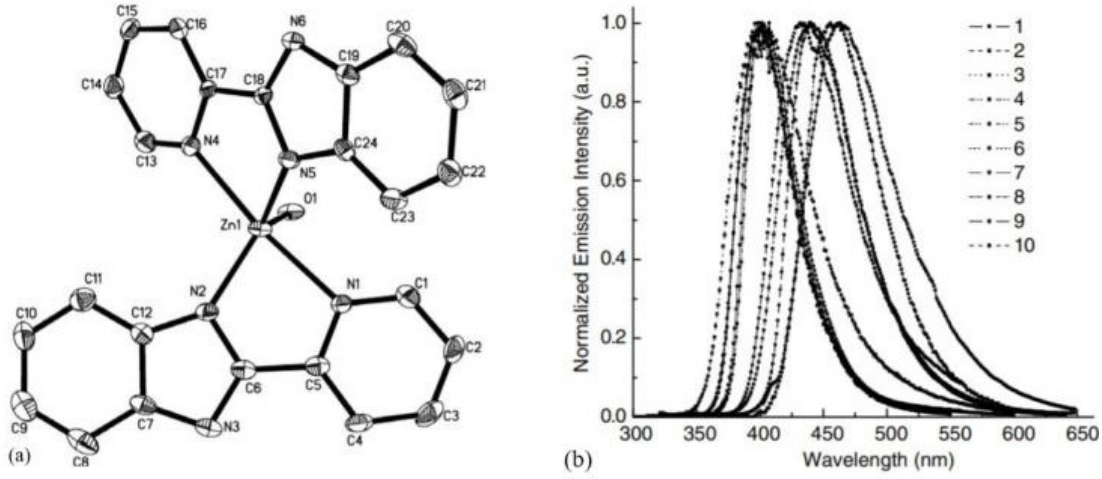

Figure 20: (a) Molecular structure of ligand and (b) The excitation and emission spectra for ten complexes.[51]

DimL containing extended π-conjugated phenanthrene ligands, namely NN1, NN2 (**Figure 21 a**)[53] and NN3, NN4, NN5 (**Figure 21 b**)[53] containing R groups of anthracene, diphenylamino-anthracene, anthracene-ethynyl-dimethylaniline (**Figure 22**)[53] were studied. Moreover, ligand binds through diimine site on reacting with rhenium(I) chloro tricarbonyl to form complex [Re (CO)3Cl(diimine) (**Figure 22**)[53] and were studied to investigate the effect of ligand structure in photophysical properties. NN1 and NN2 are chromophores with $\pi\pi^*_{phenanthrene}$ exhibits LC fluorescence, both generate deep blue emission at 380 nm and 37% and 22% QY. Thus, second chromophore of anthracene or its derivatives was introduced to phenanthrol-imidazole-pyridine motif to synthesize NN3, NN4 and NN5. The new ligand design has less electronic communication between these two chromophores that impact on photophysical properties of ligand and complexes. NN3 exhibited luminescence approximately like anthracene derivatives with QY 62%, while NN4 and NN5 has electron donating substituents that increases energy of HOMO orbital resulting decrease in optical band gap and increases wavelength for maximum absorption.

Moreover, NN4 and NN5 in DCM displayed intense ILCT luminescence from yellow to orange region (566-602 nm) and showed fluorescence solvatochromism (emission red shifted) attributed to the intramolecular charge transfer due to their donor acceptor (D-A) architecture. The coordination complexes, ReNN1 to ReNN5 and ReNN1-CN displayed photoluminescence with Φ_{em} up to 22% and excitation of ReNN1, ReNN2 resulted dual luminescence showing two bands at 400 nm for LC and at 620 nm for ML'LCT and ReNN1-CN is blue-shifted (**Figure 23**).[53] Fascinatingly, complexes of NN3−NN5 displayed optical properties like the ligands and ReNN4, ReNN5 complexes showed ILCT transitions.[53]

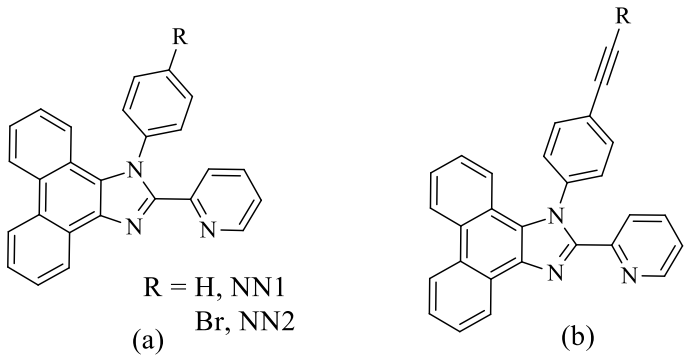

Figure 21: Varying R group to synthesized (a) NN1, NN2 and (b) NN3, NN4, NN5.[53]

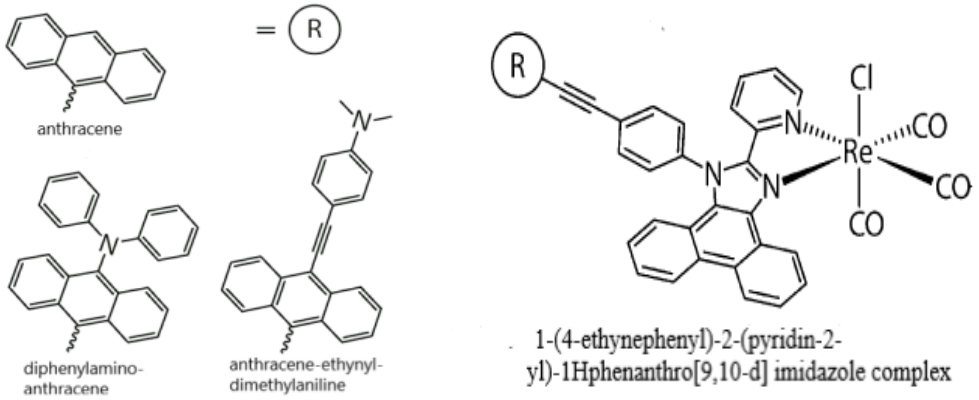

Figure 22: DimL used to form [Re (CO)3Cl(diimine)] a complex.[53]

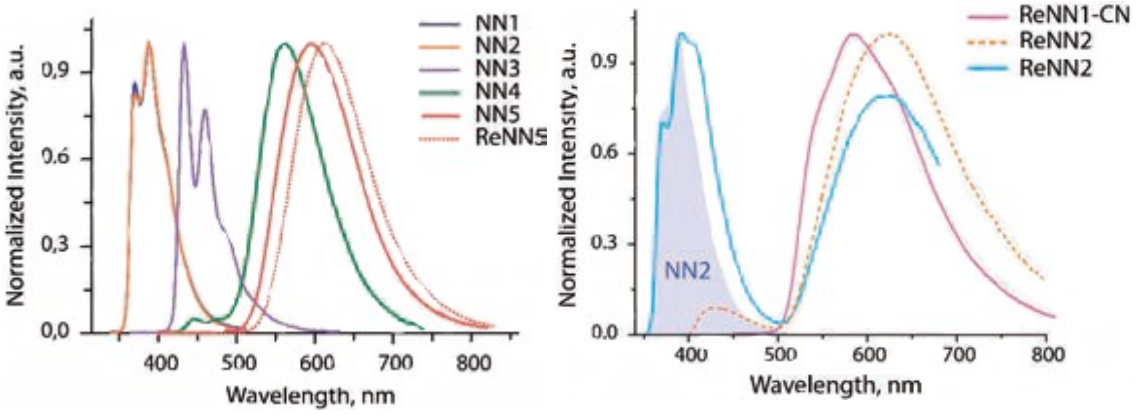

Figure 23: Normalized emission spectra of diimine ligands and their complexes.[53]

The DimL, N-(1-(pyridin-2-yl) ethylidene) pyridine-2-carbohydrazide (asymmetric alkoxy diazine) containing bidentate and tridentate coordination sites (**Figure 24**).[54] This ligand in deprotonated form shows two possibly bridging sites, one from μ-O and other from μ-N-N due to unrestricted rotation of N–N bond. Thus, it is stable in two distinctive conformations capable for forming dinuclear and polynuclear complexes showing changed magnetic features.[54]

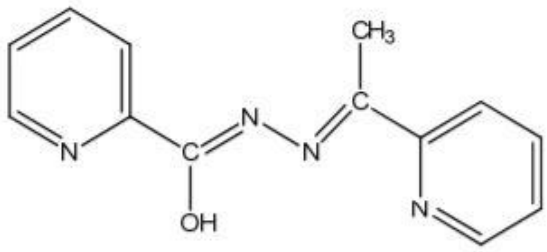

Figure 24: DimL, asymmetric alkoxy diazine is a enol-imino configuration.[54]

1.5.1. π -Acceptor ability of diimine ligands (DimL)

Acceptor ability of ligand can be determined by energy of the LUMO. In 1953, Krumholz synthesized iron (II) complexes of glyoxalbismethylimine and biacetylbismethylimine ligands and concluded chemical and spectral properties of these complexes are almost similar to complexes having aromatic ligands e.g., bipy and phen because of the good acceptance ability of aliphatic diimines.[55] Busch and Bailar synthesized iron (II) chelates with 2-pyridinealdehydemethylimine and successfully found out the correlation between the aliphatic and aromatic diimines.[56] Study of diimine complexes $[Mo(CO)_4(N\text{-}N)]$ regarding absorption solvatochromism by electron spin resonance spectroscopy revealed, aliphatic ligands were strong π-acceptors as compared to aromatic diimines, e.g., bipy. Furthered, LUMO Energy was calculated by neglect of diatomic differential overlap (NDDO) technique through Pople and co-workers used to evaluate the π-acceptor ability for ligands concerned with d-block metal ions.[57]

The NDDO-LUMO energies were compared and CT absorption of these complexes recorded (**Figure 25**)[58] for following diimines; α-diimine (dim), glyoxalbismethylimine (gmi), glyoxaldianil (gda), methylglyoxalbismethyliminc (mgmi), biacetylbismethylimine (bmi), 2-pyridinealdehydemethylimine (pm), bipy and 9,10-phenanthrenequinonediimine (phi). The result shows the π-acceptor ability decreasing in following order: o-bqui > phi > gda > gmi > mgmi > bmi > > pmi > bipy.[58]

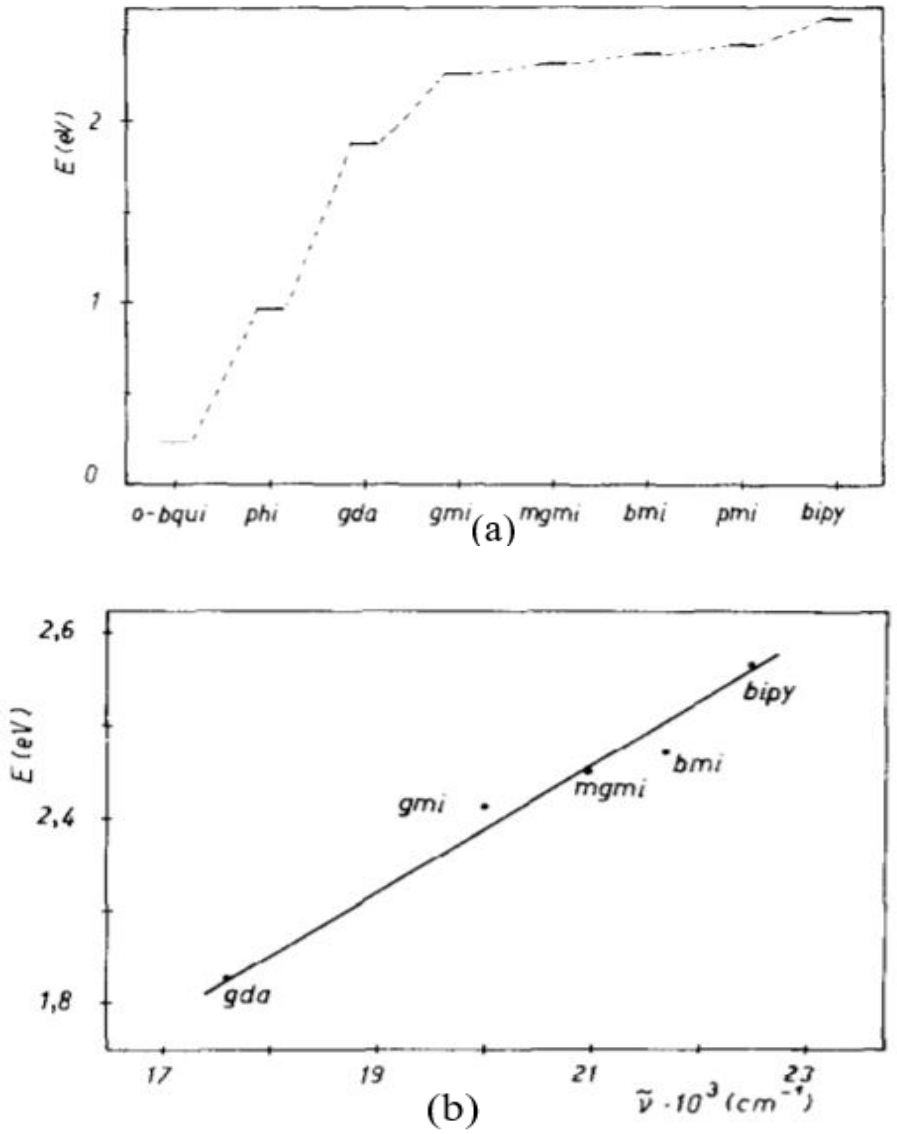

Figure 25: (a) Comparison of NDDO-LUMO for DimL and (b) correspondence of NDDO-LUMO energies with CT absorption of complexes.[58]

1.5.2. Ligand's symmetry considerations in supramolecular assemblies

Symmetry is an important aspect of ligand's design that can be demonstrated by the structural features (sterically and electronically) of 10 isomers of disubstituted naphthalene (**Figure 26**).[21] Symmetric ligand produces only one isomer of metal complex, single molecular architectural assemblies (unidirectional) and single reaction pathways. Six isomers have symmetrical structure presenting two metal binding sites are equivalent and give a single crystalline product to form unidirectional assemblies while four isomers have unsymmetrical environments that shows two ways of incorporation of ligand into assemblies and cannot form single molecular architecture.[21]

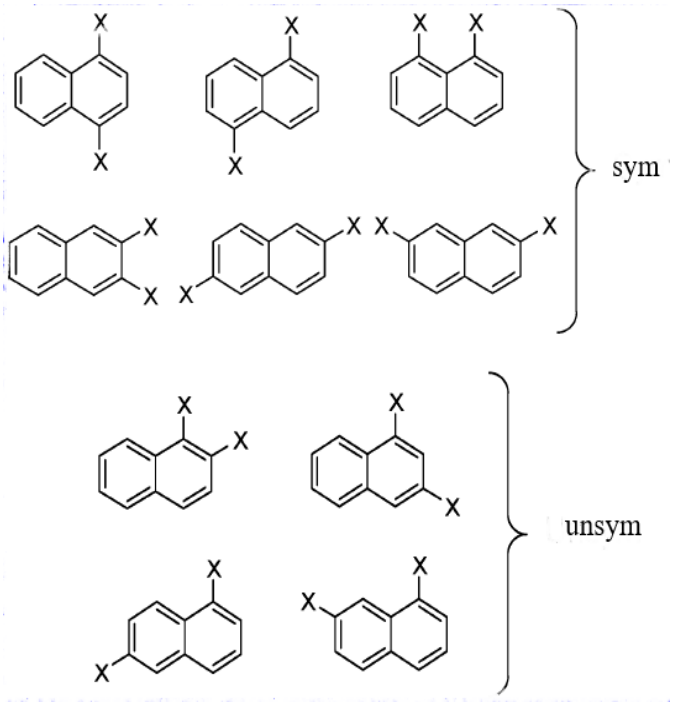

Figure 26: 10 isomers of disubstituted naphthalene, 6 symmetric and four unsymmetric.[21]

Another example of a ligand containing central benzene ring with four substituted chelating groups through methylene linkers. The ligand has two isomers, and one is 1,2,4,5-substituted groups having four symmetrically equivalent arms, thus readily coordinates with four metal ions as 4-fold connector in numerous complexes to form unidirectional assemblies. While, the other ligand's isomer is 1,2,3,4-substituted groups with four unsymmetrical arms (two pairs of equivalent arms with 1,4-substitution and 2,3-substitution) showed different behaviour. This asymmetric ligand yields cleft-shaped (because 4 groups present arranged at similar position on benzene) binuclear complexes upon complexation with silver (I) salt (tetrafluoroborate) in which one silver atom is chelated by two adjacent arms (**Figure 27**).[59] Therefore, these binuclear units assembled to form self-complementary two-folded construction due to π -π stacking and C-H……M interactions.[59]

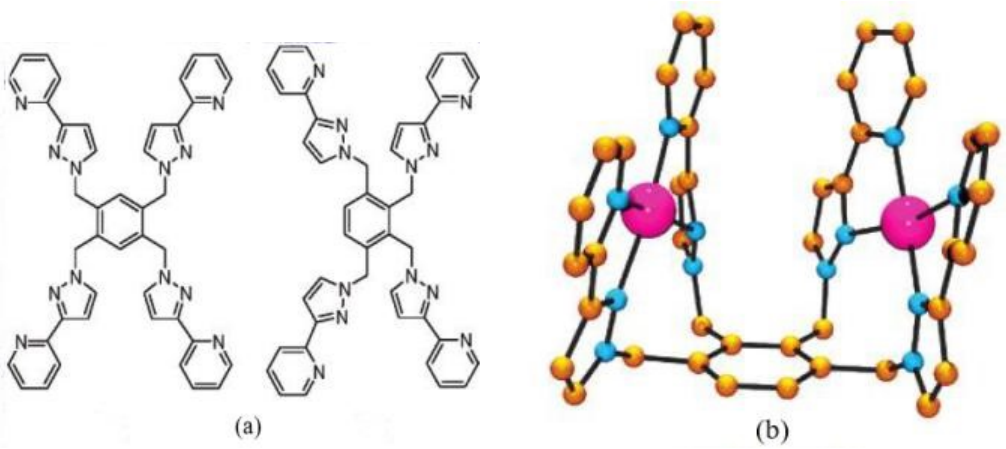

Figure 27: (a) Two isomers of ligand, central benzene ring with 1,2,4,5-substituted (symmetric) and 1,2,3,4-substituted (asymmetric) (b) binuclear silver (I) complexes of the asymmetric isomer.[59]

1.6. Ligand structure and environment influence on photophysical properties

From the past few decades, a lot of researches have been done to determine the effect of ligand and its environment on the electronic and photophysical properties of complexes. Bis(dipyrrinato) Zn (II) complexes have been studied to investigate the changes in emissive characteristics of complexes due to the presence of bulky substituents on meso-aryl group of dipyrrin ligands (**Scheme 1**).[60] The spectroscopic properties were study through absorption and emission spectra that represented maximum absorption at 488−511 nm range, molar extinction coefficients (1.2×10^5–1.6×10^5 M^{-1} cm^{-1}) and emission band at 510−558 nm are due to π−π* transition of dipyrrin structure. $2a_2Zn$−$2c_2Zn$ complexes shows additional absorption band at 370 nm due to π−π* transition of anthracene group. Absorption spectra of solid thin films are similar to the solution one, in addition to red shifts of 15−30 nm and broad bands due to the stronger intermolecular forces in solid. The fluorescence properties of the solid are distinctive from solution one due to the different crystal packing of complexes.

This analysis reveals that $2a_2Zn$ shows bands at longer wavelength 635 nm (ΦF = 0.03) with lifetimes (0.43 ns and 1.0 ns) due to the extended conjugation system of π electrons of anthracene that decreases in energy gap between HOMO LUMO orbitals. Comprablely,$1a_2Zn$ shows bands at lower wavelengths 615 nm (ΦF = 0.02) with lifetimes (0.64 ns and 2.0 ns) and $3b_2Zn$ shows bands at lowest wavelength at 560 nm (ΦF = 0.03) with lifetimes (0.088 ns and 1.1 ns) due to less π-conjugated system that increase energy gap between HOMO LUMO orbitals. (**Figure 28**).[60] It was concluded that emission wavelengths, fluorescence QY and lifetimes are completely different for the solid and solution, that results variation in photo physics of dipyrrinato−zinc complexes in solid state.

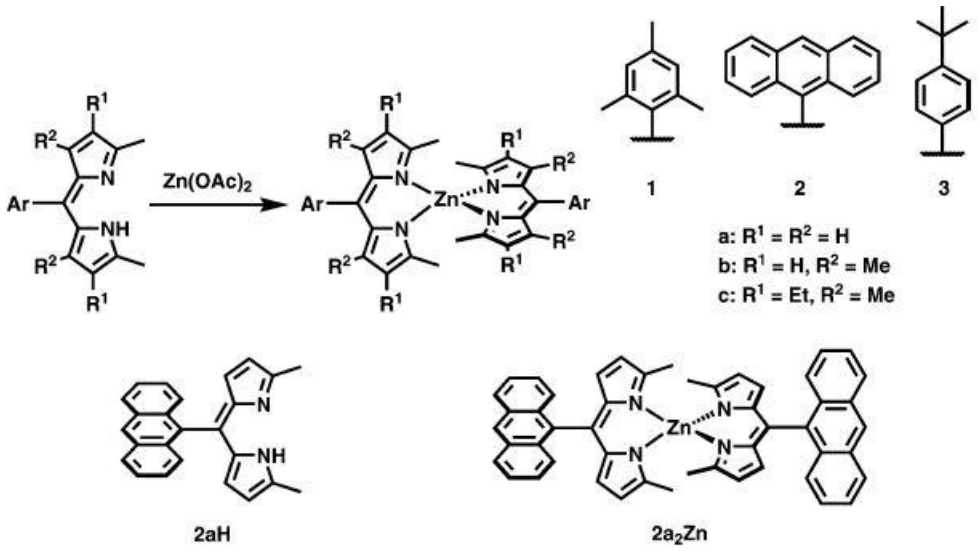

Scheme 1: Synthesis of Bis(dipyrrinato) zinc (II) Complexes.[60]

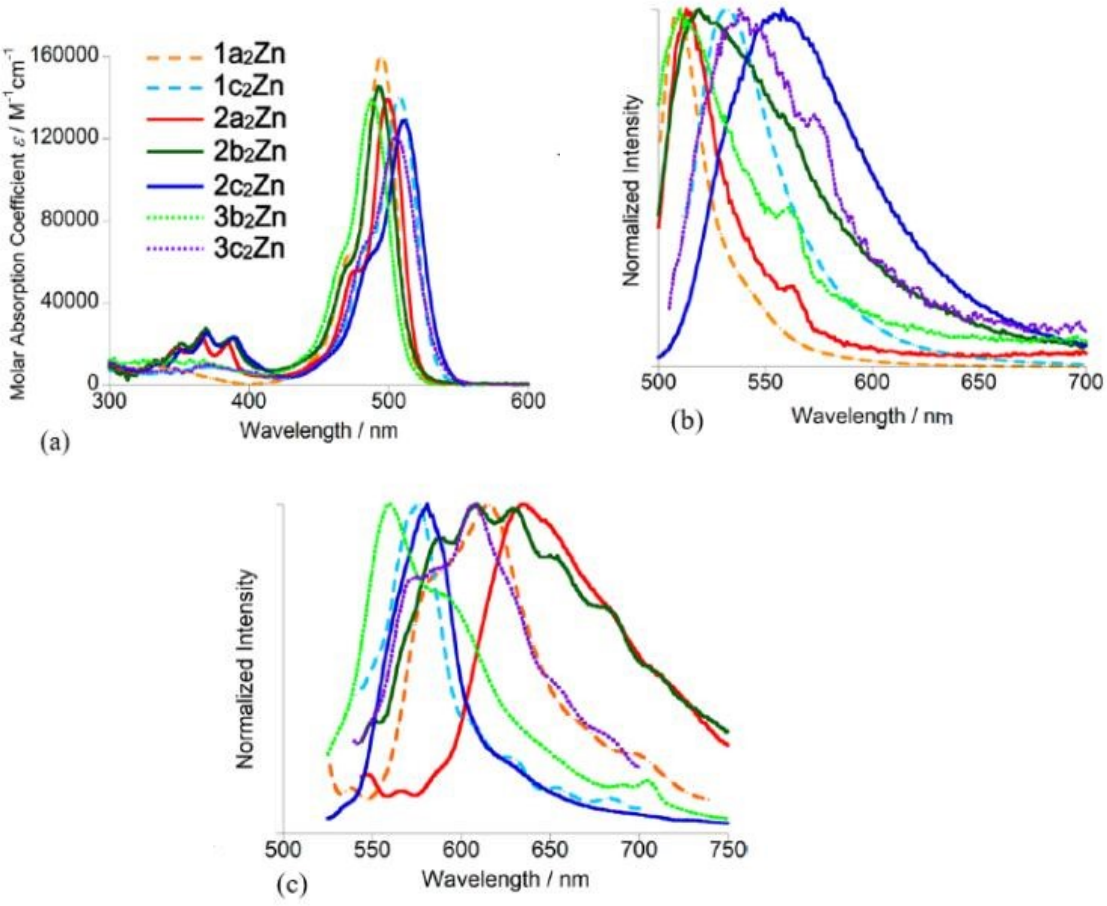

Figure 28: Spectroscopic properties of Zn complexes (a) absorption, (b) emission in toluene and (c) emission in solid state.[60]

Luminescent complexes of different metals, e.g. Au (I), Zn (II), Pt (II), Cu (I), Ag (I), Al (III) and Ir (III) have recently fascinated interest in different fields. Mechano-chromic luminescence is applied in switches, security papers, mechanosensory indicators, data storage and optoelectronic devices.[61]

Luminescent features of complexes containing zinc (II) with ligand 4 -phenyl-2,2 :6 ,2-terpyridine (ptpy) were explored.[62] Phenyl's para-position of ligand replaced by following groups, e.g. (1) tert-butyl (t-Bu), (2) hexyloxy (OHex),(3) carbazole-9-yl (Cz), (4) naphthalen-1-yl-phenyl-amine-N-yl (NPA) and (5) diphenyl amine-N-yl (DPA) have the variable electron contributing capacity (**Figure 29**).[62] It was noticed that complexes show emission colours in range of purple and reddish orange ((392-604 nm) (**Figure 30**)[62] due to the increase in donor capacity of 1 to 5 groups and in photoexcited luminescence intra-ligand CT occurs to demonstrate solvatochromism.[62]

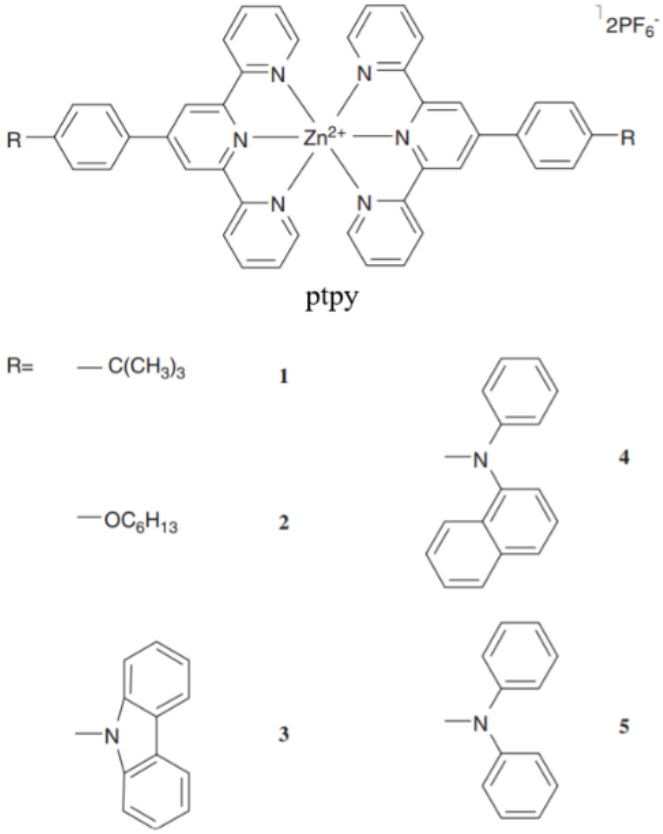

Figure 29: Zinc (II) complexes with ptpy, para-position of phenyl replaced by groups 1, 2, 3, 4 and 5.[62]

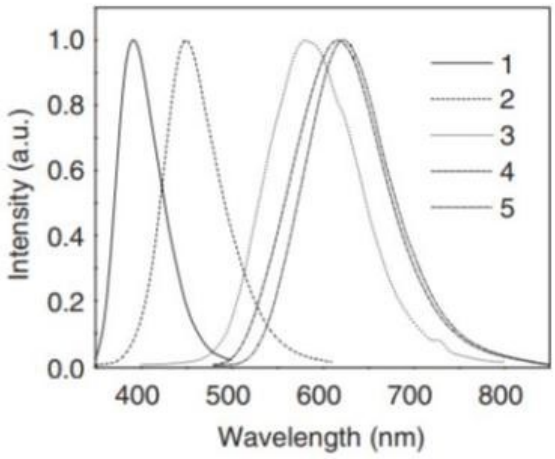

Figure 30: Emission spectra of five different zinc (II) complexes.[62]

The Ru (II) complexes, e.g. $[Ru(bipy)_2L]^{2+}$, $[Ru(phen)_2L]^{2+}$ and $[Ru(Biquin)_2L]^{2+}$ (L is 2-(4-formylphenyl)imidazo[4,5-f][1,10] phenanthroline (FPIP), 2-(4-nitrophenyl)imidazo[4,5- f][1,10] phenanthroline (NPIP) and 2-(4-cyanophenyl)imidazo[4,5-f][1,10] phenanthroline (CPIP) respectively (**Figure 31**)[63], where R_1 defined as −CHO, NO_2, and CN for ligands (L) FPIP, NPIP, and CPIP respectively. Reduction potential is the ability of ligand to reduce by gaining electrons, so it shows the extent of auxiliary ligands (AL) for electrons donation towards Ru centre. Ru (II) complexes show variation in reduction potential as varying AL that factor gives difference in electron donation capacity. The normalized absorption spectra for Ru (II) complexes (**Figure 32**).[63] Absorption at nearly 300 for ligand centred and 460 nm for MLCT absorptions. The energy of singlet state of MLCT due to the long-wavelength absorption bands and a bathochromic shift occurs for MLCT transition towards more electronegative AL, and it is independent to the electronic character of major ligand.

Detailed explanation for electronic variations through FPIP, CPIP and NPIP ligands are given in spectra.[63] Absorption patterns for MLCT transition varies with changing electronic nature of AL e.g., series of FPIP having phen shows peaks by 456 and 470 nm combinedly give MLCT band but when phen replaced by bipy, in MLCT band small bathochromic shift occurs and on replacing with conjugated biq, in MLCT band large bathochromic shift occurs.

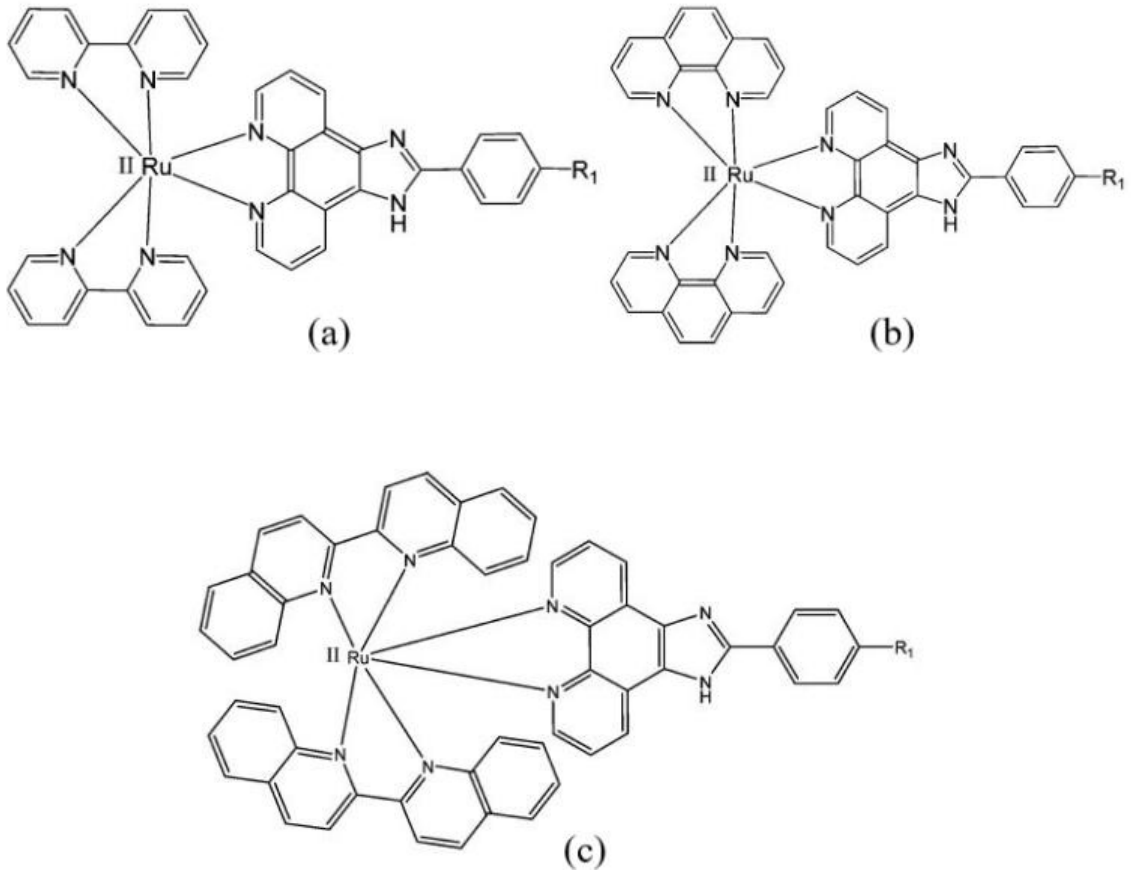

Figure 31: Ru (II) complexes (a) $[Ru(bipy)_2L]^{2+}$, (b) $[Ru(phen)_2L]^{2+}$ and (c) $[Ru(Biquin)_2L]^{2+}$ where L is 2-(4-R_1phenyl)imidazo[4,5-f][1,10] phenanthroline.[63]

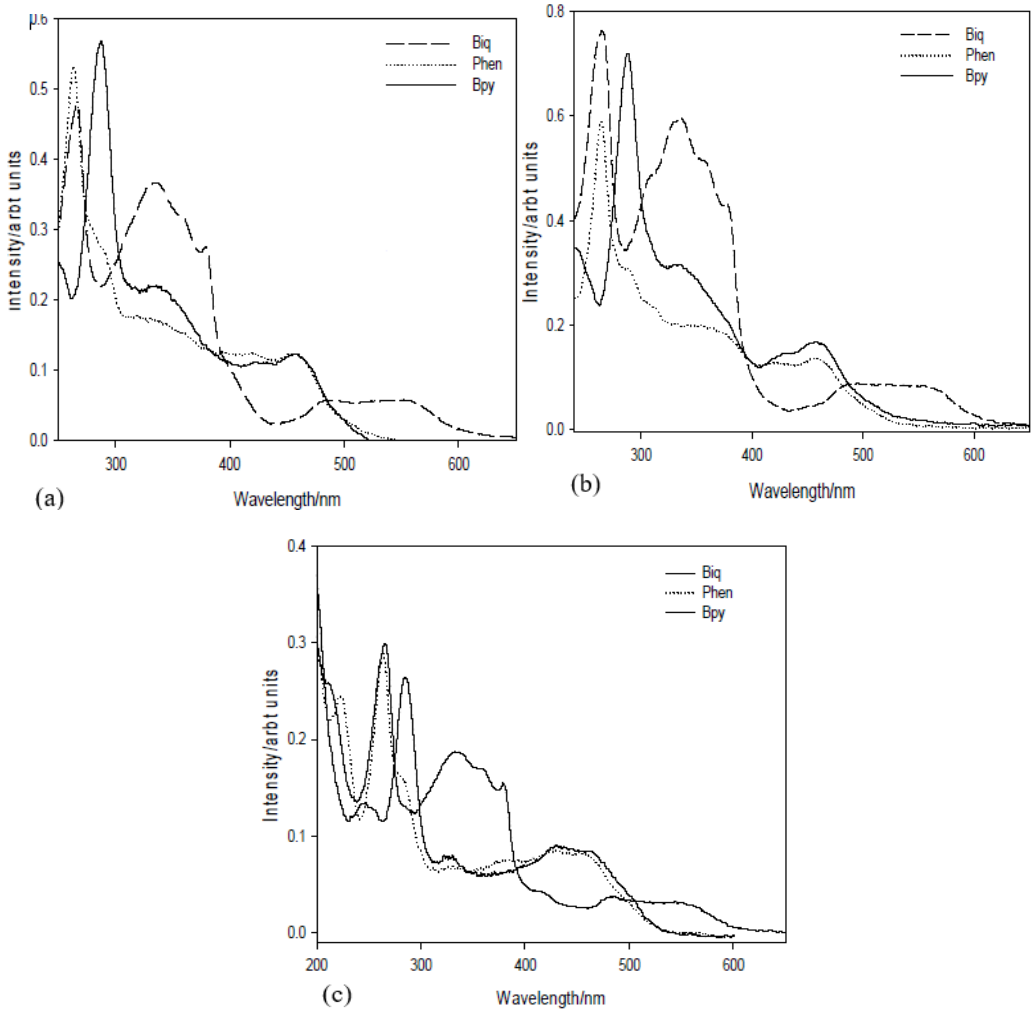

Figure 32: Normalized absorption spectra for Ru (II) complexes having major ligands with (a) FPIP, (b) CPIP, (c) NPIP.[63]

Normalised luminescence spectra for Ru (II) complexes (**Figure 33**).[63] Similar bathochromic shift exists as more electronegative AL but it shows more distinct shifts than the absorption spectra. The Ru (II) complexes having FPIP demonstrate peaks at 589 nm for phen, 598 nm for bipy and 750 nm for biq.

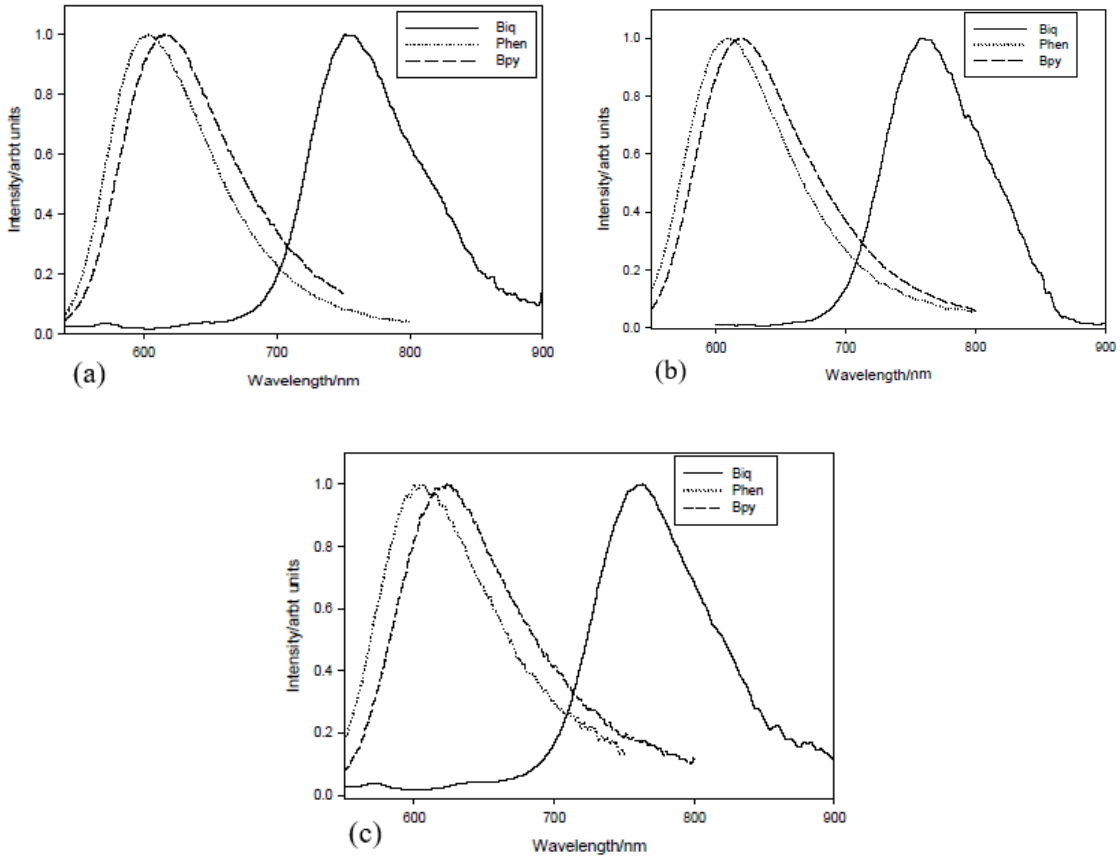

Figure 33: Normalised luminescence spectra for Ru (II) complexes having major ligands (a) FPIP, (b) CPIP, (c) NPIP.[63]

Other two series CPIP and NPIP series exhibits same trend, as a result electronic transitions decreases energies for excitation and emission by varying AL from phen-bipy-biq to tune the bandgap.[63]

1.7. Applications

1.7.1. Photoactive supramolecular structures

SmS (cages and capsules) have been constructed by self-assemble ability of metal ions with bridging ligands. The photoactive supramolecular cages and their desirable properties (emission tuning, electron transfer) can be achieved by using only one phosphorescent component either metal ion or ligand. The cages of phosphorescent e.g., Ir(III)/Ru(II) complexes have been studied aimed at wide applications in the field of sensing, photocatalysis and solar fuels production.[64]

Ru (II) complexes can be integrated into polymers, metalorganic frameworks and discrete 2D macrocycles. Cook and co-workers[65] investigated a 3D supramolecular cage of Ru (II) complexes (RuCtpt) by the reaction of 2,4,6-tris(4-pyridyl)-1,3,5-triazine (tpt) with cis-bis(bipy) Ru (II) (**Figure 34**).[65] RuCtpt was inspected for photophysical properties, showing broad emission at λ_{PL} = 577 nm at r.t., Φ_{PL} < 0.1%, lifetime τ_{PL} = 2, 790 ns, shifted towards red and intensely quenched as compared to $[Ru(bipy)_3]Cl_2$ (λ_{PL} = 613 nm, Φ_{PL} = 5%, τ_{PL} = 821 ns) whereas RuCtpt showed emission shifted towards red at 77K (λ_{PL} = 689 nm).[65] Therrien group has been explored that metal organic cage having phosphorescent ruthenium centre shows anticancer[66] biological applications and interactions with DNA.[67]

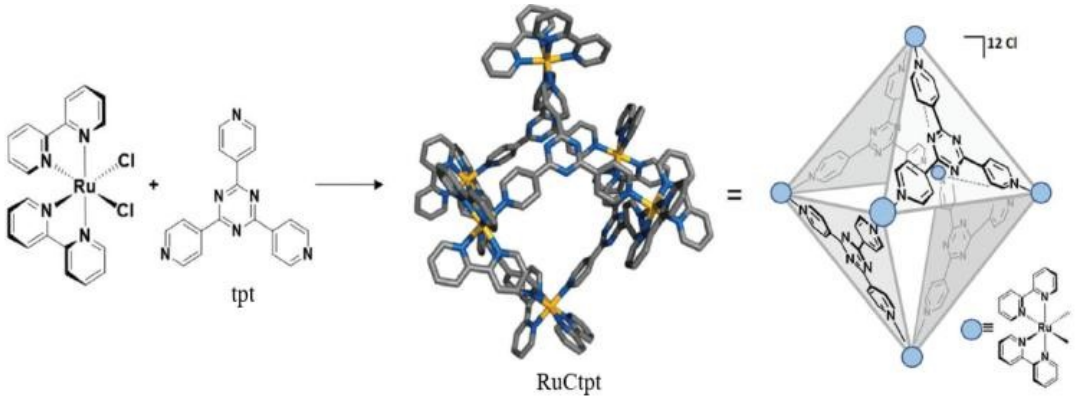

Figure 34: Reaction for RuCtpt supramolecular structure.[65]

1.7.2. Function of supramolecular structures

1.7.2.1. Catalysis

SmS have been considered as enzyme mimics because they show enzymatic activity in the same manner as enzymes in catalysis i.e., they have catalytic pockets for the selection and regulation of substrate molecules, and they have active sites to proceed catalytic reaction. The principle attention has been given to the selectivity of substrate in enzyme-mimicking catalysis. Porphyrin moieties containing SmS are commonly used as

epoxidation catalyst in catalysis. In this structure (**Figure 35 a**)[68], the molecular square, comprising Zn (II) porphyrin, stabilizes the active site of Mn (III) porphyrin, as well as regulate the substrate size. For example, the lifetime of free Mn (III) porphyrin is 10 min as compared to supramolecular structure's lifetimes that is 3 h in styrene epoxidation reaction. Additionally, these enzyme mimic structures demonstrate selectivity towards substrate's size e.g., in competitive reaction, cis-stilbene is more reactive towards supramolecular structure (catalyst) as compared to cis-3,3',5,5'-tetra(tert-butyl) stilbene because of less sterically hindered structure[69] (**Figure 35 b**).[68]

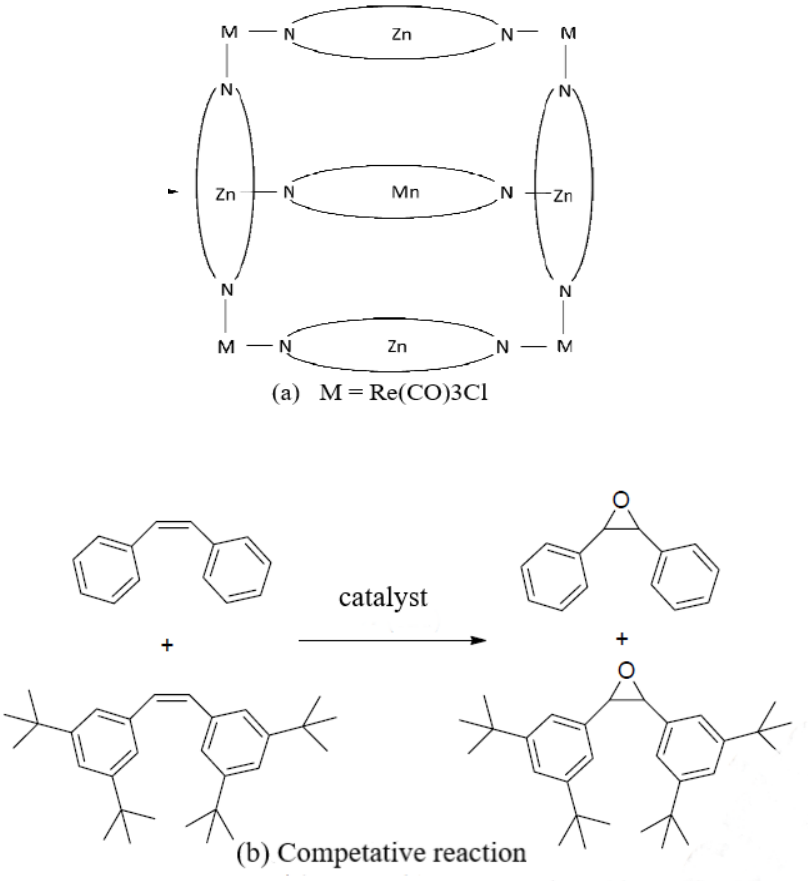

Figure 35: (a) Molecular square containing Zn (II) and Mn (III) porphyrins (b) competitive reaction showing selectivity between cis-stilbene and cis-3,3',5,5'-tetra(tert-butyl).[68]

1.7.2.2. Host-guest chemistry and molecular sensing

SmS with planar heterometallic centres have been revealed to exhibits anchoring ability due to the unsaturated metals, contributes to distinctive properties like host-guest chemistry and molecular sensing.[70]

Organometallic crown complex has been used for anion recognition by Severin group in which anion access towards the ligand L+ centre depends upon the steric effect e.g., small F- (guest) has ability to enter the crown (host) and binds with L+, although bigger anions can face steric hindrances by host (**Figure 36**)[71] and these recognitions have been detected by electrochemical and crystallographic methods.

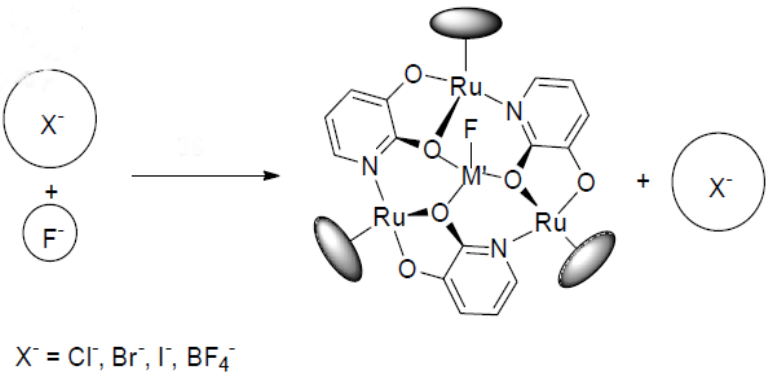

Figure 36: Small F- anion (guest) has encapsulated into crown complex.[71]

Porphyrin metal complexes show weak interactions with small molecules as compared to the cages containing porphyrin due to higher π-electron density. Therefore, porphyrin moiety in cages have been broadly studied for the guest encapsulation properties, e.g., planar polyaromatic compounds such as pyrene, coronene and peptide fragments.[69]

2. Aims of the study

From the literature survey, it is evident that ditopic ligands with *N,N*-functions (diimine) and their complexes display luminescence with interesting structure, fascinating characteristics and potential applications. These complexes have ability to self-assemble to form polymeric aggregates and supramolecular structures through intermolecular interactions (hydrogen bonding, metal-metal, C-H……M interactions etc). The synthesis and characterization of diimine ligand based on two chromophores with electronic communication, one is pyridyl-imidazole chelating moiety fused with phenanthrene and second electron donating substituents have been reported. Their photophysical properties have been studied with different electron donating substituents (anthracene derivatives).

The objective of the thesis was to design a chromophore-functionalized novel non-symmetrical ditopic ligand with *N,N*-functions (diimine) by using previous strategy in addition to ligand is capable to coordinate with different metal centres through both coordination sites. The framework of ligand based on coupling of two chromophores, one is phenanthro-imidazole-pyridine moiety that may result $\pi \rightarrow \pi^*_{phen}$ and ILCT transitions and second chromophore is phenyl-bpy motifs that is electron deficient, and these two motifs have minimized electronic communication between them. It was supposed that the presence of electron deficient motif (bpy) effect the photophysical properties of ligand and complex. The ligand is capable to coordinate with metals from pyridyl-imidazole and bpy motifs resulting in organo-metallic complexes at both sites. The ligand and its zinc complexes were synthesized and characterized by XRD crystallography, NMR spectroscopy, elemental and photophysical analysis.

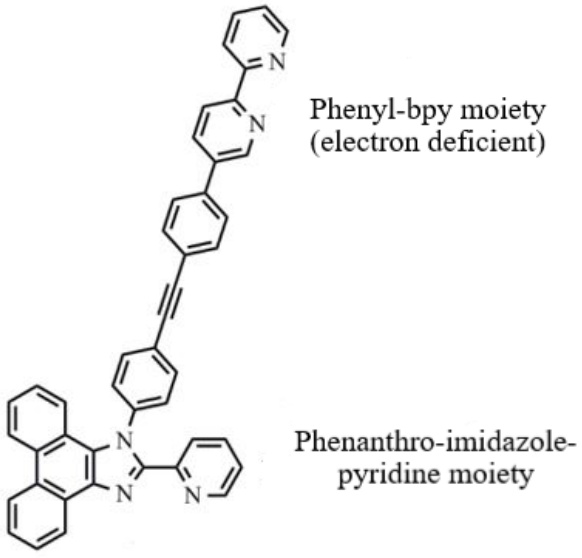

Figure 37: Design of a chromophore-functionalized novel non-symmetrical ditopic ligand with *N,N*-functions (diimine).

3. Experimental Procedures

3.1. Instrumentation

Nuclear magnetic resonance (NMR) spectra were taken on Bruker Avance-400 spectrometer. Single crystal X-ray diffraction (XRD) was recorded on Bruker Smart Apex II diffractometer and Bruker Kappa Apex II Duo diffractometer. Other photophysical investigations, UV-Vis spectra and elemental analysis were measured in analytical research laboratory of University of Eastern Finland.

3.2. Chemical reagents and solvents

The chemical reagents and solvents includes isopropyl alcohol, hydrochloric acid (HCl), sodium nitrite ($NaNO_2$), sodium bicarbonate ($NaHCO_3$), Magnesium sulphate ($MgSO_4$), sodium (Na), 4- bromoacetophenone, hydrazine hydrate (N_2H_4), pyridinecarboxaldehyde, 2,5-Norbornadiene, o-xylene ($C_6H_4(CH_3)_2$), silica gel, ammonium acetate, 9,10-phenanthrenequinone, 4-bromoaniline, 2-pyridinecarboxaldehyde, anhydrous sodium sulphate (Na_2SO_4), trimethyl-silane acetylene, triphenylphosphine (PPh_3), n-propylamine (NPAM), $pd(dba)_2$, copper (I) iodide, ammonium chloride (NH_4Cl), potassium carbonate (K_2CO_3), zinc (II) acetate, dichloromethane (DCM), ethanol (EtOH), methanol (MeOH), water (H_2O), acetic acid (AcOH), deuterated chloroform ($CDCl_3$), diethyl ether (Et_2O), dimethyl sulfoxide (DMSO), and toluene (tol) and tetrahydrofuran (THF) was purified by distillation using Na and benzophenone under inert nitrogen atmosphere.

3.3. Synthetic procedures

3.3.1. Synthesis of ditopic ligand with *N,N*-functions

Synthesis of (2*Z*)-2-(4-bromophenyl)-2-hydrazonoacetaldehyde oxime (L1) and 6-(4-bromophenyl)-3-(pyridine-2-yl)-1,2,4-triazines (L2)

2.00 g of Na was allowed to be dissolved in 35.00 mL of EtOH to make solution, 17.12 g (86.00 mmoles) of 4- bromoacetophenone was added into the solution at 10 ˚C. Further, 18.00 mL of isopropylnitrite[72] was poured into the above solution after the interval of 2 minutes, reaction mixture was left on continuous magnetic stirring for 2 h at 10-15 ˚C and, then left for overnight at room temperature(r.t.). Orange brown colored precipitates of sodium salt of iso-nitroso acetophenone was filtered by suction filtration, dried and dissolved in 35.00 mL of H_2O. To that solution, 3.60 mL of AcOH was poured to attained creamy color mixture and it was cooled on ice bath, filtered off crystals and dried them to obtain creamy color product. The product was liquify in combination of 25.00 mL of EtOH and 4.60 mL (147.30 mmoles) of hydrazine hydrate at 40-50 ˚C and was permitted

to cool down at r.t. for 1 h. 86.00 mL of H_2O was added to the mixture, creamy colored crystals were filtered and dried.[50] The obtained compound, **L1** was weighted 11.88 g (49.00 mmoles), 57 %.

Obtained amount of **L1** was liquified in 30.00 mL of EtOH, 5.26 g (49.00 mmoles) of 2-pyridinecarboxaldehyde was poured to the above solution and mixture was left on magnetic stirring for 12 h at 23 ˚C. Yellow colored product was formed, that was allowed for suction filtration and dried, then dissolved in 10.00 mL of AcOH at 90 ˚C and heated furthered for 1 h at the same temperature. The mixture was permitted to cool till r.t. and diluted with 10.00 mL of H_2O. The bright yellow precipitates were formed, that was filtered, washed with H_2O and excess EtOH and dried to obtained product.[50] The obtained compound, ligand **L2** was weighted as 5.30 g (17.00 mmoles) and percentage yield was calculated as 35 %. ^{1}H NMR (400 MHz, DMSO-d_6) δ 9.58 (s, 1H), 8.84 (d, 1H), 8.50 (d, 1H), 8.26 (d, 2H), 8.07 (t, 1H), 7.87 (d, 2H), 7.64 (t, 1H). Elemental Analysis for **L2** ($C_{14}H_9BrN_4$): Theoretical: C, 53.70; H, 2.90; N, 17.89. Experimental: C, 53.75; H, 2.95; N, 17.71.

Synthesis of 5-(4-bromophenyl)-2,2-bipyridine (L3)

3.00 g (9.60 mmoles) of **L2**, 4.90 mL (48.00 mmoles) of 2,5-Norbornadiene and 93.00 mL of o-xylene were mixed together and allowed to reflux for 24 h, after that allowed to cool till r.t. Under reduced pressure, solvent was removed to get dried residue, that was purified by column chromatography using silica gel in column and an eluent, mixture of DCM and Et_2O in 3:1 to yield pure compound. The obtained compound was recrystallized by EtOH, filtered by suction filtration, dried.[50] The obtained yellow colored ligand **L3** was weighted 2.31 g (8.00 mmoles) and percentage yield was calculated as 45 %. Elemental Analysis for **L3** ($C_{16}H_{11}BrN_2$): Theoretical: C, 61.76; H, 3.56; N, 9.00. Experimental: C, 61.72; H, 3.59; N, 8.94.

Synthesis of 1-(4-bromophenyl)-2-(pyridine-2-yl)-1*H*-phenanthro [9,10-d] imidazole (LBr)

0.93 g (12.00 mmoles) of ammonium acetate and 13.00 mL of AcOH was taken in Schlenk flask and degassed, in another Schlenk flask 1.00 g (4.80 mmoles) of 9,10-phenanthrenequinone, 2.06 g (12.00 mmoles) 4-bromoaniline, 0.51 g (4.80 mmoles) 2-pyridinecarboxaldehyde and 35.00 mL of freshly distilled toluene were added and degassed. Now, pour the ammonium acetate and AcOH mixture into another flask and the mixture was stirred at 68 ˚C for overnight under nitrogen flow. Next day, the mixture was allowed to cool down to the r.t. and solvent was evaporated. The synthesized compound was extracted by 100.00 mL of DCM, transferred to separating funnel, washed with 100.00 mL of H_2O 3 times, organic layer was collected and soaked in excess anhydrous Na_2SO_4 for 15 minutes. Filtered the solution, evaporated and residue was purified by column chromatography and DCM and Et_2O in 10:1 as eluent.[73] The yellow creamy coloured **LBr** was obtained, weighted 1.70 g (3.40 mmoles) with percentage yield 71 % and synthesized product was confirmed by NMR. ^{1}H NMR (400 MHz, Chloroform-

d) δ 8.88 (d, 1H), 8.78 (d, *J* = 8.4 Hz, 1H), 8.72 (d, *J* = 8.3 Hz, 1H), 8.37 (d, 1H), 8.22 (d, *J* = 8.1 Hz, 1H), 7.76 (t, 1H), 7.70 (d, 2H), 7.68 (t, *J* = 3.6, 2.1 Hz, 1H), 7.55 (t, 1H), 7.44 (d, 2H), 7.34 (t, *J* = 8.3, 6.9, 1.3 Hz, 1H), 7.26 (t, *J* = 8.1 Hz, 1H), 7.22 (t, *J* = 1.7 Hz, 1H), 7.20 (d, 1H). Elemental Analysis for **LBr** ($C_{26}H_{16}BrN_3$*CH_2Cl_2); Theoretical: C, 60.59; H, 3.39; N, 7.85. Experimental: C, 59.61; H, 3.60; N, 8.84.

Synthesis of 2-(pyridine-2-yl)-1-[4-((Trimethylsilyl)ethynyl) phenyl]-1*H*-phenanthro [9,10-d] imidazole (LTMS)

1.00 g (2.00 mmoles) of **LBr**, 0.55 g (5.60 mmoles) trimethyl-silane acetylene, 0.06 g (0.24 mmoles) of triphenylphosphine (PPh_3) and 15.00 mL of NPAM were taken in 100.00 mL of Schlenk flask and proceeded degasation 3 times by performing freeze thaw cycle. To the same Schlenk flask, 0.03 g (50.00 mmoles) of ($pd(dba)_2$) and 0.02 g (0.11 mmoles) of copper (I) iodide were added, and mixture was stirred under nitrogen flow for 48 h at 60 ˚C. The reaction mixture was cooled down to the r.t., product was extracted by 40.00 mL of DCM and washed by solution of 5.00 g of NH_4Cl in 50.00 mL of H_2O. Organic layer was soaked in excess of anhydrous Na_2SO_4 for 15 minutes to remove aqueous content, solution was filtered, evaporated and crude product was purified by column chromatography (eluent = DCM: MeOH 40: 1).[53]

Synthesis of 1-(4-ethynylphenyl)-2-(pyridine-2-yl)-1*H*-phenanthro [9,10-d] imidazole (LA)

Synthesized mass of **LTMS** in previous step, 15.00 mL of THF and 10.00 mL of MeOH were added in 100.00 mL of Schlenk flask under nitrogen flow and degassed by alternate vacuum and N_2 cycles. Then, 1.00 g (7.00 mmoles) of K_2CO_3 was added into the mixture, degassed again in same manner and left on magnetic stirring under N_2 flow for overnight at r.t. in the absence of sunlight. Furthered, evaporated the solvent, 30.00 mL of DCM was poured into product and washed twice with 20.00 mL of H_2O, then organic part was separated from aqueous layer and soaked in Na_2SO_4 for 15 minutes. The mixture was filtered, solvent was evaporated, and product was purified by column chromatography (eluent = DCM: MeOH: 40: 1), solvent evaporated.[53] The pure product obtained were weighted 0.41 g (2.20 mmoles) and percentage yield was calculated as 47 %. ^{1}H NMR (400 MHz, Chloroform-*d*) δ 8.98 (d, *J* = 8.0 Hz, 1H), 8.88 (d, *J* = 8.5 Hz, 1H), 8.81 (d, *J* = 8.3 Hz, 1H), 8.46 (d, 1H), 8.29 (d, 1H), 7.85 (t, 1H), 7.79 (d, 2H), 7.76 (t, *J* = 7.2 Hz, 1H), 7.64 (t, 1H), 7.62 (d, *J* = 7.9 Hz, 2H), 7.42 (t, 1H), 7.34 – 7.26 (m, 3H), 3.36 (s, 1H). Elemental Analysis for **LA** ($C_{32}H_{27}N_3O$*CH_3OH): Theoretical: C, 81.48; H, 4.95; N, 9.83. Experimental: C, 77.96; H, 4.32; N, 9.43.

Synthesis of 1-((4-([2,2'-bipyridine]-5-yl-) phenyl) ethynyl)-2-phenyl-1*H*-phenanthro [9,10-d] imidazole (LF)

LF (diimine) ligand was synthesized with the same procedure as **LTMS** except that 0.36 g (1.10 mmoles) of **L3** and 0.41 g (2.20 mmoles) of **LA** were used instead of **LBr** and trimethyl-silane acetylene. The mixture was cooled down to r.t., product was washed with MeOH and EtO_2 and purified by column chromatography (eluent = DCM: MeOH: 40: 1).[74] 0.53 g (1.30 mmoles) creamy solid was obtained and percentage yield was calculated as 70 %. ^{1}H NMR (500 MHz, Chloroform-*d*) δ 8.96 (s, 1H), 8.88 (d, 1H), 8.79 (d, 1H), 8.77 – 8.67 (m, 2H), 8.50 (d, 1H), 8.45 (d, 1H), 8.38 (d, 1H), 8.18 (d, 1H), 8.07 (d, 1H), 7.84 (t, 1H), 7.79 (d, 1H), 7.76 – 7.64 (m, 8H), 7.61 – 7.50 (m, 4H), 7.36 – 7.27 (m, 2H), 7.19 (t, 1H).Elemental Analysis for **LF** ($C_{44}H_{27}N_5$*C_2H5OH): Theoretical: C, 82.24; H, 4.95; N, 10.42. Experimental: C, 83.24; H, 4.43; N, 10.93.

3.3.2. Synthesis of complexes from ditopic ligand with *N,N*-functions

3.3.2.1. LF-(Zn $(OAc)_2)_2$ complex

20.00 mg (0.03 mmoles) of **LF** was allowed to be dissolved in 3.00 mL of DCM to make clear solution and 0.012 g (0.06 mmoles) of Zn $(OAc)_2$ was dissolved in 2.00 mL of MeOH. Then, Zn $(OAc)_2$ solution was poured into **LF** solution, resulting mixture (light yellow) showed blue emission and it was stirred for 30 minutes. The mixture was filtered with cotton wool and left for vapor diffusion Et_2O into reaction mixture to get pure yellow crystals.[74] The obtained mass was 0.009 g (0.011 mmoles) with 35% yield and needle like crystals showed bluish green emission. ^{1}H NMR (500 MHz, Chloroform-*d*) δ 9.27 (s, 1H), 9.01 (d, *J* = 5.1 Hz, 3H), 8.77 (d, *J* = 8.5 Hz, 1H), 8.69 (d, *J* = 8.5 Hz, 1H), 8.31 (d, *J* = 8.4 Hz, 1H), 8.27 (d, *J* = 8.4 Hz, 1H), 8.23 (d, *J* = 8.0 Hz, 1H), 8.13 (t, *J* = 7.8 Hz, 1H), 7.98 (s, 2H), 7.84 – 7.74 (m, 7H), 7.76 – 7.65 (m, 5H), 7.59 (t, *J* = 7.7 Hz, 1H), 7.39 – 7.27 (m, 1H), 7.11 (s, 1H), 2.05 (s, 12H). Elemental Analysis for **LF-(Zn $(OAc)_2)_2$** complex ($C_{52}H_{39}N_5O_8Zn_2$*CH_3OH): C, 62.12; H, 4.23; N, 6.83. Experimental: C, 60.90; H, 4.21; N, 6.70.

3.3.2.2. LF-Zn $(OAc)_2$ complex

Another zinc complex synthesis reaction was carried out in similar way by adding 20.00 mg (0.03 mmoles) of **LF** in 3.00 mL of DCM and 0.006 g (0.03 mmoles) of Zn $(OAc)_2$ in 2.00 mL of MeOH and followed by mixing of metal and ligand solutions. The light yellow coloured reaction mixture was kept on stirring for 30 minutes and it exhibited blue emission.[74] Then, mixture was filtered and left for vapor diffusion in MeOH/DCM solvent system to get pure crystals.

4. Results and discussion

4.1. Synthesis of ditopic/diimine ligand and it's Zinc complexes

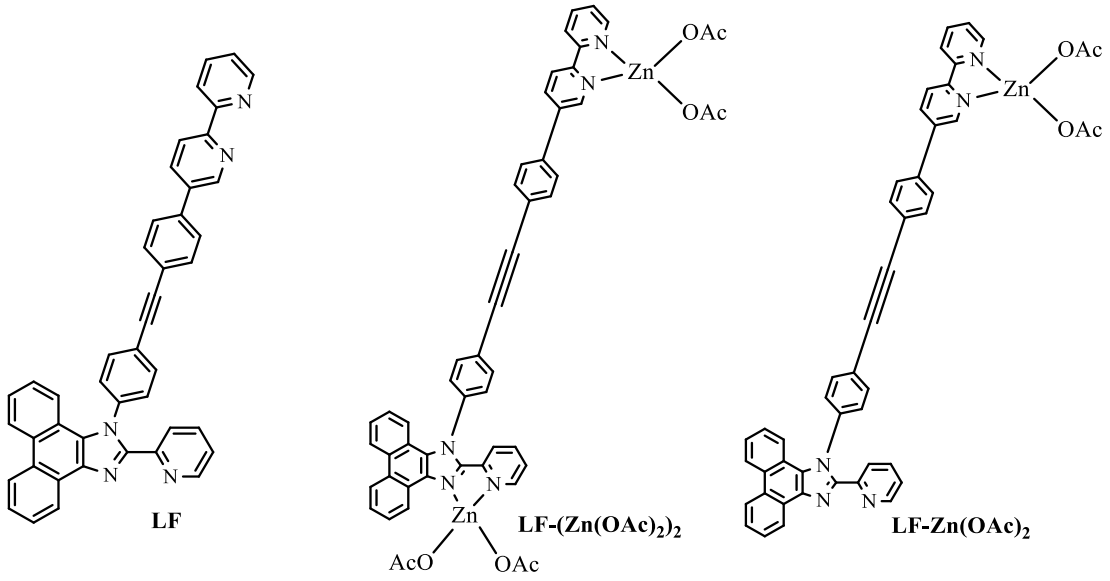

Figure 38: Novel ditopic ligand (**LF**), **LF-(Zn (OAc)2)2** and **LF-Zn (OAc)2** complexes.

4.1.1 Synthesis of ditopic/diimine ligand

For the synthesis of organometallic complexes from ditopic/diimine ligand (**LF**), a series of reactions was carried out to synthesized **L1, L2, L3, LBr, LTMS, LA** ligands to get final desired ligand **LF**.

Synthesis of L1 and L2 ligands

The synthesis of **L1** ligand (hydrazones) was carried out by alkylation reaction of 4-bromoacetophenone and isopropyl nitrite in the presence of reagents AcOH and EtOH to acquire creamy coloured crystals with 57 % yield. Then, triazines, **L2** ligand was synthesized by condensation reaction of hydrazones **L1** and 2-pyridinecarboxaldehyde under the same conditions to obtain bright yellow precipitates with 35% yield.[50] The reaction sequence for **L1** and **L2** can be depicted (**Scheme 2**)[50] and structure of both ligands was confirmed by ^{1}H-NMR.

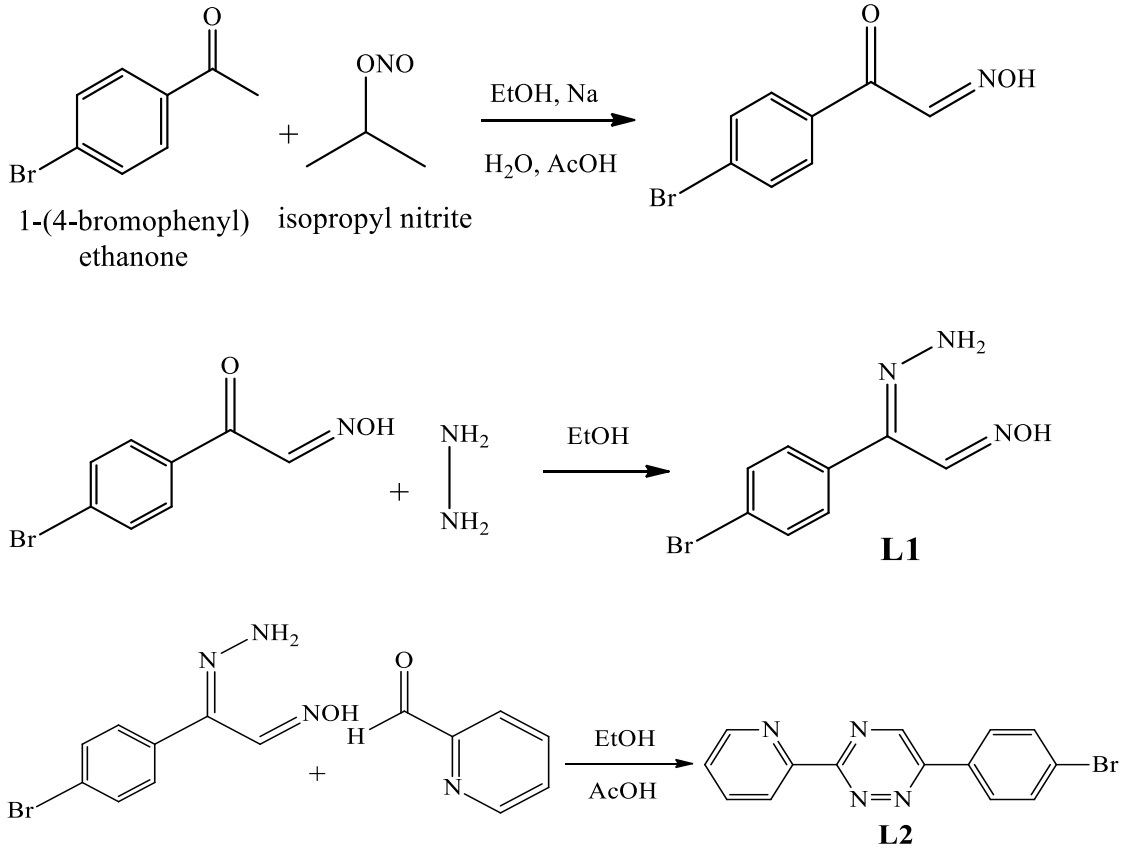

Scheme 2: Synthesis reactions for ligands **L1**, EtOH, AcOH, H_2O, Na, 40-50 ˚C, 57% and for **L2**, EtOH, AcOH, 90 ˚C, 35 %.[50]

Synthesis of L3 ligand

Cycloaddition reaction was proceeded to synthesized **L3** ligand (bipyridine) by addition of 2,5-Norbornadiene and **L2** (triazines) in the presence of o-xylene under specific conditions (**Scheme 3**).[50] The yellow coloured product was gained with 45% yield and structural analysis was supported by ^{1}H-NMR.

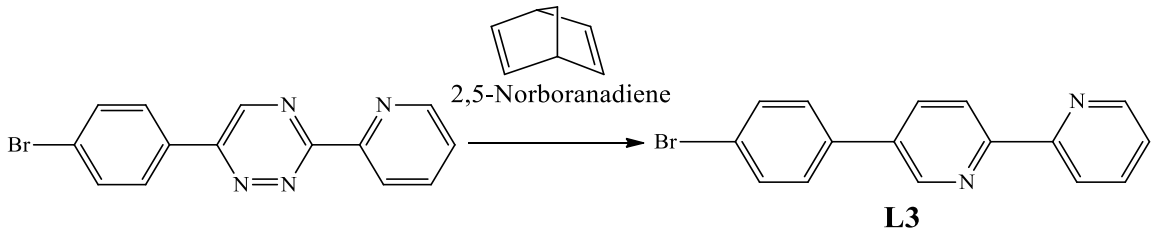

Scheme 3: Synthesis reaction of ligand **L3**, o-xylene, 25 ˚C, 24 h, 45 %.[50]

Synthesis of LBr ligand

Debus−Radziszewski condensation reaction was progressed for the synthesis of **LBr** ligand by reacting 9,10-phenanthrenequinone, 4-bromoaniline, 2-pyridinecarboxaldehyde and ammonium acetate by the addition of solvents tol. AcOH at certain conditions (**Scheme 4**).[73] The yellow creamy product **LBr** obtained with 71% yield and confirmed by ^{1}H-NMR.

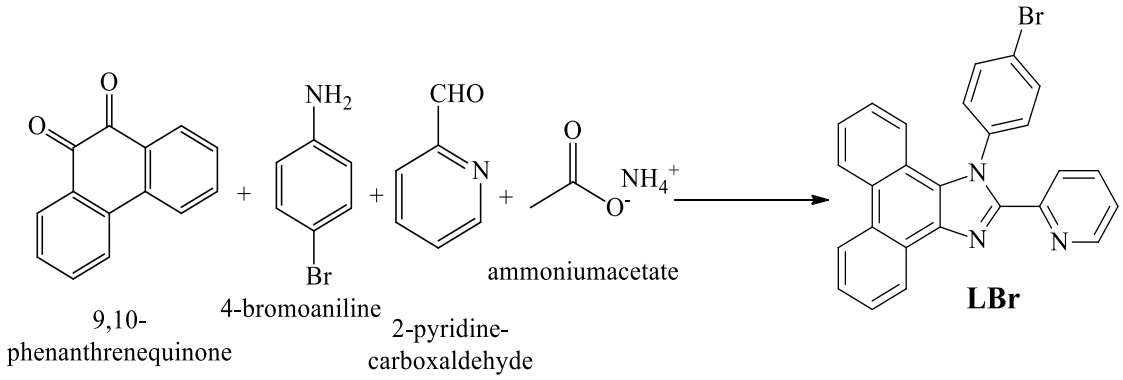

Scheme 4: Synthesis reaction of ligand **LBr**, tol, AcOH, 68 ˚C, 24 h, 71 %.[73]

Synthesis of LTMS ligand

Synthesis of **LTMS** ligand was carried by Sonogashira cross-coupling reaction.[75] The reaction was proceeded by using PPh_3, NPAM and two catalysts of palladium complex ($pd(dba)_2$) and copper (I) halide salt. Copper (I) salt act as activated specie to react with terminal alkyne (trimethyl-silane acetylene) and helps in coupling with aryl halide (**LBr**) to yield aryl acetylene (**Scheme 5**).[53] Coordination centre (imidazole) is suitable for Sonogashira cross-coupling reaction to proceed furthered synthesis of ditopic ligands because of its affinity towards metals centre to form extended frameworks.

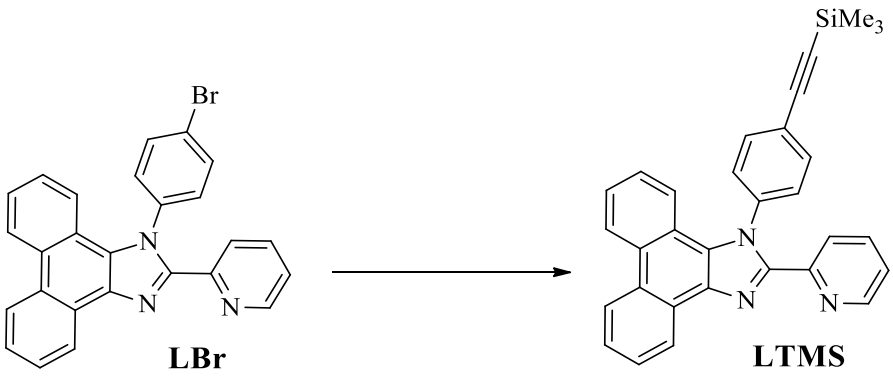

Scheme 5: Synthesis reaction of ligand **LTMS**, trimethyl-silane acetylene, NPAM, $pd(dba)_2$, CuI, PPh_3, 60 ˚C, 48 h.[53]

Synthesis of LA ligand

LA was synthesized by reaction of **LTMS** with K_2CO_3 in the presence of THF and MeOH to yield 47% product (**Scheme 6)**[53] and confirmed by ^{1}H-NMR.

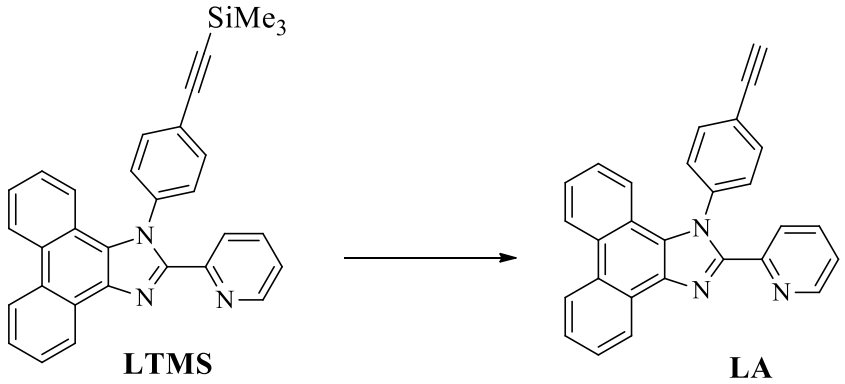

Scheme 6: Synthesis reaction of ligand **LA**, K_2CO_3, THF, MeOH, 25 ˚C, 24 h, 47 %.[53]

Synthesis of ditopic/diimine (LF) ligand

Sonogashira cross coupling reaction[75] proceeded to synthesize a chromophore-functionalized novel non-symmetrical ditopic ligand with *N,N*-functions (diimine) **LF** from **LA** and **L3** in the presence of PPh_3, NPAM, (pd $(dba)_2$) and CuI with 70% yield of creamy crystals (**Scheme 7**).[74] The structural verification was approved by ^{1}H-NMR spectroscopy and XRD crystallography.

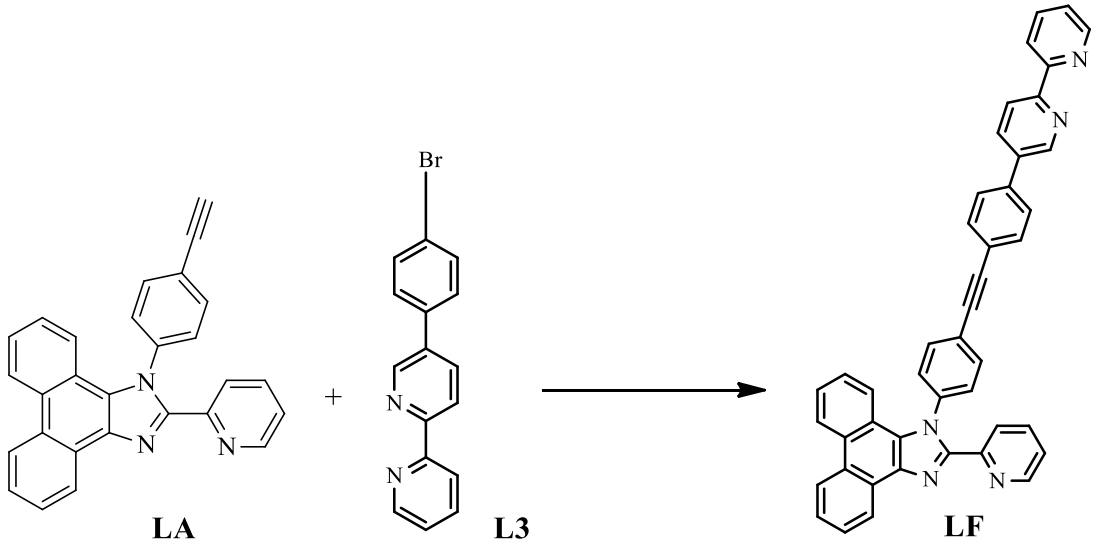

Scheme 7: Synthesis reaction of ligand **LF**, NPAM, pd$(dba)_2$, CuI, PPh_3, 60 ˚C, 48 h, 70 %.[74]

4.1.2. Synthesis of complexes from ditopic/diimine ligand (LF-Zn)

LF-(Zn (OAc)$_2$)$_2$ complexation was carried out by simple mixing of **LF** solution in DCM and Zn (OAc)$_2$ solution in MeOH in 1 to 2 ratio, allowed for stirring and left for vapour diffusion to get pure yellow crystals of complex with 70% yield **(Scheme 8)**. The structural analysis of complex was supported by ^{1}H-NMR and XRD crystallography.

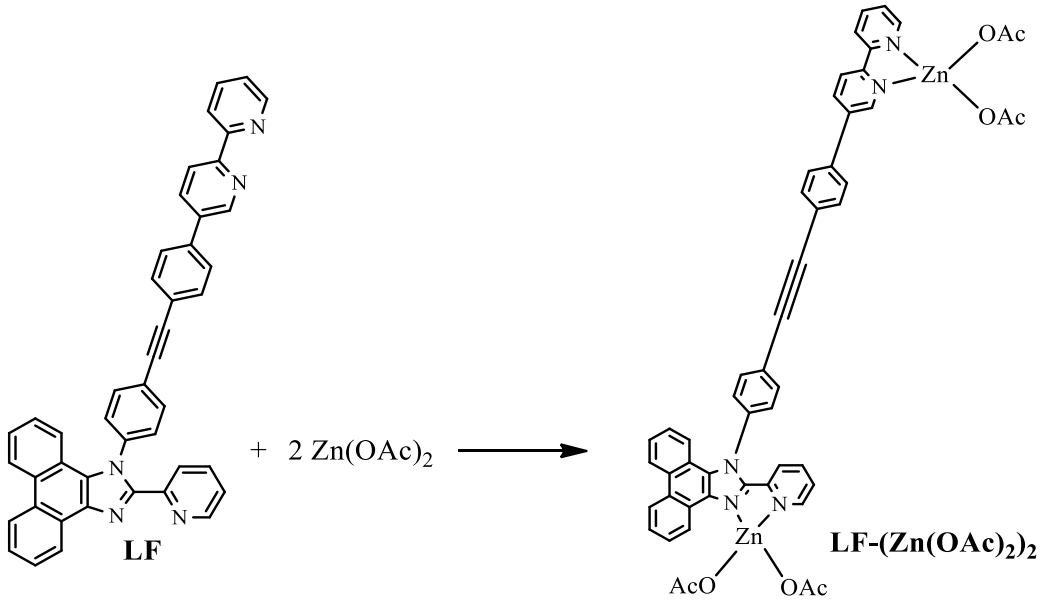

Scheme 8: Synthesis reaction for complex **LF-(Zn (OAc)$_2$)$_2$**, DCM, MeOH, 25 ˚C, 30 minutes, 75%.

LF-Zn (OAc)$_2$ complex was synthesized by mixing **LF** solution in DCM and Zn (OAc)$_2$ solution in MeOH in 1 to 1 ratio, followed by stirring and vapour diffusion in MeOH/DCM solvent system to get pure crystals **(Scheme 9)**. The structural analysis of complex was verified by XRD crystallography.

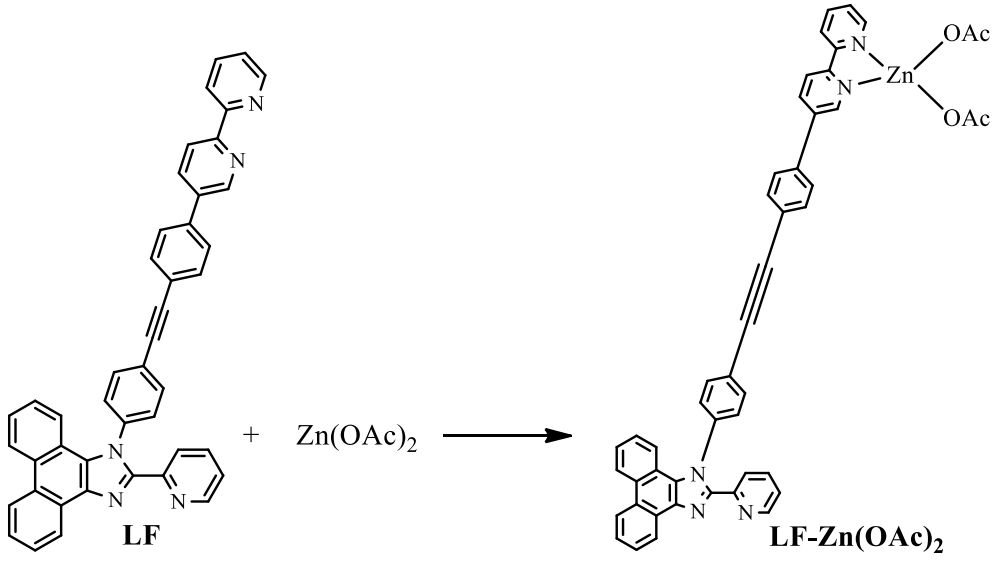

Scheme 9: Synthesis reaction for complex **LF-Zn (OAc)$_2$**, DCM, MeOH, 25 ˚C, 30 minutes.

The zinc metal is coordination at bipy moiety of ligand instead of coordinated at pyridine-imidazole fragment in case of **LF-Zn (OAc)$_2$** complex due to more feasible binding. The coordination is facile due to absence of bulky groups at adjacent position that reduce steric handiness. But in pyridyl-imidazole moiety, adjacent phenanthrene group create steric hindrances for incoming metal atom.

The complexation reaction of **LF** ligand in different stochiometric ratio was carried out with other zinc salts including, zinc (II) bromide, zinc (II) chloride, zinc (II) iodide, zinc (II) trifluoro-acetate, zinc (II) perchlorate hexahydrate and zinc (II) acetyl acetonate but didn't result in any complex formation. This anomalous behaviour of **LF** ligand might be due to large extended aromatic structure that restrict binding with metal salts and other zinc salts. Additionally, the lower solubility of this reaction mixture of this ligand with metal salts in different solvents further deters the complex formation.

4.2. Characterization and analysis

4.2.1. Nuclear magnetic resonance spectroscopy (^{1}H-NMR)

The structure of ditopic/diimine ligand **LF**, of all synthesized precursor of **LF** and of **LF-Zn (OAc)$_2$** complex was confirmed and supported by ^{1}H-NMR spectroscopy. Spectrum demonstrates number of peaks, relative integral intensity and multiplicity that describe number of protons to relevant carbon atom and nature of its surrounding environment for specific synthesized compound. The ^{1}H-NMR spectra for **L2, LBr, LA** and **LF** ligand are as follows:

Characterization of L2 by ^{1}H-NMR

The evaluation of **L2** measured spectrum demonstrates total seven peaks for triazines, py and bromophenol fragments. In bromophenol fragment, two peaks F for 2/3 at δ 7.87 ppm and D for 1/4 at δ 8.26 ppm shows integral intensity of two and are doublets due to direct attachment with one protonated carbon but F is more high fielded (H.F) due to direct bonding with Br as compared to D. Similarly, peak A for 5 (triazines) at δ 9.58 ppm and B for 9 (py) at δ 8.84 ppm with integral intensity of one are situated towards low field (L.F) due to direct attachment with N atom and are singlet and doublet due to no and one neighbouring proton respectively. Moreover, for py part, peak G for 8 (triplet) at δ 7.64 ppm, E for 7 (triplet) at δ 8.07 ppm and C for 6 (doublet) at δ 8.50 ppm moves from high to low field with one integral value (**Figure 39**). This spectral interpretation provides reliable correspondence of number of signals, relative integral intensity and multiplicity to the **L2** synthesized compound.

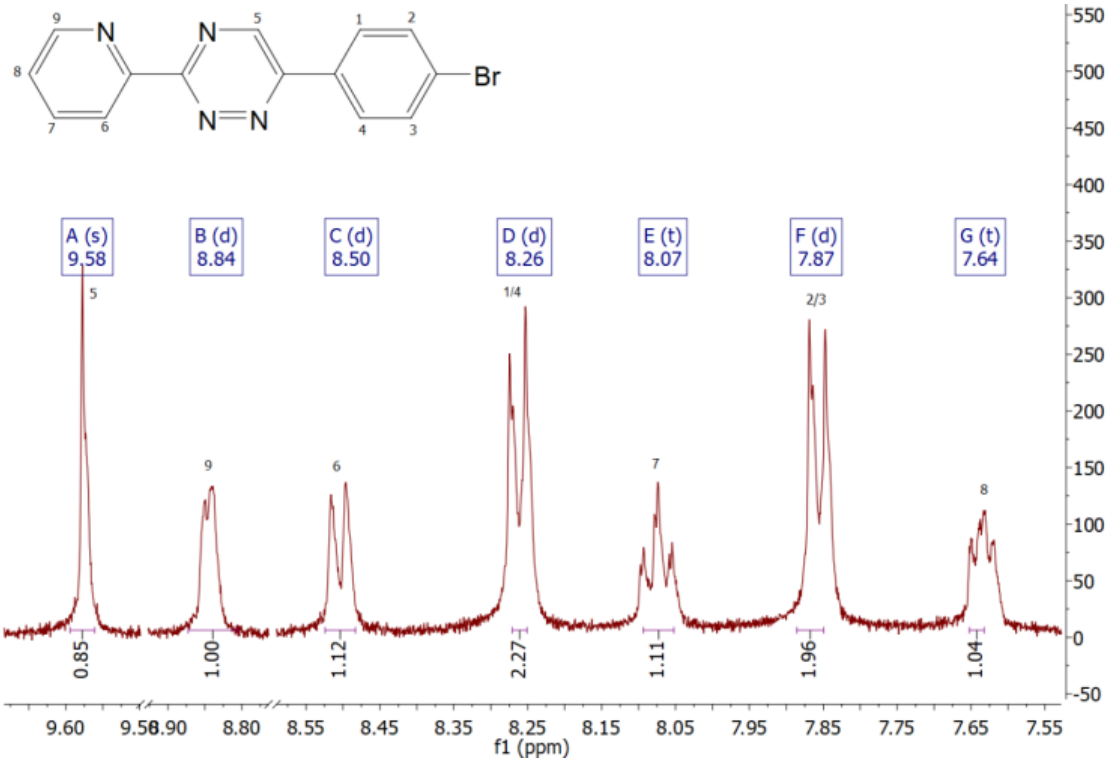

Figure 39: [1]H-NMR spectrum of ligand **L2**, DMSO, 298 K.

Characterization of LBr by [1]H-NMR

Analysis of measured [1]H-NMR spectrum for **LBr** represents cumulatively fourteen peaks for phenanthrene, imidazole, bromophenol and py parts. For phen fragment, peak A for 12 at δ 8.88 ppm, B for 13 at δ 8.78 ppm and C for 16 at δ 8.72 ppm with integral intensity of one are towards L.F region and show multiplicity of doublets due to the presence of one proton at their respective adjacent position. While, H for 15 at δ 7.68 ppm (triplet), I for 14 at δ 7.55 ppm (triplet), K for 10 at δ 7.34 ppm (triplet), L for 11 at δ 7.26 ppm (triplet) and N for 9 at δ 7.20 ppm (doublet) with integral intensity of one situated towards H.F region and somehow overlapped. In py fragment, peak D for 1 at δ 8.37 ppm and E for 4 at δ 8.22 ppm with integral intensity of one are found to be doublets due to the presence of one proton at adjacent carbon and situated towards L.F due to in vicinity of imidazole ring. While, signal F for 3 at δ 7.76 ppm (triplet) and M for 2 at δ 7.22 ppm (triplet) with integral intensity of one move towards H.F region. Moreover, in bromophenol part, peak G for 6/7 at δ 7.76 ppm and J for 5/8 at δ 7.44 ppm with integral intensity of two are doublet due to neighbouring one proton, and J is towards more H.F region due to the attachment with Br group (**Figure 40**). In short, number of the signals, integral intensity and multiplicity correspond well with the stoichiometry of the synthesized compound.

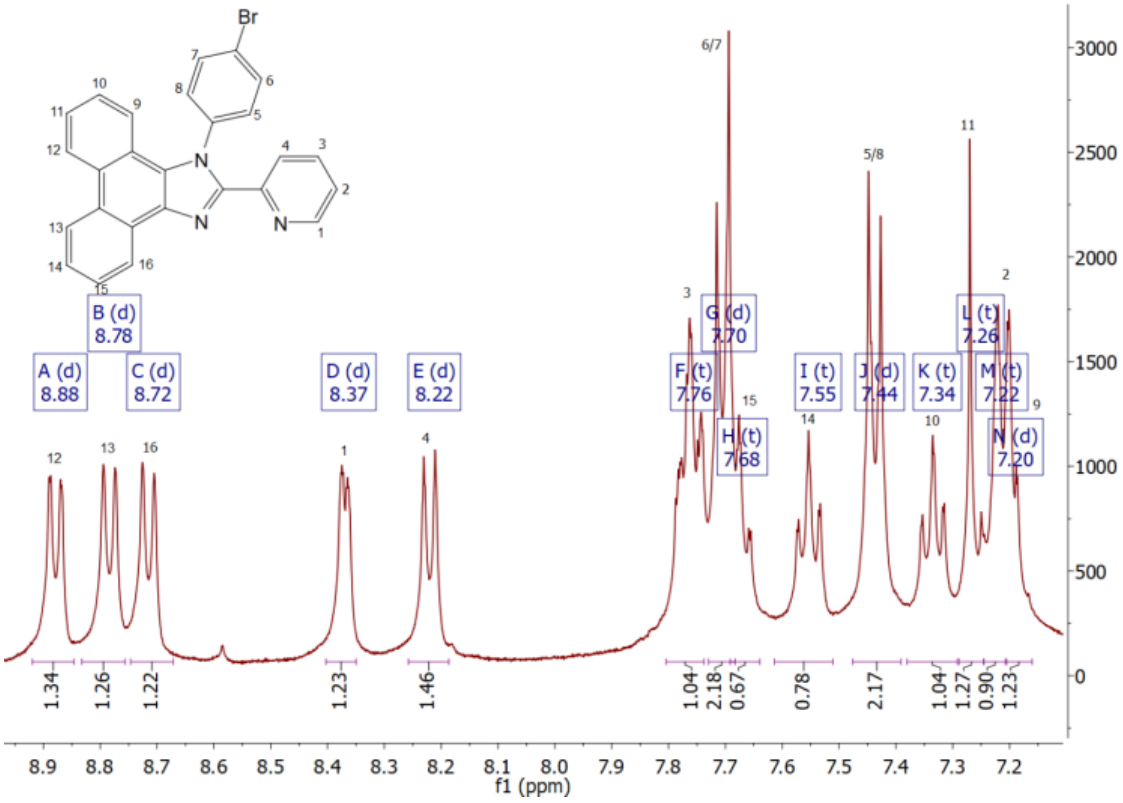

Figure 40: ^{1}H-NMR spectrum of ligand **LBr**, $CDCl_3$, 298 K.

Characterization of LA by ^{1}H-NMR

^{1}H-NMR spectrum of **LA** depicts major five parts of this ligand, phenanthrene, imidazole, py, phenyl, acetylene and shows total thirteen number of signals. Additionally, spectra show one signals M for acetylene fragment denoted proton number 17 at δ 3.36 ppm with integral intensity of one and shows multiplicity of singlet due to absence of any neighbouring proton and one more signal for $CDCl_3$ solvent. All signals are almost like **LBr** spectra except overleaped signal L at δ 7.30 ppm (multiplet) that represents proton numbers 9, 11, 12 with integral intensity of three. There is slight increment in chemical sift values for all peaks of **LA** as compared to **LBr** due to the presence of acetylene group instead of bromo group. Moreover, signal G for 5/8 at δ 7.79 ppm appear towards more L.F region as compared to signal J for 6/7 at δ 7.62 ppm due to the presence of acetylene group (**Figure 41**). This spectral analysis confirmed the structure of synthesized compound.

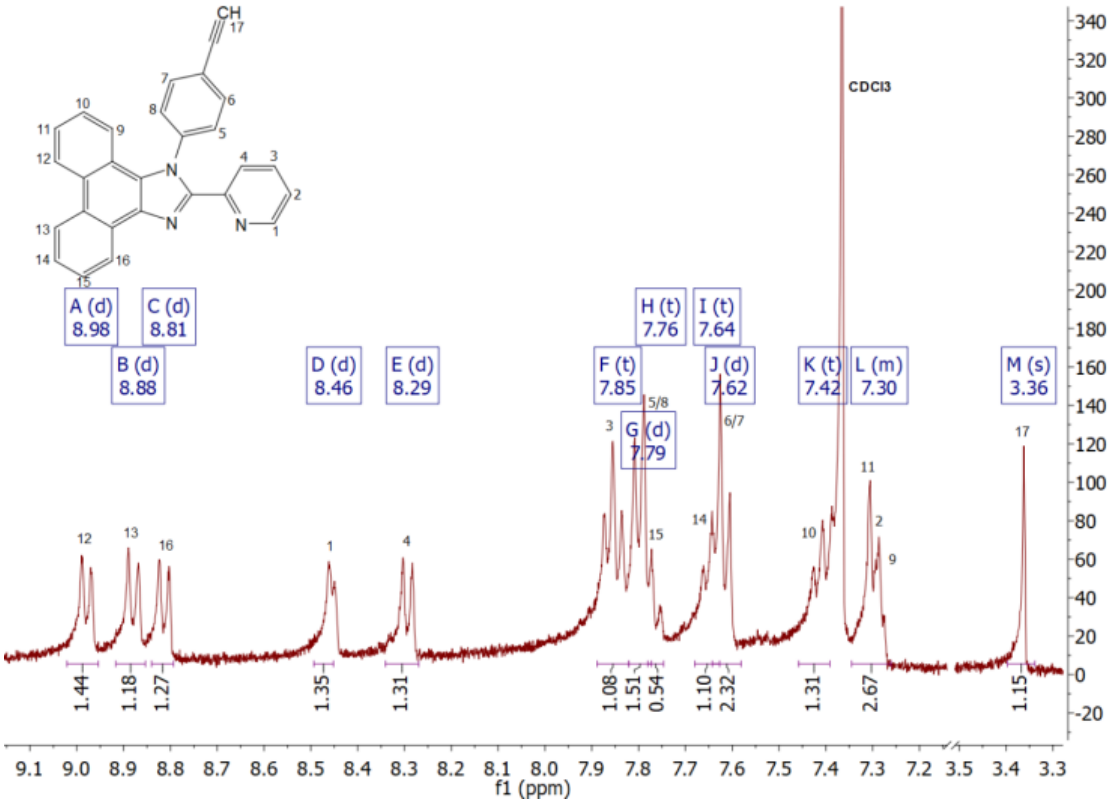

Figure 41: ^{1}H-NMR spectrum of ligand **LA**, $CDCl_3$, 298 K.

4.2.1.1. Characterization of LF by ^{1}H-NMR

Spectral interpretation of experimental data of **LF** demonstrates several distinct and overlapped peaks, and an additional solvent ($CDCl_3$) peak. This final ligand consists two functional motifs **L3** and **LA** containing phenyl, bipyridine and phenanthrene, imidazole, pyridine, acetylene fragments. For phen fragment, signals B for 12 at δ 8.88 ppm, C for 13 at δ 8.79 ppm and G for 16 at δ 8.38 ppm shows doublets due to one protonated carbon at respective adjacent position with integral intensity of one and moves slightly towards H.F region as compared to **LA** spectra. Whereas, signals H for 9 at δ 8.18 ppm, J for 15 at δ 7.84 ppm with integral value of one show doublet and triplet peaks, and L is overlapped peak for 10, 11/14 at δ 7.71 ppm (multiplet) with integral value of one and two respectively. These all signals show slight difference in chemical shift values as compared to **LA**. For py fragment, signal D for 1 at δ 8.71 ppm, N for 2 at δ 7.31 ppm, K for 4 at δ 7.79 ppm and L for 3 at δ 7.71 ppm with integral intensity of one are found to be overlapped peaks.

Moreover, in phenol part overlapped peaks L for 5/8 at δ 7.71 ppm and M for 6/7 at δ 7.56 ppm with integral intensity of two are is towards more H.F region due to the presence of **L3** group at acetylene. For **L3** motif, protons of phenol appear as overlapped signals L for 17/20 and M for 18/19 with integral intensity of two are is towards H.F region. For bpy part, signal A for 21 at δ 8.96 ppm (singlet due to absence of neighbouring protons) and E for 24 at δ 8.50 (doublet) with integral intensity of one situated at L.F region due

to the direct attachment with N -atom. Signal D for 22 at δ 8.71 ppm (multiplet), I for 23 at δ 8.07 ppm (doublet), F for 27 at δ 8.45 ppm (doublet), N for 26 at δ 7.31 ppm (multiplet) and O for 25 at δ 7.19 ppm (triplet) with integral intensity of one are assigned for bpy protons (**Figure 42**). Although all evaluated data corresponds to the stoichiometry of synthesized compound.

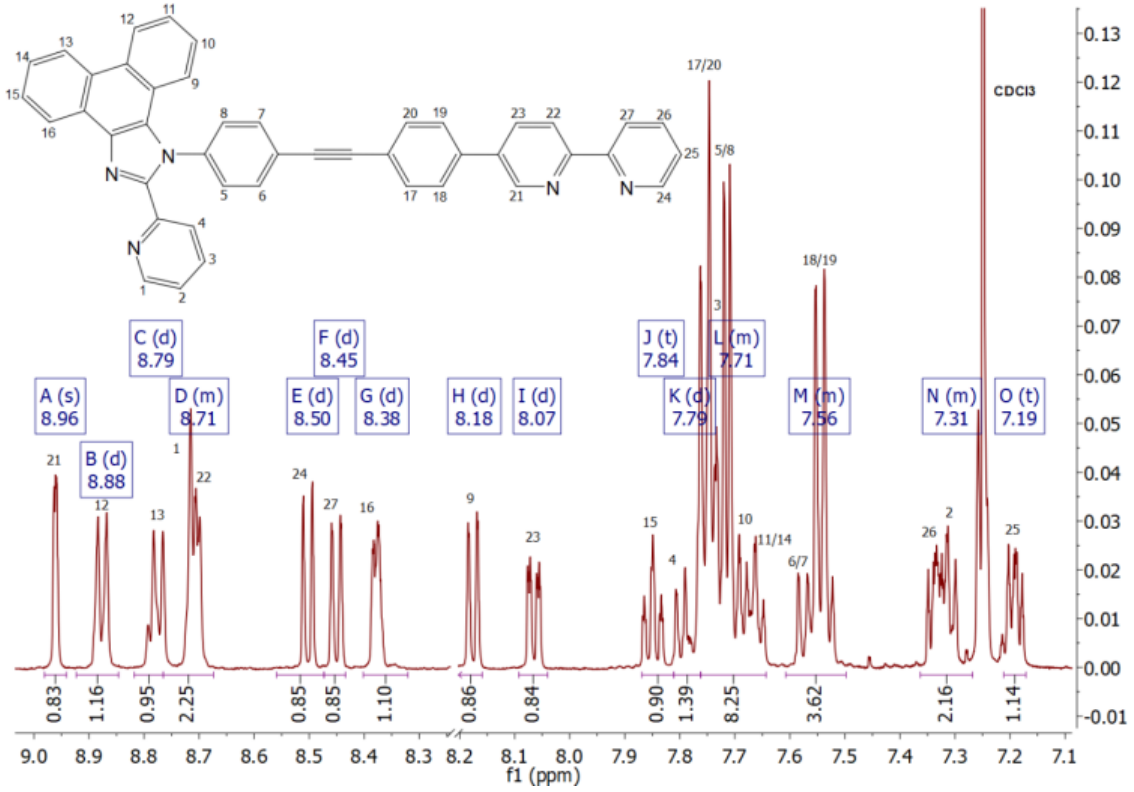

Figure 42: ^{1}H-NMR spectrum of ligand **LF**, $CDCl_3$, 298 K.

4.2.1.2. Characterization of complex LF-(Zn (OAc)$_2$)$_2$ by ^{1}H-NMR

Spectral analysis of experimental data for **LF-(Zn (OAc)$_2$)$_2$** complex shows eleven peaks. Complexation of **LF** with Zn^{+2} metal represents metal impact on spectroscopic measurements. It can be seen clearly from spectral data of **LF** and **LF-(Zn (OAc)$_2$)$_2$** complex (**Figure 43**) that peaks at δ 8.50 ppm, δ 8.71 ppm and δ 8.96 ppm in ligand spectra shifted to at δ 8.69 ppm, δ 8.77 ppm and δ 9.27 ppm respectively in complex spectra. The chemical shift value of protons adjacent to nitrogen at both coordination centres, i.e, pyridyl-imidazole and bpy fragments moves significantly towards lower field region upon ligand complexation. It indicates that metal binds at both coordination sites of ligands.

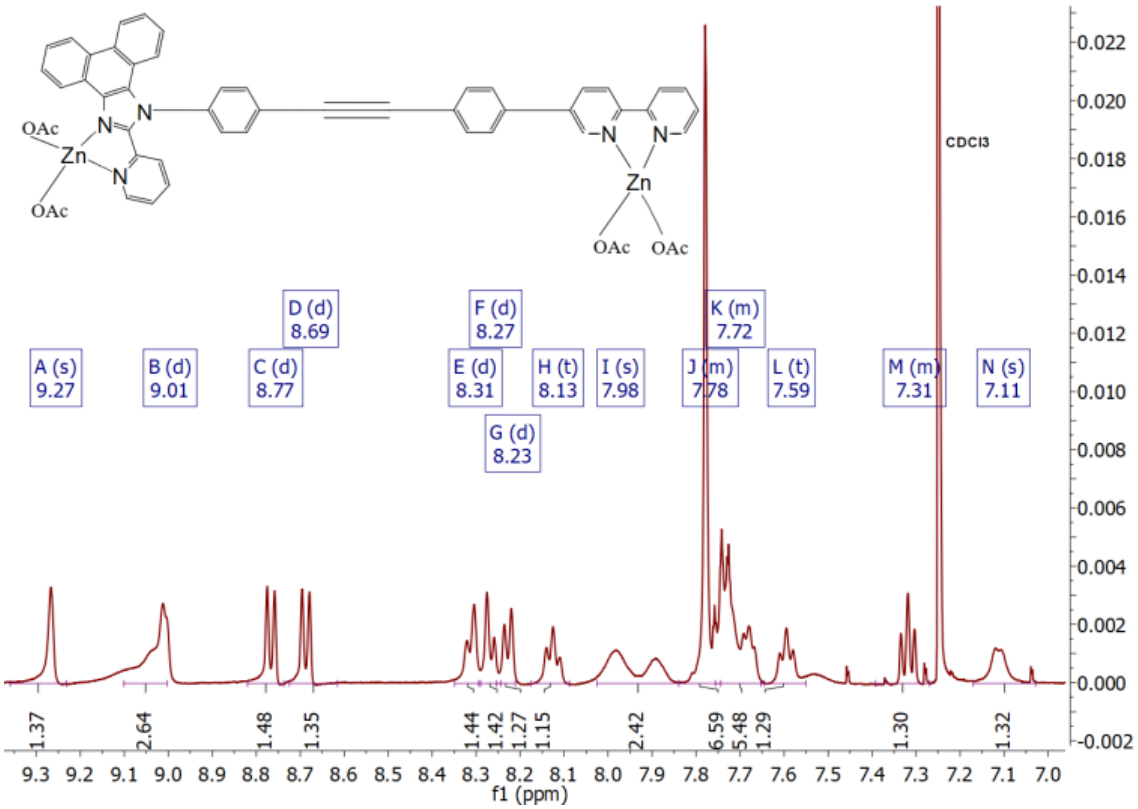

Figure 43: ^{1}H-NMR spectrum of **LF-(Zn (OAc)$_2$)$_2$** complex, $CDCl_3$, 298 K.

4.2.2. Single crystal X-ray diffraction (XRD)

The proposed structures of ditopic/diimine ligand **LF** and it's zn-complexes were confirmed by single crystal X-ray diffraction study. Crystallographic data for ligand and complexes is illustrated in (**Table 1**) that represents **LF** and **LF-(Zn (OAc)$_2$)$_2$** have triclinic crystal systems whereas **LF-Zn (OAc)$_2$**, has monoclinic crystal system with their characteristics cell lengths, cell angles and cell volumes. According to XRD studies of ligand and complexes, phenanthro-imidazole fragment is planner and almost perpendicular to the py ring that restrict the conjugation between the polyaromatic rings in chromophore ligand. The molecular structure of **LF** is asymmetric containing phenanthro-imidazole, py and phenolic fragments on one side of acetylene and bipy fragments on other side (**Figure 44**).

Table 1: Crystallographic data for **LF**, **LF-Zn (OAc)$_2$**, and **LF-(Zn (OAc)$_2$)$_2$**.

Parameters	**Ligand LF**	**LF-Zn (OAc)$_2$,**	**LF-(Zn (OAc)$_2$)$_2$**
Chemical formula	$C_{44}H_{27}N_5$	$C_{48}H_{33}N_5O_4Zn$	$C_{52}H_{39}N_5O_8Zn_2$
Molecular weight	625.72	809.19	992.65
Temperature	298 K	298 K	298 K
Crystal system	Triclinic	Monoclinic	Triclinic
Space group	P -1	P 2_1/c	P -1
Cell length (a/Å)	10.1067(4)	18.68(3)	8.2982(5)
Cell length (b/Å)	13.4684(6)	15.72(3)	15.1652(9)
Cell length (c/Å)	13.6739(6)	14.44(3)	22.6958(13)
Cell angle ($\alpha/^0$)	110.327(2)	90	105.219(2)
Cell angle ($\beta/^0$)	109.394(2)	97.79(3)	90.326(2)
Cell angle ($\gamma/^0$)	100.503(2)	90	97.703(2)
Cell volume (Å3)	1550.35	4202.09	2728.6

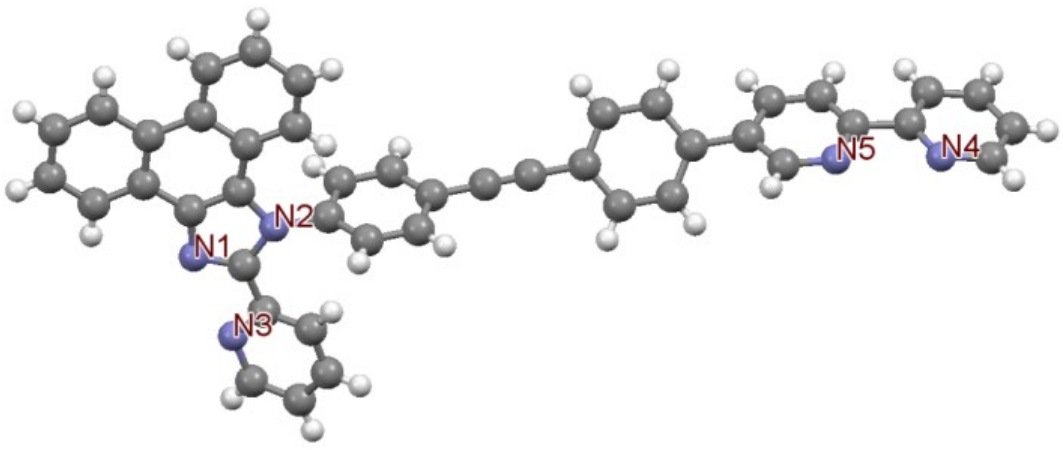

Figure 44: Molecular structure of **LF** ligand.

Luminescent properties of ligand and its ability to construct supramolecular organometallic structures depends upon molecular packing patterns including π···π stacking between aromatic rings and intermolecular interactions of ligand molecule. The intermolecular distance of acetylene with py fragment (aromatic ring) and ph fragment of adjacent **LF** molecule is measured 2.811 Å and 2.789 Å (**Figure 45**). Additionally, hydrogen bonding N···H distance between nitrogen of imidazole and hydrogen of phenyl group is observed as 2.581 Å and 2.712, and π···π stacking distance between aromatic rings of same fragment of adjacent molecules varies from 2.744 Å to 3.395 Å (**Figure 46**), and these values are comparable with literature.[76,77]

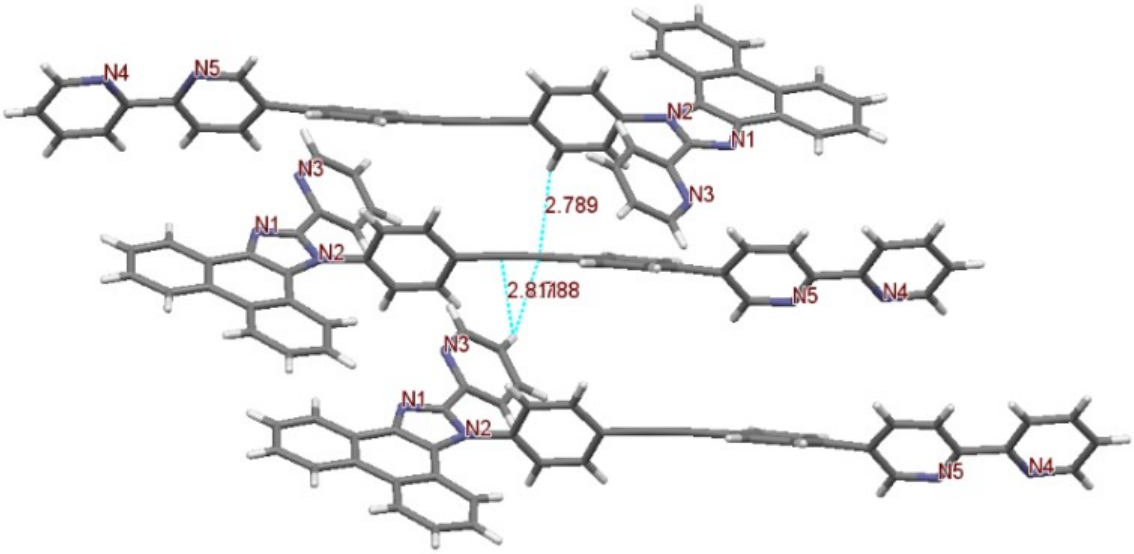

Figure 45: Molecular packing patterns of **LF**.

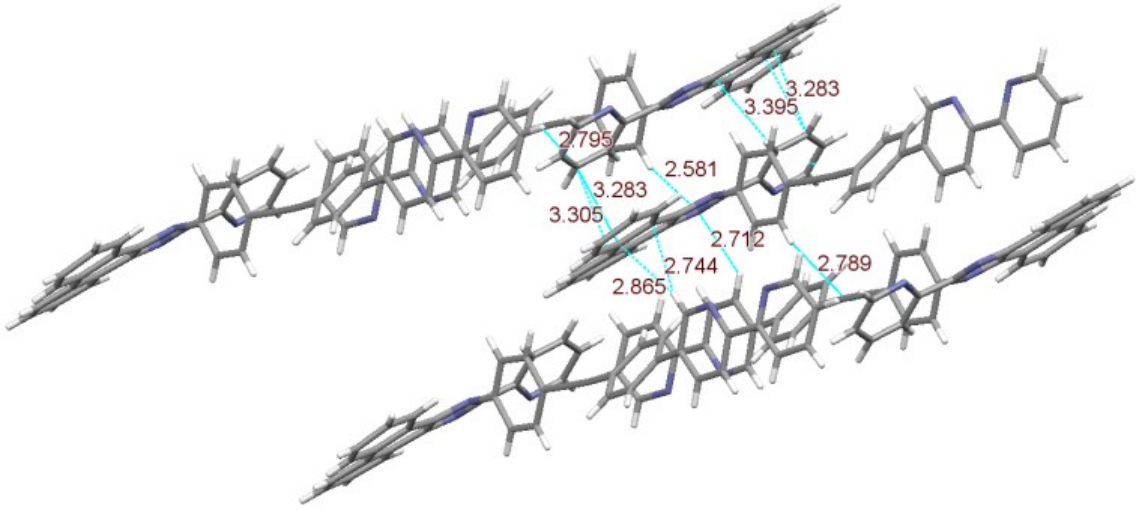

Figure 46: Hydrogen bonding N···H and π···π stacking patterns of **LF**.

LF upon complexation with zinc acetate yields needle like crystals of **LF-Zn**, zinc metal can coordinate at two different sites of ditopic ligand, either at pyridyl-imidazole or bpy fragments or at both. Two types of molecular structures, **LF-Zn $(OAc)_2$**, and **LF-$(Zn(OAc)_2)_2$** were obtained due to variable molar ratios of ligand and complex. In **LF-Zn $(OAc)_2$**, zinc metal atom coordinated at bpy fragment while in **LF-$(Zn(OAc)_2)_2$**, metal atom is coordinated at both bpy and pyridyl-imidazole fragments (**Figure 47, 48**). The coordination of diimine ligand to zinc metal through the pyridyl-imidazole fragment create steric hindrance between acetate group of metal and nearby H−C group of phenanthrene that leads to produce distortion in tetrahedral geometry.

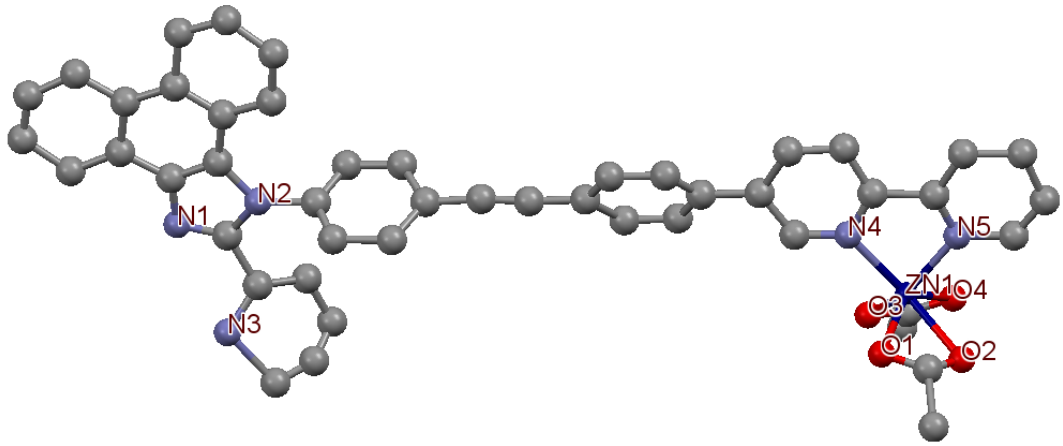

Figure 47: Molecular structure of **LF-Zn $(OAc)_2$.**

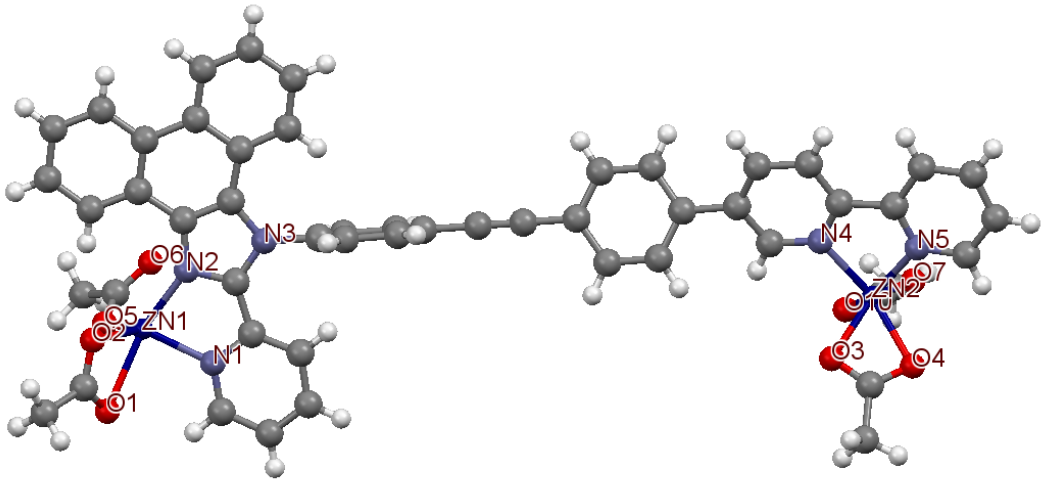

Figure 48: Molecular structure of **LF-$(Zn(OAc)_2)_2$.**

The characteristic parameters including bond distance and angle along metal for both complexes are recorded (**Table 2, 3**). The bond distances of Zn-N for bpy and pyridal-imidazole motifs were found to be comparable with reported zinc complexes. Zn-N bond distances for bpy fragment in both complexes were found to be almost similar to the reported example, i.e., 6-(2-Methoxyphenyl)-2,2-bipyridinezinc dichloride complex.[78]

Similarly, bond distances of Zn-N for pyridal-imidazole motif were found to be almost similar to the reported zinc complexes, e.g., 3- phenyl-1-(pyridin-2-yl)-1H-pyrazol-5-aminezincdichloride[79],1-(4-(anthracen-9-yl-ethynyl)phenyl)-2-(pyridin-2-yl)-1*H*-phenanthro[9,10-*d*]imidazole zinc dichloride and zinc diiodide, and 9,10-bis((4-(2-(pyridin-2-yl)-1*H*-phenanthro[9,10-*d*]imidazol-1-yl)phenyl)ethynyl) anthracene zinc diacetate.[74] It can be seen from table that intermolecular interactions of metal are much stronger in **LF-(Zn (OAc)$_2$)$_2$** as compared to **LF-Zn (OAc)$_2$,** due to shorter bond distance between metal and neighbouring atoms. This can be influenced by the addition of another zin acetate group to pyridyl-imidazole fragment and due to different coordination modes.

Table 2: Selected bond distances and angles in **LF-Zn (OAc)$_2$**.

Distance (Å)	**LF-Zn (OAc)$_2$**	**Angle °**	**LF-Zn (OAc)$_2$**
Zn1-N4	2.158	N4-Zn1-N5	79.01
Zn1-N5	2.055	N4-Zn1-O1	92.58
Zn1-O1	2.153	N4-Zn1-O2	141.24
Zn1-O2	2.238	N4-Zn1-O3	99.20
Zn1-O3	2.051	N4-Zn1-O4	58.86
Zn1-O4	2.308	N5-Zn1-O1	112.93
		N5-Zn1-O2	90.30
		N5-Zn1-O3	142.27
		N5-Zn1-O4	93.90
		O1-Zn1-O2	57.39
		O1-Zn1-O3	104.79
		O1-Zn1-O4	132.94
		O2-Zn1-O3	111.16
		O2-Zn1-O4	86.01

Table 3: Selected bond distances and angles in **LF-(Zn (OAc)$_2$)$_2$**.

Distance (Å)	**LF-(Zn (OAc)$_2$)$_2$**	**Angle °**	**LF-(Zn (OAc)$_2$)$_2$**
Zn1-N1	2.0574	N1-Zn1-N2	80.07
Zn1-N2	2.0643	N1-Zn1-O1	88.05
Zn1-O1	2.3871	N1-Zn1-O2	123.40
Zn1-O2	2.0140	N1-Zn1-O5	118.61
Zn1-O5	1.9255	N2-Zn1-O1	147.88
Zn2-N4	2.0860	N2-Zn1-O2	103.24
Zn2-N5	2.0677	N2-Zn1-O5	121.73
Zn2-O3	2.0696	O1-Zn1-O2	59.31
Zn2-O4	2.1666	O1-Zn1-O5	90.17
Zn2-O7	2.1594	O2-Zn1-O5	107.22
Zn2-O10	2.3471	N4-Zn2-N5	78.10
		N4-Zn2-O3	97.01
		N4-Zn2-O4	148.66
		N4-Zn2-O7	115.84
		N4-Zn2-O10	99.67
		N5-Zn2-O3	128.35
		N5-Zn2-O4	97.68
		N5-Zn2-O7	93.06
		N5-Zn2-O10	140.70
		O3-Zn2-O4	61.03
		O3-Zn2-O7	132.43
		O3-Zn2-O10	90.95
		O4-Zn2-O7	95.29
		O4-Zn2-O10	102.57
		O7-Zn2-O10	52.08

Shorts contacts for both complexes illustrated (**Figure 49, 50**). In **LF-Zn (OAc)$_2$**, phenanthrene and carbon atom of zinc acetate fragments make intermolecular interactions with carbon atom of bpy rings of adjacent ligand molecules that characterise by bond distance of 3.370 Å and 3.394 Å respectively. While, in **LF-(Zn (OAc)$_2$)$_2$**, the distance between acetylene and ph fragments increases to 2.837 Å due to metal binding. π···π stacking between aromatic rings of phenanthrene and ph exists with characteristics distance of 3.248 Å. Moreover, oxygen atoms of zinc acetate fragments make intermolecular interactions with hydrogen atom of bpy and ph of adjacent ligand molecules with bond lengths of 2.591 Å, 2.499 Å, 2.522 Å and 2.422 Å respectively (**Figure 51**). Aromatic fragments are arranged in antiparallel pattern in both complexes.

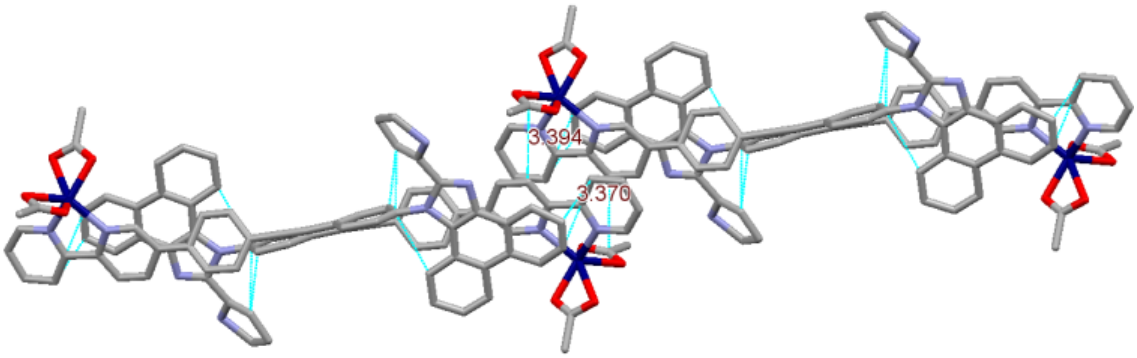

Figure 49: Molecular packing patterns of **LF-Zn (OAc)$_2$**.

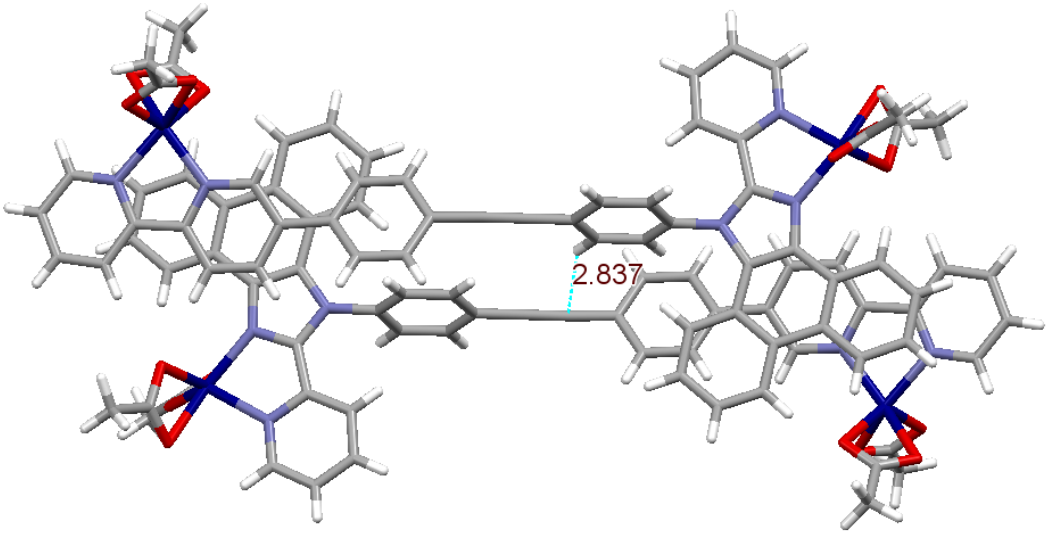

Figure 50: Molecular packing patterns of **LF-(Zn (OAc)$_2$)$_2$.**

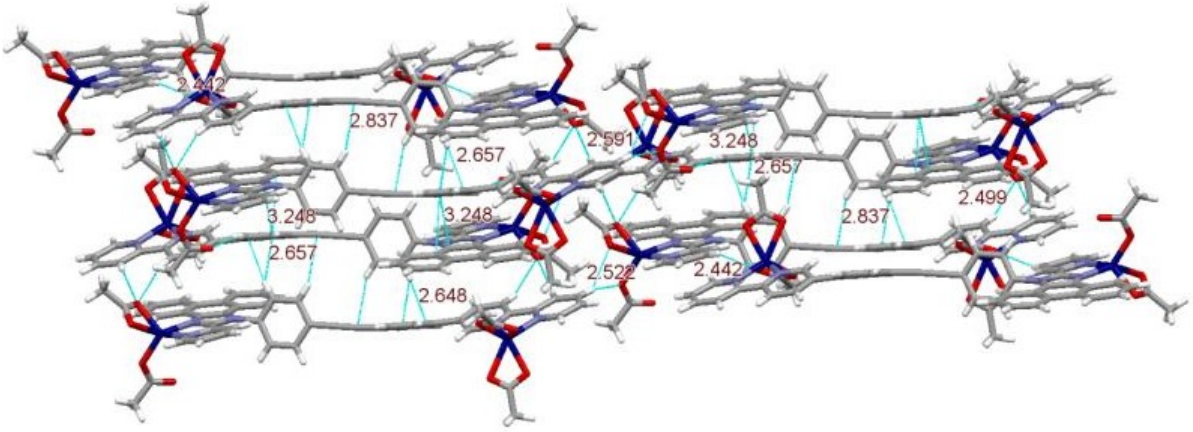

Figure 51: Hydrogen bonding O···H and π···π stacking patterns of **LF-(Zn (OAc)$_2$)$_2$**.

4.2.3. Photophysical properties

Photophysical measurements were performed for ditopic/diimine ligand containing two chromophore moieties and its zinc complexes in solution form and recorded (**Table 4**). Two different concentrations of ligand and complex solutions in DCM were taken to measure absorption spectra. These concentrations for **LF** (a) 2.66×10^{-5} mole L^{-1}, (b) 1.07×10^{-5} mole L^{-1}, and for its zinc complex **LF-(Zn (OAc)$_2$)$_2$** (a) 3.36×10^{-5} mole L^{-1}, (b) 1.68×10^{-5} mole L^{-1}.

Table 4: Photophysical data of **LF** and zinc complex.

Samples	**λ_{abs} wavelength (nm) for maximum absorption**	**$\varepsilon \times 10^4$ (L mol^{-1}cm^{-1})**
LF	262 (P1)	11.95
	325 (P2)	12.69
	364 (sh)	3.49
LF-(Zn (OAc)$_2$)$_2$	261 (P1)	7.95
	335 (P2)	7.79
	362 (sh)	5.15

The maximum absorption intensity (λ_{ab}) of **LF** is observed on wavelength 262 nm, 325 nm, 364 (sh) with molar absorptivity/molar extinction coefficient 11.95×10^4 L mol^{-1}cm^{-1}, 12.69×10^4 L mol^{-1}cm^{-1} and 3.49×10^4 L mol^{-1}cm^{-1} respectively. Similarly, maximum intensity λ_{ab} for **LF-(Zn (OAc)$_2$)$_2$** complex is found to be on wavelength 261 nm, 335 nm, 362 (sh) with molar absorptivity 7.95×10^4 L mol^{-1}cm^{-1}, 7.79×10^4 L mol^{-1}cm^{-1} and 5.15×10^4 L mol^{-1}cm^{-1} respectively (**Figure 52**). The photophysical data of ligand, **LF** and complex is compared with literature example of diimine ligand containing two chromophores, phenanthrol-imidazole-pyridine moiety and electron donating moeity. It illustrates absorption bands at 363 and 490 nm for LC due to phenanthrene-localized $\pi \rightarrow \pi^*_{phen}$ transition and ILCT due to phenanthrene → pyridyl charge transfer. Synthesized novel ditopic ligand also has two chromophores, phenanthrol-imidazole-pyridine motif and electron deficient bpy moiety. Thus, same absorption bands occur for phenanthrene-localized $\pi \rightarrow \pi^*_{phen}$ (LC) and phenanthrene → pyridyl charge transfer (ILCT) but comparatively at lower wavelength (262 and 325 nm) due to presence of electron deficient fragment (bpy) that increases energy gap between HOMO LUMO orbitals resulting decrease in absorption wavelength.

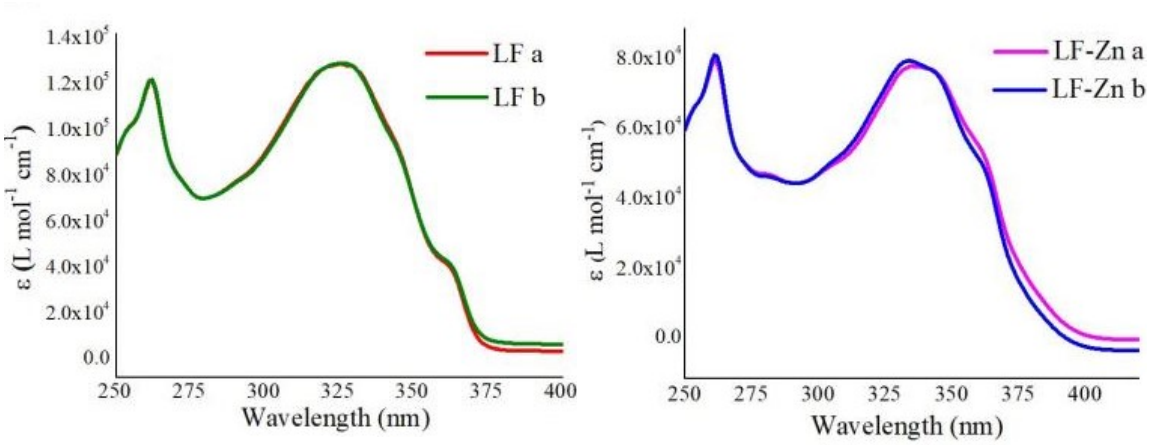

Figure 52: Absorption spectra of different concentrations of **LF** (a) 2.66 $\times 10^{-5}$ moleL^{-1}, (b) 1.07 $\times 10^{-5}$ mole L^{-1} and its zinc complex **LF-(Zn (OAc)$_2$)$_2$** (a) 3.36$\times 10^{-5}$ mole L^{-1}, (b) 1.68$\times 10^{-5}$ mole L^{-1} in DCM, 298 K.

The absorption spectra were normalized for ligand and complex solutions. Then, ligand and complex normalized spectra were merged to monitor change in spectrum. The intensity of maximum absorption of complex at 335 nm is slightly red shifted as compared to ligand at 325 nm that confirm complexation and molar absorptivity of complex is smaller than the ligand (**Figure 53**). The slight red shift in spectra of **LF** complex is comparable with literature[50,78,51] and shows different photophysical properties due to binding with zinc metal. The photophysical properties also depended on solution behavior, e.g., ligand and complex show blue emission in solid form and deep bluish color in solution form. Ligand contain two different chromophores phenanthrene and bpy that are responsible for their color and emission. Moreover, **LF** is chromophore-functionalized ditopic/diimine can be used as building blocks to synthesized transition metal complexes which aggregate to create supramolecular structures that might have wide application in different fields.

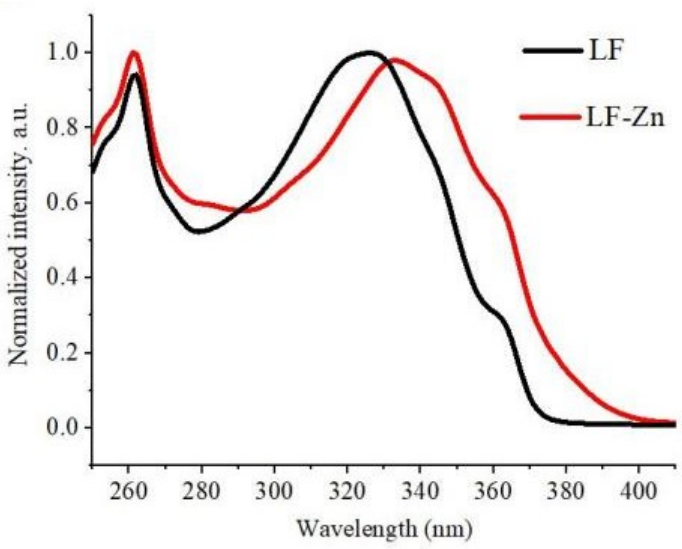

Figure 53: Merged normalized absorption spectra of **LF** and **LF-(Zn (OAc)$_2$)$_2$**.

Conclusions

The main purpose of thesis is synthesis, characterization and single crystal X-ray diffraction (XRD) analysis of a chromophore-functionalized novel non-symmetrical ditopic ligand with *N,N*-functions (diimine) and their complexes. Following conclusions are made:

- Novel ditopic ligand with *N,N*-functions (diimine) **LF** has been synthesized by integration of a secondary chromophore based on phenyl-bipyrdine moiety into primary chromophore based on phenanthrol-imidazole-pyridine moiety. Ditopic ligand has two coordination sites based on pyridyl-imidazole and bipyridine moieties to coordinate with zinc metal atom. Complexes of **LF-Zn** were prepared and showed two type of coordination modes.

- All precursors, desired ditopic/diimine ligand and its complexes were confirmed and characterized by nuclear magnetic resonance (^{1}H-NMR), UV-Vis spectroscopy, single crystal X-ray diffraction (XRD) and elemental analysis.

- The single crystal X-ray diffraction (XRD) analysis was performed for ligand and its zinc complexes. The intermolecular interactions from acetylene to py and ph fragments, hydrogen bonding (N···H, O···H) and π···π stacking were observed that is responsible to create self-assemblies to construct solid state supramolecular structures.

- Photophysical analysis revealed that ligand and its zinc complexes shows two absorption bands due to phenanthrene-localized $\pi \rightarrow \pi^*_{phen}$ transitions (LC) and phenanthrene → pyridyl intra-ligand charge transitions (ILCT) with maximum absorption intensity (λ_{ab}) at 262 and 325 nm due to presence of electron deficient moiety (bpy) that increases energy gap between HOMO LUMO orbitals resulting decrease in absorption wavelength.

.

Acknowledgements

I would like to express my sincere appreciation and great gratitude to the Department of Chemistry, University of Eastern Finland for providing me a great opportunity to enhance my knowledge and to get master's degree.

I am very thankful to Professor Igor O. Koshevoy for providing me an opportunity to do research under his supervision, for his patient guidance, encouragement, moral support, valuable suggestions and critiques for research.

I am greatly indebted to my co-supervisor Diana Temerova, all my teachers and colleagues at Department of Chemistry for their support and help which they have ever made to end up my research perfectly.

Finally, my warm gratitude goes to my parents and family for their appreciation, continuous support, encouragement, love and patience. Without them none of my accomplishments would have been achieved.

References

1. Chirnside, R. C. *Inorganic chemistry*. *The Analyst, Fifth edition.;* Gary L. Miessler, St. Olaf College, Paul J. Fischer, Macalester College. 1944; pp 1-682.
2. Fianchini, M. Synthesis Meets Theory: Past, Present and Future of Rational Chemistry. *Physical Sciences Reviews* **2017**, *2* (12), 1-32.
3. Cotton, F. A.; Geoffrey, W.; Carlos, A. M. *Advanced Inorganic Chemistry*. Wiley-Interscience. 1999; pp 1-1396.
4. Omae, I. Organometallic Intramolecular-Coordination Compounds Containing a Nitrogen Donor Ligand. *Chemical Reviews* **1979**, *79* (4), 287–321.
5. Atkins, P. W. *Shriver & Atkins inorganic chemistry by Peter Atkins, 5th edition*; Cram 101, 2012; pp 1-824.
6. Bradley, P. G.; Kress, N.; Hornberger, B. A.; Dallinger, R. F.; Woodruff, W. H. Vibrational Spectroscopy of the Electronically Excited State. 5. Time-Resolved Resonance Raman Study of Tris (Bipyridine)Ruthenium (II) and Related Complexes. Definitive Evidence for the "Localized" MLCT State. *Journal of the American Chemical Society* **1981**, *103* (25), 7441–7446.
7. Neves, A.; Vencato, I.; Verani, C. N. The Synthesis and Characterization of the Novel Pseudo-Octahedral Complex Bis[(2-Hydroxybenzyl) - (2-Methylpyridyl)-Amine] Zinc (II), [ZnII(Bpa)2].2H2O as a Model for Astacin. *Journal of the Brazilian Chemical Society* **1997**, *8* (3), 265–270.
8. Buncel, E.; Rajagopal, S. Solvatochromism and Solvent Polarity Scales. *Accounts of Chemical Research* **1990**, *23* (7), 226–231.
9. Smith, M.; March, J. *Marchs advanced organic chemistry: reactions, mechanisms, and structure*; John Wiley & Sons: Hoboken, NJ, 2007. pp 1-2357.
10. Prakash, M. J.; Lah, M. S. Metal–Organic Macrocycles, Metal–Organic Polyhedra and Metal–Organic Frameworks. *Chemical Communications* **2009**, 23, 3326-3341.
11. Shiga, T.; Newton, G. N.; Oshio, H. Pre-Programmed Self-Assembly of Polynuclear Clusters. *Dalton Transactions* **2018**, *47* (22), 7384–7394.
12. Lehn, J. M.; Rigault, A.; Siegel, J.; Harrowfield, J.; Chevrier, B.; Moras, D. Spontaneous Assembly of Double-Stranded Helicates from Oligobipyridine Ligands and Copper(I) Cations: Structure of an Inorganic Double Helix. *Proceedings of the National Academy of Sciences* **1987**, *84* (9), 2565–2569.
13. Seidel, S. R.; Stang, P. J. High-Symmetry Coordination Cages via Self-Assembly. *Accounts of Chemical Research* **2002**, *35* (11), 972–983.
14. Sun, Q.-F.; Iwasa, J.; Ogawa, D.; Ishido, Y.; Sato, S.; Ozeki, T.; Sei, Y.; Yamaguchi, K.; Fujita, M. Self-Assembled M24L48 Polyhedra and Their Sharp Structural Switch upon Subtle Ligand Variation. *Science* **2010**, *328* (5982), 1144–1147.
15. Caulder, D. L.; Raymond, K. N. Supermolecules by Design. *Accounts of Chemical Research* **1999**, *32* (11), 975–982.
16. Eryazici, I.; Moorefield, C. N.; Newkome, G. R. Square-Planar Pd (II), Pt (II), and Au (III) Terpyridine Complexes: Their Syntheses, Physical Properties, Supramolecular Constructs, and Biomedical Activities. *Chemical Reviews* **2008**, *108* (6), 1834–1895.

17. Smulders, M. M. J.; Riddell, I. A.; Browne, C.; Nitschke, J. R. Building on Architectural Principles for Three-Dimensional Metallosupramolecular Construction. *Chem. Soc. Rev.* **2013**, *42* (4), 1728–1754.
18. Gianneschi, N. C.; Masar, M. S.; Mirkin, C. A. Development of a Coordination Chemistry-Based Approach for Functional Supramolecular Structures. *Accounts of Chemical Research* **2005**, *38* (11), 825–837.
19. You, C.-C.; Würthner, F. Self-Assembly of Ferrocene-Functionalized Perylene Bisimide Bridging Ligands with Pt (II) Corner to Electrochemically Active Molecular Squares. *Journal of the American Chemical Society* **2003**, *125* (32), 9716–9725.
20. Hofmeier, H.; Schubert, U. S. Recent Developments in the Supramolecular Chemistry of Terpyridine–Metal Complexes. *Chem. Soc. Rev.* **2004**, *33* (6), 373–399.
21. Steel, P. J. Ligand Design in Multimetallic Architectures: Six Lessons Learned. *Accounts of Chemical Research* **2005**, *38* (4), 243–250.
22. Steel, P. J. Aromatic Nitrogen Heterocycles as Bridging Ligands; a Survey. *Coordination Chemistry Reviews* **1990**, *106*, 227–265.
23. Fujita, M.; Yu, S.-Y.; Kusukawa, T.; Funaki, H.; Ogura, K.; Yamaguchi, K. Self-Assembly of Nanometer-Sized Macrotricyclic Complexes from Ten Small Component Molecules. *Angewandte Chemie International Edition* **1998**, *37* (15), 2082–2085.
24. Olenyuk, B.; Whiteford, J. A.; Fechtenkötter, A.; Stang, P. J. Self-Assembly of Nanoscale Cuboctahedra by Coordination Chemistry. *Nature* **1999**, *398* (6730), 796–799.
25. Steel, P. Nitrogen Heterocycles as Building Blocks for New Metallo-Supramolecular Architectures. *Molecules* **2004**, *9* (6), 440–448.
26. Constable, E. C. N,N′-Chelating Biheteroaromatic Ligands; a Survey. *Coordination Chemistry Reviews* **1989**, *93* (2), 205–223.
27. Chichak, K. S. Molecular Borromean Rings. *Science* **2004**, *304* (5675), 1308–1312.
28. Wu, Z.; Zhou, K.; Ivanov, A. V.; Yusobov, M.; Verpoort, F. The Simplest and Fascinating Metal–Organic Polyhedra: Tetrahedra. *Coordination Chemistry Reviews* **2017**, *353*, 180–200.
29. Nugent, P.; Belmabkhout, Y.; Burd, S. D.; Cairns, A. J.; Luebke, R.; Forrest, K.; Pham, T.; Ma, S.; Space, B.; Wojtas, L.; Eddaoudi, M.; Zaworotko, M. J. Porous Materials with Optimal Adsorption Thermodynamics and Kinetics for CO2 Separation. *Nature* **2013**, *495* (7439), 80–84.
30. Black, S. P.; Stefankiewicz, A. R.; Smulders, M. M. J.; Sattler, D.; Schalley, C. A.; Nitschke, J. R.; Sanders, J. K. M. Generation of a Dynamic System of Three-Dimensional Tetrahedral Polycatenanes. *Angewandte Chemie* **2013**, *125* (22), 5861–5864.
31. Hirscher, M. Hydrogen Storage by Cryoadsorption in Ultrahigh-Porosity Metal-Organic Frameworks. *Angewandte Chemie International Edition* **2010**, *50* (3), 581–582.
32. Hastings, C. J.; Pluth, M. D.; Bergman, R. G.; Raymond, K. N. Enzymelike Catalysis of the Nazarov Cyclization by Supramolecular Encapsulation. *Journal of the American Chemical Society* **2010**, *132* (20), 6938–6940.
33. Paquin, F.; Rivnay, J.; Salleo, A.; Stingelin, N.; Silva-Acuña, C. Multi-Phase

Microstructures Drive Exciton Dissociation in Neat Semicrystalline Polymeric Semiconductors. *Journal of Materials Chemistry C* **2015**, *3* (41), 10715–10722.

34. Tidmarsh, I. S.; Faust, T. B.; Adams, H.; Harding, L. P.; Russo, L.; Clegg, W.; Ward, M. D. Octanuclear Cubic Coordination Cages. *Journal of the American Chemical Society* **2008**, *130* (45), 15167–15175.
35. Ward, M. D. Polynuclear Coordination Cages. *Chemical Communications* **2009**, No. 30, 4487-4499.
36. Cook, T. R.; Zheng, Y.-R.; Stang, P. J. Metal–Organic Frameworks and Self-Assembled Supramolecular Coordination Complexes: Comparing and Contrasting the Design, Synthesis, and Functionality of Metal–Organic Materials. *Chemical Reviews* **2012**, *113* (1), 734–777.
37. Kharisov, B. I.; Martínez, P. E.; Jiménez-Pérez, V. M.; Kharissova, O. V.; Martínez, B. N.; Pérez, N. Recent Advances on Ditopic Ligands. *Journal of Coordination Chemistry* **2009**, *63* (1), 1–25.
38. Ringenbach, C.; Nicola, A. D.; Ziessel, R. A Concise Modular Synthesis of 2,5-Diethynyl-3,4-Dibutyl-Thiophene-Bridged Back-to-Back Terpyridine Ligands. *The Journal of Organic Chemistry* **2003**, *68* (12), 4708–4719.
39. Roland, B. K.; Flora, W. H.; Selby, H. D.; Armstrong, N. R.; Zheng, Z. Dendritic Arrays of [Re6(μ3-Se)8]2 Core-Containing Clusters: Exploratory Synthesis and Electrochemical Studies. *Journal of the American Chemical Society* **2006**, *128* (20), 6620–6625.
40. Thomas, K. R. J.; Lin, J. T.; Lin, Y.-Y.; Tsai, C.; Sun, S.-S. Self-Assembly Molecular Architectures Incorporating Fluorene- and Carbazole-Based Bichromic Oligopyridines. Novel Photoactive Materials. *Organometallics* **2001**, *20* (11), 2262–2269.
41. Ramírez Juan; Stadler, A.-M.; Rogez, G.; Drillon, M.; Lehn, J.-M. Copper (II) Dinuclear Pyrazine-Based Rack-Type Complexes: Preparation, Structure, and Magnetic Properties. *Inorganic Chemistry* **2009**, *48* (6), 2456–2463.
42. Sykes, D.; Parker, S. C.; Sazanovich, I. V.; Stephenson, A.; Weinstein, J. A.; Ward, M. D. d→f Energy Transfer in Ir(III)/Eu(III) Dyads: Use of a Naphthyl Spacer as a Spatial and Energetic "Stepping Stone." *Inorganic Chemistry* **2013**, *52* (18), 10500–10511.
43. Chen, F.-F.; Wei, H.-B.; Bian, Z.-Q.; Liu, Z.-W.; Ma, E.; Chen, Z.-N.; Huang, C.-H. Sensitized Near-Infrared Emission from IrIII-LnIII (Ln = Nd, Yb, Er) Bimetallic Complexes with a (N∧O)(N∧O) Bridging Ligand. *Organometallics* **2014**, *33* (13), 3275–3282.
44. Zhao, Q.; Liu, Y.; Cao, Y.; Lv, W.; Yu, Q.; Liu, S.; Liu, X.; Shi, M.; Huang, W. Rational Design of Nanoparticles with Efficient Lanthanide Luminescence Sensitized by Iridium(III) Complex for Time-Gated Luminescence Bioimaging. *Advanced Optical Materials* **2014**, *3* (2), 233–240.
45. Jana, A.; Crowston, B. J.; Shewring, J. R.; Mckenzie, L. K.; Bryant, H. E.; Botchway, S. W.; Ward, A. D.; Amoroso, A. J.; Baggaley, E.; Ward, M. D. Heteronuclear Ir(III)–Ln(III) Luminescent Complexes: Small-Molecule Probes for Dual Modal Imaging and Oxygen Sensing. *Inorganic Chemistry* **2016**, *55* (11), 5623–5633.

46. Dmitriev, R. I.; Papkovsky, D. B. O2-Sensitive Probes Based on Phosphorescent Metalloporphyrins. *Phosphorescent Oxygen-Sensitive Probes SpringerBriefs in Biochemistry and Molecular Biology* **2012**, 1–28.
47. Miao, Q.; Xie, C.; Zhen, X.; Lyu, Y.; Duan, H.; Liu, X.; Jokerst, J. V.; Pu, K. Molecular Afterglow Imaging with Bright, Biodegradable Polymer Nanoparticles. *Nature Biotechnology* **2017**, *35* (11), 1102–1110.
48. Wang, Z.; Zhu, C. Y.; Yin, S. Y.; Wei, Z. W.; Zhang, J. H.; Fan, Y. N.; Jiang, J. J.; Pan, M.; Su, C. Y. A Metal–Organic Supramolecular Box as a Universal Reservoir of UV, WL, and NIR Light for Long-Persistent Luminescence. *Angewandte Chemie* **2019**, *131* (11), 3519–3523.
49. Alan, R. K.; Otho Meth, C.; Charles, W. R.; Comprehensive Organic Functional Group Transformations, by Alan R. Katritzky, Volume 3; Elsevier, 2003; pp 1-856.
50. Kozhevnikov, V. N.; Shabunina, O. V.; Kopchuk, D. S.; Ustinova, M. M.; König, B.; Kozhevnikov, D. N. Facile Synthesis of 6-Aryl-3-Pyridyl-1,2,4-Triazines as a Key Step toward Highly Fluorescent 5-Substituted Bipyridines and Their Zn(II) and Ru(II) Complexes. *Tetrahedron* **2008**, *64* (37), 8963–8973.
51. Yue, S.-M.; Xu, H.-B.; Ma, J.-F.; Su, Z.-M.; Kan, Y.-H.; Zhang, H.-J. Design and Syntheses of Blue Luminescent Zinc(II) and Cadmium(II) Complexes with Bidentate or Tridentate Pyridyl-Imidazole Ligands. *Polyhedron* **2006**, *25* (3), 635–644.
52. Klappa, J. J.; Geers, S. A.; Schmidtke, S. J.; Macmanus-Spencer, L. A.; Mcneill, K. Pyridylpyrrolides as Alternatives to Cyclometalated Phenylpyridine Ligands: Synthesis and Characterization of Luminescent Zinc and Boron Pyridylpyrrolide Complexes. *Dalton Trans.* **2004**, No. 6, 883–891.
53. Kisel, K. S.; Eskelinen, T.; Zafar, W.; Solomatina, A. I.; Hirva, P.; Grachova, E. V.; Tunik, S. P.; Koshevoy, I. O. Chromophore-Functionalized Phenanthro-Diimine Ligands and Their Re(I) Complexes. *Inorganic Chemistry* **2018**, *57* (11), 6349–6361.
54. Pilichos, E.; Spanakis, E.; Maniaki, E.-K.; Raptopoulou, C. P.; Psycharis, V.; Turnbull, M. M.; Perlepes, S. P. Diversity of Coordination Modes in a Flexible Ditopic Ligand Containing 2-Pyridyl, Carbonyl and Hydrazone Functionalities: Mononuclear and Dinuclear Cobalt(III) Complexes, and Tetranuclear Copper(II) and Nickel(II) Clusters. *Magnetochemistry* **2019**, *5* (3), 39.
55. Krumholz, P. Studies on the Coördinate Bond. II. Ferrous Complexes of α-Diimines1. *Journal of the American Chemical Society* **1953**, *75* (9), 2163–2166.
56. Busch, D. H.; Bailar, J. C. The Iron (II)-Methine Chromophore. *Journal of the American Chemical Society* **1956**, *78* (6), 1137–1142.
57. Pople, J. A.; Segal, G. A. Approximate Self-Consistent Molecular Orbital Theory. III. CNDO Results for AB2 and AB3 Systems. *The Journal of Chemical Physics* **1966**, *44* (9), 3289–3296.
58. Reinhold, J.; Benedix, R.; Birner, P.; Hennig, H. Quantum Chemical Investigations of the π-Acceptor Ability of α-Diimine Ligands. *Inorganica Chimica Acta* **1979**, *33*, 209–213.
59. Mcmorran, D. A.; Steel, P. J. A Self-Complementary Molecular Cleft. *Chemical Communications* **2002**, 67, 2120–2121.
60. Tsuchiya, M.; Sakamoto, R.; Shimada, M.; Yamanoi, Y.; Hattori, Y.; Sugimoto, K.; Nishibori, E.; Nishihara, H. Bis (Dipyrrinato)Zinc (II) Complexes: Emission in the

Solid State. *Inorganic Chemistry* **2016**, *55* (12), 5732–5734.

61. Wang, X.; Zhang, H.; Yu, R.; Dong, L.; Peng, D.; Zhang, A.; Zhang, Y.; Liu, H.; Pan, C.; Wang, Z. L. Dynamic Pressure Mapping of Personalized Handwriting by a Flexible Sensor Matrix Based on the Mechanoluminescence Process. *Advanced Materials* **2015**, *27* (14), 2324–2331.
62. Chen, X.; Zhou, Q.; Cheng, Y.; Geng, Y.; Ma, D.; Xie, Z.; Wang, L. Synthesis, Structure and Luminescence Properties of Zinc (II) Complexes with Terpyridine Derivatives as Ligands. *Journal of Luminescence* **2007**, *126* (1), 81–90.
63. O'Neill, L.; Perdisatt, L.; O'Connor, C. Influence of Auxiliary Ligands on the Photophysical Characteristics of a Series of Ruthenium (II)–Polypyridyl Complexes. *The Journal of Physical Chemistry A* **2012**, *116* (44), 10728–10735.
64. Martir, D. R.; Zysman-Colman, E. Photoactive Supramolecular Cages Incorporating Ru (Ii) and Ir(Iii) Metal Complexes. *Chemical Communications* **2019**, *55* (2), 139–158.
65. Hauke, C. E.; Oldacre, A. N.; Fulong, C. R. P.; Friedman, A. E.; Cook, T. R. Coordination-Driven Self-Assembly of Ruthenium Polypyridyl Nodes Resulting in Emergent Photophysical and Electrochemical Properties. *Inorganic Chemistry* **2017**, *57* (7), 3587–3595.
66. Smith, G. S.; Therrien, B. Targeted and Multifunctional Arene Ruthenium Chemotherapeutics. *Dalton Transactions* **2011**, *40* (41), 10793-10800.
67. Ostrowski, A. D.; Ford, P. C. Metal Complexes as Photochemical Nitric Oxide Precursors: Potential Applications in the Treatment of Tumors. *Dalton Transactions* **2009**, 48, 10660–10669.
68. Merlau, M. L.; Mejia, M. D. P.; Nguyen, S. T.; Hupp, J. T. Artificial Enzymes Formed through Directed Assembly of Molecular Square Encapsulated Epoxidation Catalysts. *Angewandte Chemie* **2001**, *113* (22), 4369–4372.
69. Li, H.; Yao, Z.-J.; Liu, D.; Jin, G.-X. Multi-Component Coordination-Driven Self-Assembly toward Heterometallic Macrocycles and Cages. *Coordination Chemistry Reviews* **2015**, *293-294*, 139–157.
70. Tong, J.; Jia, L.-M.; Shang, P.; Yu, S.-Y. Controlled Synthesis of Supramolecular Architectures of Homo- and Heterometallic Complexes by Programmable Self-Assembly. *Crystal Growth & Design* **2018**, *19* (1), 30–39.
71. Severin, K. Supramolecular Chemistry with Organometallic Half-Sandwich Complexes. *Chemical Communications* **2006**, 37, 3859-3867.
72. Liang, S.; Cao, X.; Yan, X.; Chen, L. A Mild and Practical Synthesis of Biphenyl Compounds. *Journal of Chemical Research* **2012**, *36* (9), 555–556.
73. Qiu, K.; Ouyang, M.; Liu, Y.; Huang, H.; Liu, C.; Chen, Y.; Ji, L.; Chao, H. Two-Photon Photodynamic Ablation of Tumor Cells by Mitochondria-Targeted Iridium (Iii) Complexes in Aggregate States. *Journal of Materials Chemistry B* **2017**, *5* (27), 5488–5498.
74. Supervisor, D. B. Polyaromatic diimine ligands and their late transition metal complexes as materials with mechanochromic luminescence. 2018, 1-60.
75. Eckhardt, M.; Fu, G. C. The First Applications of Carbene Ligands in Cross-Couplings of Alkyl Electrophiles: Sonogashira Reactions of Unactivated Alkyl

Bromides and Iodides. *Journal of the American Chemical Society* **2003**, *125* (45), 13642–13643.

76. Roesky, H. W.; Andruh, M. The Interplay of Coordinative, Hydrogen Bonding and π–π Stacking Interactions in Sustaining Supramolecular Solid-State Architectures. *Coordination Chemistry Reviews* **2003**, *236* (1-2), 91–119.
77. Janiak, C. A Critical Account on π–π Stacking in Metal Complexes with Aromatic Nitrogen-Containing Ligands†. *Journal of the Chemical Society, Dalton Transactions* **2000**, 21, 3885–3896.
78. Liu, X.-M.; Mu, X.-Y.; Xia, H.; Ye, L.; Gao, W.; Wang, H.-Y.; Mu, Y. Synthesis, Structures, and Luminescent Properties of d10 Group 12 Metal Complexes with Substituted 2,2′-Bipyridine Ligands. *European Journal of Inorganic Chemistry* **2006**, *2006* (21), 4317–4323.
79. Hiscock, L. K.; Joekar, D.; Balonova, B.; Piqueras, M. T.; Schroeder, Z. W.; Jarvis, V.; Maly, K. E.; Blight, B. A.; Dawe, L. N. Structures, Phase Behavior, and Fluorescent Properties of 3-Phenyl-1-(Pyridin-2-Yl)-1H-Pyrazol-5-Amine and Its ZnCl2 Complex. *Inorganic Chemistry* **2019**, *58* (24), 16317–16321.